

1 **Impact of Intercontinental Pollution Transport on North American Ozone Air Pollution:**  
2 **An HTAP Phase 2 Multi-model Study**

Deleted: II

3  
4 Min Huang<sup>1,2</sup>, Gregory R. Carmichael<sup>3</sup>, R. Bradley Pierce<sup>4</sup>, Duseong S. Jo<sup>5</sup>, Rokjin J. Park<sup>5</sup>,  
5 Johannes Flemming<sup>6</sup>, Louisa K. Emmons<sup>7</sup>, Kevin W. Bowman<sup>8</sup>, Daven K. Henze<sup>9</sup>, Yanko Davila<sup>9</sup>,  
6 Kengo Sudo<sup>10</sup>, Jan Eiof Jonson<sup>11</sup>, Marianne Tronstad Lund<sup>12</sup>, Greet Janssens-Maenhout<sup>13</sup>,  
7 Frank J. Dentener<sup>13</sup>, Terry J. Keating<sup>14</sup>, Hilke Oetjen<sup>8,\*</sup>, Vivienne H. Payne<sup>8</sup>

8  
9 <sup>1</sup>George Mason University, Fairfax, VA, USA

10 <sup>2</sup>University of Maryland, College Park, MD, USA

11 <sup>3</sup>University of Iowa, Iowa City, IA, USA

12 <sup>4</sup>NOAA National Environmental Satellite, Data, and Information Service, Madison, WI, USA

13 <sup>5</sup>Seoul National University, Seoul, Korea

14 <sup>6</sup>European Center for Medium range Weather Forecasting, Reading, UK

15 <sup>7</sup>National Center for Atmospheric Research, Boulder, CO, USA

16 <sup>8</sup>Jet Propulsion Laboratory, California Institute of Technology, Pasadena, CA, USA

17 <sup>9</sup>University of Colorado-Boulder, Boulder, CO, USA

18 <sup>10</sup>Nagoya University, Furocho, Chigusa-ku, Nagoya, Japan

19 <sup>11</sup>Norwegian Meteorological Institute, Oslo, Norway

20 <sup>12</sup>Center for International Climate and Environmental Research, Oslo, Norway

21 <sup>13</sup>European Commission, Joint Research Center, Ispra, Italy

22 <sup>14</sup>US Environmental Protection Agency, Washington, DC, USA

Deleted: Research Triangle Park, NC

23 \*Now at: University of Leicester, Leicester, UK

24  
25 *Correspondence to:* Min Huang (mhuang10@gmu.edu)

Formatted: Suppress line numbers

28 **Abstract**

29  
30 The recent update on the US National Ambient Air Quality Standards of the ground-level  
31 ozone (O<sub>3</sub>) can benefit from a better understanding of its source contributions in different US  
32 regions during recent years. In the Hemispheric Transport of Air Pollution experiment Phase 1  
33 (HTAP1), various global models were used to determine the O<sub>3</sub> source-receptor relationships  
34 among three continents in the Northern Hemisphere in 2001. In support of the HTAP Phase 2  
35 (HTAP2) experiment that studies more recent years and involves higher-resolution global models  
36 and regional models' participation, we conduct a number of regional scale Sulfur Transport and  
37 dEposition Model (STEM) air quality base and sensitivity simulations over North America during  
38 May-June 2010. STEM's top and lateral chemical boundary conditions were downscaled from  
39 three global chemical transport models' (i.e., GEOS-Chem, RAQMS, and ECMWF C-IFS) base  
40 and sensitivity simulations in which the East Asian (EAS) anthropogenic emissions were reduced  
41 by 20%. The mean differences between STEM surface O<sub>3</sub> sensitivities to the emission changes,  
42 and its corresponding boundary condition model's are smaller than those among its boundary  
43 condition models, in terms of the regional/period mean (<10%) and the spatial distributions. An  
44 additional STEM simulation was performed in which the boundary conditions were downscaled  
45 from a RAQMS simulation without EAS anthropogenic emissions. The scalability of O<sub>3</sub>  
46 sensitivities to the size of the emission perturbation, is spatially varying, and the full source  
47 contribution obtained by linearly scaling the North American mean O<sub>3</sub> sensitivities to a 20%  
48 reduction in the EAS anthropogenic emissions may be underestimated by at least 10%.

49 The three boundary condition models' mean O<sub>3</sub> sensitivities are ~8% (May-June 2010)/~11%  
50 (2010 annual) lower than those estimated by multiple global models, and the multi-model  
51 ensemble estimates are higher than the HTAP1 reported 2001 conditions, due to the growing EAS  
52 anthropogenic emissions, the interannual variability in atmospheric circulation (i.e., stronger trans-  
53 Pacific transport in spring 2010 following an El Niño event), and the different experiment designs  
54 of HTAP1 and HTAP2. GEOS-Chem sensitivities indicate that the EAS anthropogenic NO<sub>x</sub>  
55 emissions matter more than the other EAS O<sub>3</sub> precursors to the North American O<sub>3</sub>, qualitatively  
56 consistent with previous adjoint sensitivity calculations.

57 In addition to the analyses on large spatial/temporal scales relative to the HTAP1, we also  
58 show results on subcontinental- and event-scale that are more relevant to the US air quality  
59 management. Satellite O<sub>3</sub> (TES, JPL-IASI, and AIRS) and carbon monoxide (TES and AIRS)  
60 products, along with surface measurements and model calculations, show that during certain  
61 episodes stratospheric O<sub>3</sub> intrusions and the transported EAS pollution influenced O<sub>3</sub> in the western  
62 and the eastern US differently. Free-running global models underpredicted the transported  
63 background O<sub>3</sub> during these episodes, posing difficulties for STEM to accurately simulate the  
64 surface O<sub>3</sub> and its source contribution. Although we effectively improved the modeled O<sub>3</sub> by  
65 incorporating satellite O<sub>3</sub> (OMI and MLS) and evaluated the quality of the HTAP2 emission  
66 inventory with the KNMI OMI nitrogen dioxide, using observations to evaluate and improve O<sub>3</sub>  
67 source attribution still remains to be further explored.

<del>Deleted: The STEM</del>
<del>Deleted: (</del>
<del>Deleted: %). We perform analyses not only on large spatial/temporal scales relative to the HTAP1, but also on subcontinental- and event-scale that are more relevant to the US air quality management. The</del>
<del>Deleted: (including the 24h mean and the US policy-relevant maximum daily 8h average (MDA8) metric averaged throughout the study period and during a selected pollution transport event)</del>
<del>Deleted: often</del>
<del>Deleted: . The STEM sensitivities are also compared with the mean sensitivities estimated by multi- global models, which are higher than the HTAP1 reported 2001 conditions, as well as the 2001-2005 conditions studied using the tagged tracer approach. This indicates the increasing impacts</del>
<del>Deleted: East Asian anthropogenic pollution on North America during 2001-2010. The GEOS-Chem sensitivities indicate that the East Asian anthropogenic NO<sub>x</sub> emissions matter more than the other East Asian O<sub>3</sub> precursors to the North American O<sub>3</sub>, qualitatively consistent with previous adjoint sensitivity calculations</del>
<del>Deleted: global</del>
<del>Deleted: East Asian</del>
<del>Deleted: , to assess the</del>
<del>Deleted: . The scalability</del>
<del>Deleted: regional</del>
<del>Deleted: y</del>
<del>Deleted: the</del>
<del>Deleted: East Asian</del>
<del>Deleted: .</del>
<del>Deleted: Satellite NO<sub>2</sub> (KNMI OMI) and O<sub>3</sub> (TES, JPL-IASI, OMI, MLS, and AIRS) products help detect pollution episodes, quantify or/and reduce the uncertainties in the bottom-up NO<sub>x</sub> emissions and the model transported background O<sub>3</sub>. Based on model calculations and satellite/surface observations during a selected event, we show the different influences from stratospheric O<sub>3</sub> intrusions along with the transported East Asian pollution on O<sub>3</sub> in the western and the eastern US. Future directions of using satellite data in air quality research are also suggested.</del>
<del>Formatted: Suppress line numbers</del>

99 **1. Introduction**

100  
101  
102  
103  
104  
105  
106  
107  
108  
109  
110  
111  
112  
113  
114  
115  
116  
117  
118  
119  
120  
121  
122  
123  
124  
125  
126  
127  
128  
129  
130  
131  
132  
133  
134  
135  
136  
137  
138  
139  
140  
141  
142  
143  
144

Tropospheric ozone (O<sub>3</sub>), a short-lived trace gas with a lifetime ranging from hours in the boundary layer to weeks in the free troposphere, affects tropospheric chemistry, harms human and ecosystem health, and induces climate change on local, regional and global scales (Jerrett et al., 2009; Smith et al., 2009; Anenberg et al., 2010; Mauzerall and Wang, 2001; Avnery et al., 2011a, b; Shindell et al., 2009, 2013; Bowman and Henze, 2012; Stevenson et al., 2006, 2013; Monks et al., 2015). It has been recognized that the uneven distributions of tropospheric O<sub>3</sub> can be attributed to the stratosphere as well as local, regional and distant emission sources, through complicated processes that occur on synoptic, meso- and micro-scales (Task Force on Hemispheric Transport of Air Pollution (HTAP), 2010; National Research Council (NRC), 2009; Maas and Grennfelt, 2016). The mitigation of O<sub>3</sub>'s climate and health impacts would benefit from efforts to control the emissions of its precursors from the various emission sources (United Nations Environment Programme (UNEP) and World Meteorological Organization (WMO), 2011), such as nitrogen oxides (NO<sub>x</sub>), carbon monoxide (CO), methane (CH<sub>4</sub>), and non-methane volatile organic compounds (NMVOCs).

Ground-level O<sub>3</sub> is one of the six criteria air pollutants regulated by the US Environmental Protection Agency (EPA), and the US National Ambient Air Quality Standards (NAAQS) has recently been lowered to 70 ppbv to better protect Americans' health and the environment. Issues regarding making accurate estimates of the total O<sub>3</sub> as well as the background O<sub>3</sub> level (defined as the concentration that is not affected by recent locally-emitted or produced anthropogenic pollution) (e.g., McDonald-Buller et al., 2011; Zhang et al., 2011; Fiore et al., 2014; Huang et al., 2015), have been recently discussed as part of the implementation of the new US O<sub>3</sub> standard (US EPA, 2016a, b). This includes assessing the impacts of various components of the background O<sub>3</sub>, such as stratospheric O<sub>3</sub>, local natural sources such as biogenic, lightning and wildfire emissions, as well as the long-range transport (LRT) of pollution. The impact of the trans-Pacific pollution transport on US air quality has been evaluated in numerous studies over the past decades (e.g., Fiore et al., 2009; Reidmiller et al., 2009; Zhang et al., 2008, 2009; Huang et al., 2010, 2013a; Lin et al., 2012a, 2015, 2016; US EPA, 2016a). It has been found that the increasing trends of pollution in the upwind continents, especially the populated East Asia (e.g., Zhang et al., 2014; Susaya et al., 2013; Wang et al., 2012), may partially offset the US air quality improvements in recent decades due to the regional and local emission controls (e.g., Jacob et al., 1999; Verstraeten et al., 2015; Ambrose et al., 2011; Wigder et al., 2013; Cooper et al., 2010; Parrish et al., 2009, 2012; Gratz et al., 2014). A better understanding of the processes that determine the O<sub>3</sub> pollution levels, as well as an improved capability of attributing the air pollution to nearby or distant sources is needed to assist with designing and implementing effective local emission control strategies to comply with the tighter air quality standards.

Chemical transport models are often used to reproduce and attribute the observed O<sub>3</sub> levels, including assessing the impacts of the internationally transported O<sub>3</sub> on the US air quality. In the HTAP modeling experiment Phase 1<sub>a</sub> (HTAP1<sub>a</sub>), various global models with horizontal resolutions ranging from 1°×1° to 5°×5°, only around half of which are finer than 3°×3°, were used to determine the O<sub>3</sub> source-receptor (SR) relationships among three continents in the Northern Hemisphere in 2001 (Chapter 4 in HTAP, 2010). The global model based SR relationships in HTAP1<sub>a</sub> determined using the emission perturbation approach (i.e., calculating the changes of O<sub>3</sub>

Deleted: 1

146 at the receptor regions in response to a 20% reduction in the emission inputs in a given source  
147 region) were reported as either monthly 24h mean values or policy-relevant metrics such as the  
148 maximum daily 8h average (MDA8) for the US (e.g., Fiore et al., 2009; Reidmiller et al., 2009).  
149 Large intermodel diversity was found in the simulated total O<sub>3</sub> and the intercontinentally  
150 transported pollution for the chosen SR pairs in the northern midlatitudes, indicating the challenges  
151 with model simulations to accurately represent the key atmospheric processes. Multi-model mean  
152 results were the foci of in these studies with the assumption that this approach can reduce the  
153 uncertainty from the single model estimates for monthly or seasonal means. “Ensemble” model  
154 analyses have been suggested by some US stakeholders as one of the methods for helping with the  
155 characterization of the background O<sub>3</sub> components (US EPA, 2016b). Although the multi-model  
156 approach can help identify some of the weaknesses of the individual models and may produce  
157 more reliable estimates, it is necessary to well understand the uncertainties inherent in using the  
158 same set of anthropogenic emissions in all these model simulations. Satellite observations over the  
159 regions with limited in-situ measurements such as the East Asia can be particularly helpful for  
160 quantifying such uncertainties.

161  
162 The 20% emission perturbation in the HTAP1 modeling experiment was chosen to produce  
163 a sizeable (i.e., larger than numerical noise) and realistic impact, but small enough in the assumed  
164 near-linear atmospheric chemistry regime. The scalability of the modeled O<sub>3</sub> sensitivities to the  
165 size of the emission perturbations has been assessed on continental scale (Wu et al., 2009; Fiore et  
166 al., 2009; HTAP, 2010; Wild et al., 2012; Emmons et al., 2012). The receptor O<sub>3</sub> responses to the  
167 source-region emission perturbations are found to be fairly linear within ~50% of the perturbations.  
168 However, due to the chemical non-linearity, the full source contribution obtained by linearly  
169 scaling the receptor regional mean O<sub>3</sub> sensitivity to the 20% reduction in the source region  
170 emissions may be underestimated, and the scalability depended on seasons and the perturbed  
171 emission species. Huang et al. (2013b) investigated the scalability of the O<sub>3</sub> sensitivity between  
172 the southern California-US intermountain west SR pair for May 2010, in which study the southern  
173 California anthropogenic emissions were perturbed by multiple amounts of +50%, -50%, -100%.  
174 They reported that the scalability of the O<sub>3</sub> sensitivities changed with the distance from the source  
175 regions. Further analyses on the scalability of these modeled O<sub>3</sub> sensitivities during recent years  
176 especially for the East Asia-NAM SR pair, as well as their spatial variability, are still needed.  
177 Furthermore, results generated using the emission perturbation approach need to be compared with  
178 those based on the other methods (e.g., tagged tracers, adjoint sensitivity).

179  
180 Previous studies have demonstrated the advantages of high resolution chemical transport  
181 modeling for understanding SR relationships (e.g., Lin et al., 2010 for Europe and the East Asia;  
182 Lin et al., 2012a; Huang et al., 2010, 2013a for Asia and NAM). Using observations (satellite,  
183 sondes, aircraft) along with single model simulations, a few studies have reported that the US O<sub>3</sub>  
184 sensitivities to extra-regional sources is time- and region-dependent (e.g., Lin et al., 2012a, b;  
185 Langford et al., 2011; Ott et al., 2016), and therefore the necessity of evaluating the extra-regional  
186 source impacts on event scale has been emphasized in these studies as well as in US EPA (2016a,  
187 b). The HTAP Phase 2 (HTAP2) multi-model experiment, initiated in 2012, is designed to advance  
188 the understanding of the impact of intercontinental pollution transport during more recent years  
189 (i.e., 2008-2010) involving a number of global and regional models’ participation (Galmarini et  
190 al., 2017; Koffi et al., 2016). The regional models are anticipated to help connect the analyses over  
191 global and regional scales and enable discussions on small spatial (e.g., subcontinental) and

Deleted: 6

193 temporal scales (i.e., event based analyses). The use of satellite products for identifying the  
194 transport events as well as for quantitative model evaluation is also encouraged in the work plan.  
195 The HTAP2 modeling experiment was sequentially conducted in two steps. First, similar to the  
196 HTAP1 experiment, a group of global models with different resolutions conducted base and  
197 emission perturbation sensitivity simulations to determine the pollutants' SR relationships. All  
198 models in their base simulations used the same set of harmonized sector-based global  
199 anthropogenic emissions developed specifically for the HTAP2 modeling experiment (Janssens-  
200 Maenhout et al., 2015). Most of these global models recorded only key chemical species from their  
201 base and sensitivity simulations in varied temporal frequencies. Several global models saved the  
202 three-dimensional (3D) chemical fields of more species with a 3- or 6-hour interval, which are  
203 suitable for being used as regional models' chemical boundary conditions. In the second step,  
204 regional models conducted base and sensitivity simulations to analyze the pollutants' SR  
205 relationships in greater detail. The regional model simulations used the same set of anthropogenic  
206 emissions as the global models within their simulation domains, and the chemical boundary  
207 conditions in these regional simulations were downscaled from the base and sensitivity simulations  
208 from the selected boundary condition model outputs. For regional simulations over the North  
209 America and Europe, boundary conditions were mostly taken from a single model such as the  
210 ECMWF C-IFS or GEOS-Chem.

211  
212 This study aims to address: 1) the differences in O<sub>3</sub> sensitivities generated from the HTAP2  
213 and HTAP1 experiments to help address how the LRT impacts on NAM changed through time; 2)  
214 how the refined modeling experiment design in HTAP2 can help advance our understanding of the  
215 LRT impacts on NAM, particularly the involvement of regional models and the inclusion of small  
216 spatial/temporal scale analysis during high O<sub>3</sub> episodes that are more relevant to air quality  
217 management; 3) the usefulness of satellite observations for better understanding the sources of  
218 uncertainties in the modeled total O<sub>3</sub> (e.g., from the emission and regional models' boundary  
219 condition inputs) as well as for reducing the uncertainties in some of these model inputs via  
220 chemical data assimilation. We performed a number of regional scale STEM (Sulfur Transport  
221 and dEposition Model) base and sensitivity simulations over the NAM during May-June 2010,  
222 during which period strong trans-Pacific pollution transport were shown to episodically impact the  
223 US (Lin et al., 2012a). Extending the HTAP2 regional simulations' basic setup, the STEM top and  
224 lateral chemical boundary conditions were downscaled from three global models' (i.e., the Seoul  
225 National University (SNU) GEOS-Chem, RAQMS, and the ECMWF C-IFS) base and sensitivity  
226 simulations in which the East Asian anthropogenic emissions were reduced. The STEM surface  
227 O<sub>3</sub> sensitivities over the NAM region based on different boundary condition models were inter-  
228 compared, in terms of the regional averages and the spatial patterns on monthly basis and during  
229 a selected event identified by satellite O<sub>3</sub> and CO products. These were also compared with the  
230 sensitivities estimated by their corresponding boundary condition models as well as all HTAP2  
231 participating global models and the results from HTAP1.

## 232 2. Methods

### 233 2.1. Anthropogenic emission inputs

234 Identical anthropogenic emissions were used in all global and regional chemical transport  
235 models' base and sensitivity simulations. This monthly-varying harmonized sectoral (i.e., power,  
236 industry, transportation, residential, shipping, aircraft, agriculture) emission inventory was  
237  
238

Deleted: In this study, we

Moved (insertion) [1]

Moved up [1]: from the emission and regional models' boundary condition inputs) as well as for reducing the uncertainties in some of these model inputs via chemical data assimilation.

Deleted: . An additional regional simulation was performed in which the STEM boundary conditions were downscaled from one global model simulation without the East Asian anthropogenic emissions, and the nonlinear relationship between the O<sub>3</sub> sensitivity and the size of the emission perturbation is discussed. In the discussion, we emphasize: 1) the differences in O<sub>3</sub> sensitivities generated from the HTAP2 and HTAP1 experiments to help address how the LRT impacts on NAM changed through time; 2) how the multi-model approach, as well as the refined model experiment design in HTAP2 can help advance our understanding of the LRT impacts, especially the benefits of increasing the global models' resolutions and involving the regional models; 3) the usefulness of satellite observations for better understanding the sources of uncertainties in the modeled total O<sub>3</sub> (e.g.,

260 provided on a gridded  $0.1^\circ \times 0.1^\circ$  resolution for the years of 2008 and 2010, by compiling the  
 261 officially reported emissions at the national scale (Janssens-Maenhout et al., 2015;  
 262 [http://edgar.jrc.ec.europa.eu/htap\\_v2](http://edgar.jrc.ec.europa.eu/htap_v2)). The temporal profiles for developing the monthly-varying  
 263 emissions differ by region and sector. The amount of emissions of key O<sub>3</sub> precursors (CO, NO<sub>x</sub>,  
 264 NMVOCs) from both years are summarized in Table S1 for the four major emissions sectors, over  
 265 the NAM (US+Canada, based on data from the US EPA and the Environmental Canada, which  
 266 shows lower emissions from the previous years as also discussed in Pouliot et al., 2015), MICS-  
 267 Asia regions (south, southeast, and east Asia, based on country inventory for China and from the  
 268 Clean Air Policy Support System and the Regional Emission inventory in ASia 2.1, more  
 269 information also in Li et al., 2017), and for over the world. For all of these species, global total  
 270 emissions in 2008 and 2010 are similar. The NO<sub>x</sub>, NMVOC, and CO emissions decreased from  
 271 2008 to 2010 over the NAM by 10.7%, 9.4%, and 15.7%, respectively. In 2008, NAM NO<sub>x</sub>,  
 272 NMVOC and CO contributed to 18.0%, 11.7% and 11.9% of the global total, respectively, and in  
 273 2010, these contributions became 15.8%, 10.5% and 10.2%. For 2010, the transportation sector  
 274 contributed more than the other sectors to NAM anthropogenic NO<sub>x</sub> and CO emissions; industrial  
 275 sector contributed more than the other sectors to NMVOCs emissions. Over East Asian countries,  
 276 these emissions are ~2-5 times higher than the US emissions, and the NO<sub>x</sub>, NMVOC and CO  
 277 emissions increased over Asia by 7.3%, 7.2% and 1.0%, with the dominant emission sectors in  
 278 2010 of transportation, industry, and residential, respectively. For both years, the emissions over  
 279 the MICS-Asia regions contribute to over 40% of the global emissions. For these key O<sub>3</sub> precursors,  
 280 the East Asian countries contribute to 45% (NMVOCs)-70% (NO<sub>x</sub>) of the emissions in the MICS-  
 281 Asia domain in both years, and the south Asian countries contribute to ~22% (NO<sub>x</sub>)-34%  
 282 (NMVOCs) of the MICS-Asia emissions. The uncertainty of the emission estimates differs by  
 283 emission sector and species: i.e., the emissions from large-scale combustion sources (e.g., NO<sub>x</sub>  
 284 and CO from power and industry sectors) are less uncertain than those from small-scale and  
 285 scattered sources (e.g., CO and NMVOCs from transportation and residential sources). Non-  
 286 anthropogenic emission inputs used in different models' simulations may differ, and their impacts,  
 287 on the modeled total O<sub>3</sub> and the SR relationships will be compared, in detail in future studies.

Deleted: 5

## 2.2. Region definitions for the SR study and the model base and sensitivity simulations

### 2.2.1. Base and 20% emission perturbation simulations from global and regional models

291 The HTAP2 simulations from eight global models, used in this study, are listed in Table  
 292 1a, including the relevant references. Horizontal and vertical resolutions of these models range  
 293 from finer than 1° to coarser than 2.5°, and from 20 to 60 layers, respectively. Overall, these  
 294 resolutions are higher than the HTAP1 participating models'. Figure 1 defines the source regions  
 295 used in the HTAP2 SR relationship study and we will focus in this study on assessing the East  
 296 Asia (EAS), S Asia (SAS), Europe (EUR), and non-NAM anthropogenic source (interchangeable  
 297 in this paper with "(all) foreign") impacts on the NAM O<sub>3</sub> levels in 2010. Specifically, each model  
 298 performed a base simulation and a number of sensitivity simulations in which the original HTAP2  
 299 anthropogenic emissions for all species and sectors in a defined source region were perturbed by  
 300 a certain amount (referring to 20% as in most cases) and these cases are defined in Table 1a-b, as  
 301 *\*source region\*ALL(\*perturbation\*)*, where "ALL" refers to "all species and sectors", consistent  
 302 with HTAP1 and HTAP2's naming convention. The O<sub>3</sub> differences  $R(O_3, *source\ region*,$   
 303 *\*perturbation\*)* over the NAM were then calculated between each model's base and sensitivity  
 304 simulations:  
 305

Deleted: . As this paper focuses

Deleted: impact of anthropogenic emissions, we do not introduce this information

Formatted: Indent: First line: 0.5"

Deleted: .

Deleted: overall

Deleted: Relevant references for the RAQMS model and the SNU GEOS-Chem are Pierce et al. (2007, 2009) and Park et al. (2004) (with additional descriptions on its HTAP simulation configurations at: [http://iek8wikis.iek.fz-juelich.de/HTAPWiki/WP2.3?action=AttachFile&do=view&target=\\_README\\_GEOS-Chem.pdf](http://iek8wikis.iek.fz-juelich.de/HTAPWiki/WP2.3?action=AttachFile&do=view&target=_README_GEOS-Chem.pdf)), respectively. The descriptions of the remaining models can be found in published HTAP2 works such as in Stjern et al. (2016).

Deleted: , unless specified differently

Deleted: l

Deleted: (

Deleted: ).

324  $R(O_3, EAS, 20\%) = \text{BASE } O_3 - \text{EASALL}(-20\%) O_3$  (1a)

325  $R(O_3, SAS, 20\%) = \text{BASE } O_3 - \text{SASALL}(-20\%) O_3$  (1b)

326  $R(O_3, EUR, 20\%) = \text{BASE } O_3 - \text{EURALL}(-20\%) O_3$  (1c)

327  $R(O_3, \text{non-NAM}, 20\%) = \text{NAMALL } O_3 - \text{GLOALL}(-20\%) O_3$  (1d)

Deleted: -

Deleted: -

Deleted: -

Deleted: -

329 The monthly-mean  $R(O_3, \textit{source region}, 20\%)$  values were averaged over the NAM  
 330 region for the analysis and compared with the findings in the HTAP1 study (e.g., Fiore et al., 2009).  
 331 It is worth mentioning that the rectangular source regions defined in HTAP1 were modified in  
 332 HTAP2 to align with the geo-political borders. For EAS and SAS, the regions not overlapped by  
 333 HTAP1 and HTAP2 are mostly in the less populated/polluted regions such as the northwestern  
 334 China, according to the HTAP2 emission maps ([http://edgar.jrc.ec.europa.eu/htap\\_v2/index.php](http://edgar.jrc.ec.europa.eu/htap_v2/index.php)).  
 335 HTAP2's EUR domain excludes certain regions in Russia/Belarus/Ukraine, Middle East and  
 336 North Africa that are included in HTAP1's EUR domain. The impact of emissions over these  
 337 regions on comparing the NAM  $R(O_3, EUR, 20\%)$  values in HTAP1 and HTAP2 will be discussed  
 338 in Section 3.2.1.

339  
 340 A unitless "Response to Extra-Regional Emission Reductions (RERER)" metric  
 341 (Galmarini et al., 2017), as defined in eq. (2), was also calculated to measure the importance of  
 342 local versus non-local sources to NAM's  $O_3$  levels:

343 
$$\text{RERER}(O_3, \text{NAM}) = \frac{R_{O_3, \text{non-NAM}, 20\%}}{R_{O_3, \text{global}, 20\%}} = \frac{(\text{NAMALL } O_3 - \text{GLOALL } O_3)}{(\text{BASE } O_3 - \text{GLOALL } O_3)}$$
 (2)

Deleted: 6

344 The denominator and numerator terms of RERER represent the impacts of global and non-NAM  
 345 anthropogenic emissions on NAM  $O_3$ , respectively. The higher the NAM RERER value is, the  
 346 stronger impact from non-local sources on NAM is indicated. The RERER value can exceed 1,  
 347 when emission reductions led to increasing concentrations (e.g.  $O_3$  titration by nitrogen monoxide  
 348 (NO)).

349  
 350 The STEM (version 2K3) regional simulations were then performed on a 60 km×60 km  
 351 horizontal resolution (a typical coarse regional model resolution) grid over NAM within the  
 352 domain defined in Figure 2a during May-June 2010. The meteorological conditions in spring 2010  
 353 were compared with the climatology from the NCEP/NCAR reanalysis data for the 1981-2010  
 354 period (Kalnay et al., 1996) in Huang et al. (2013b), concluding that this spring represents a period  
 355 of stronger-than-climatological average spring trans-Pacific transport, based on a stronger  
 356 meridional gradient in the North Pacific and higher Pacific/North American (PNA) indexes. This  
 357 is consistent with the findings by Lin et al. (2014) that the El Niño conditions during the 09/10  
 358 winter strengthened the trans-Pacific transport of Asian pollution in spring 2010. The mean near-  
 359 surface air temperatures in the western US in this spring were lower than the climatology, with  
 360 larger anomalies in the mountain states, which may have led to weaker local  $O_3$  production and  
 361 decomposition of the transported peroxyacyl nitrates (PAN). In contrast, higher-than-normal  
 362 temperatures were found in the eastern US that favored anomalously strong local  $O_3$  production.

Deleted: 2b

Deleted: S

Deleted: (

Deleted: ) and stratospheric intrusion conditions (based on the tropopause pressure and the UTLS relative humidity).

Formatted: Font:Not Italic

364  
 365 STEM has been used to interpret the observations collected by satellites and during aircraft  
 366 campaigns in the past decade (e.g., Carmichael et al., 2003a, b; Huang et al., 2010, 2013a, b, 2014,  
 367 2015). STEM calculates gas-phase chemistry reactions based on the SAPRC 99 gaseous chemical  
 368 mechanism (Carter, 2000) with thirty photolysis rates calculated online by the Tropospheric  
 369 Ultraviolet-Visible radiation model (Madronich et al., 2002). Most of the key configurations of the  
 370 60 km base simulations are the same as those described in Lapina et al. (2014), i.e., meteorological

380 fields were pre-calculated by the Advanced Research Weather Research and Forecasting Model  
381 (WRF-ARW, Skamarock et al., 2008) version 3.3.1 forced by the North American Regional  
382 Reanalysis data (Mesinger et al., 2006), using a similar set of the physics configuration to those in  
383 Huang et al. (2013a). Biomass burning emissions are from the Fire INventory from NCAR (FINN)  
384 inventory version 1.0 (Wiedinmyer et al., 2011). Biogenic emissions were calculated by the Model  
385 of Emissions of Gases and Aerosols from Nature (MEGAN) version 2.1 (Guenther et al., 2012),  
386 driven by the WRF meteorology. Lightning NO<sub>x</sub> emissions are generated following the method in  
387 Allen et al. (2012), with the flash rates determined by the WRF convective precipitation and scaled  
388 to the National Lightning Detection Network flash rates. A major difference of the STEM  
389 simulations in this study from the Lapina (2014) study is that the anthropogenic emissions were  
390 replaced with the monthly-mean HTAP2 inventory with no weekday-weekend variability applied,  
391 rather than the earlier National Emission Inventory (NEI) 2005 in which the weekday-weekend  
392 variability exists. This change can introduce uncertainty for some US regions where weekday-  
393 weekend variability of some O<sub>3</sub> precursors' emissions was notable during the studied period (e.g.,  
394 weekend NO<sub>x</sub> emissions in southern California during spring/summer 2010 were 0.6-0.7 of the  
395 weekday emissions as reported by Kim et al. (2016) and Brioude et al. (2013)), but this was done  
396 to ensure consistency with the HTAP2 global model simulations, that also didn't use daily variable  
397 emissions for any regions in the world. The VOC speciation for the SPRAC 99 chemical  
398 mechanism in the NEI 2005 ([ftp://aftp.fsl.noaa.gov/divisions/taq/emissions\\_data\\_2005](ftp://aftp.fsl.noaa.gov/divisions/taq/emissions_data_2005)) were  
399 applied to break down the total NMVOC emissions provided in the HTAP2 inventory. The VOC  
400 speciation based on the year of 2005 can be unrealistic for 2005 as well as 2010 as studies have  
401 reported variable temporal changes of different VOC species in some US cities (e.g., Warneke et  
402 al., 2012). The time-varying lateral and top boundary conditions in the STEM base simulations  
403 were downscaled from three global models (i.e., 3 hourly SNU GEOS-Chem, 3 hourly ECMWF  
404 C-IFS, and 6 hourly RAQMS) base simulations. In support of the SR relationship study to quantify  
405 the East Asia anthropogenic impacts on the NAM, three STEM sensitivity simulations were also  
406 conducted in which the STEM boundary conditions were downscaled from the EASALL(-20%)  
407 sensitivity simulations by these three global models (Table 1b). All STEM simulated 3D chemical  
408 fields were saved hourly for the convenience of calculating the US primary O<sub>3</sub> standard metric  
409 MDA8 as well as the quantitative comparisons against the satellite Level 2 (L2) O<sub>3</sub> products. The  
410 STEM base case surface O<sub>3</sub> performance and its O<sub>3</sub> sensitivities were also compared with those of  
411 its boundary condition models as well as the multi- global model means. The latitude/longitude  
412 ranges (20-50°N/130-65°W) of NAM for the global and regional model based sensitivity  
413 calculations were selected to mainly account for the coverage of the STEM domain, which are  
414 slightly different from the definition of North America in HTAP1.

Deleted: This change can introduce uncertainty, but

Deleted: .

Formatted: Indent: First line: 0.5"

415  
416 Note that non-anthropogenic emission inputs used in STEM and its boundary condition  
417 models differed, as summarized in Table 1c. Figure S1 shows detailed comparisons between  
418 STEM and GEOS-Chem's non-anthropogenic (i.e., soil, lightning, biomass burning) NO<sub>x</sub>  
419 emission inputs, and their impacts on the modeled NAM background O<sub>3</sub> were included in Lapina  
420 et al. (2014). Such quantitative comparisons will also be carried out between STEM and its other  
421 boundary condition models in future studies.

#### 422 423 2.2.2. Additional base and sensitivity simulations from selected models

424



427 In addition to the base and 20% EAS all-category emission perturbation simulations, the  
428 global RAQMS model conducted a sensitivity simulation in which the East Asian anthropogenic  
429 emissions were zeroed out, which was also used as STEM's boundary conditions (Table 1b). We  
430 calculate the "S<sub>O<sub>3</sub></sub>" metric (eq. (3)) using the O<sub>3</sub> sensitivities in STEM and RAQMS at the receptor  
431 regions in response to both 20% and 100% of emission reductions, to explore the relationships  
432 between the O<sub>3</sub> sensitivity and the size of the emission perturbation. A closer-to-one "S<sub>O<sub>3</sub></sub>" value  
433 indicates higher scalability of the sensitivity based on the 20% emission perturbation method for  
434 obtaining the full "contribution" of the East Asian anthropogenic emissions on the NAM O<sub>3</sub>.

435  
436 
$$S_{O_3} = R(O_3, \text{EAS}, 100\%) / R(O_3, \text{EAS}, 20\%) / 5 \quad (3)$$
  
437 Where:  $R(O_3, \text{EAS}, 100\%) = \text{BASE } O_3 - \text{EASALL}(-100\%) O_3$

438  
439 The RAQMS model also provided a base simulation that assimilated satellite O<sub>3</sub> products  
440 from the Ozone Monitoring Instrument (OMI, Levelt et al., 2006) and Microwave Limb Sounder  
441 (MLS, Livesey et al., 2008) (Pierce et al., 2007), which was used to help better understand the  
442 regional model base run error sources, as well as for demonstrating the use of satellite observations  
443 to help improve the representation of the trans-boundary pollution.

444  
445 We also used a number of sensitivity simulations produced by the GEOS-Chem adjoint  
446 model v35f in which the emissions from selected anthropogenic emission sectors (power&industry,  
447 transportation, residential) or individual O<sub>3</sub> precursor chemical species (NO<sub>x</sub>, VOC, CO) over the  
448 East Asia were reduced by 20%. Additional simulations for the 2008-2009 periods by the SNU  
449 GEOS-Chem were also utilized to quantify the East Asia and non-NAM anthropogenic source  
450 impacts in comparison with the 2010 conditions that we mainly focus on in this study.

### 451 2.3. *In-situ and satellite observations*

#### 452 2.3.1. In-situ observations

453 Over the receptor NAM, the hourly O<sub>3</sub> observations at the Clean Air Status and Trends  
454 Network (CASTNET, <http://epa.gov/castnet/javaweb/index.html>) sites were used to evaluate the  
455 global and regional models' base simulations in four subregions: western US (i.e., the EPA regions  
456 8, 9, 10); southern US (i.e., the EPA regions 4 and 6), the Midwest (i.e., the EPA regions 5 and 7),  
457 and the northeast (i.e., the EPA regions 1-3). The numbers of sites used in global and regional  
458 models' evaluation in each US subregion are summarized in Tables 2-3. The locations of these  
459 sites and the subregions they belong to are indicated in Figure 2a, overlaid on a model-based terrain  
460 height map. A majority of the CASTNET sites in the western US are located at high elevation (>1  
461 km) remote or rural regions, more susceptible to the trans-boundary pollution (e.g., Jaffe, 2011).  
462 Most of the sites in the other three subregions are located in low elevation regions, mainly affected  
463 by local and regional pollution. The model-based terrain heights fairly well represent the reality  
464 on subregional scale – the differences between the actual and model-based subregional mean  
465 terrain heights at the CASTNET sites are smaller than 0.1 km (Table 3).

466  
467 During May-June 2010, intense ozonesonde measurements were made at multiple  
468 California locations (Cooper et al., 2011), in support of the NOAA "California Nexus (CalNex):  
469 Research at the Nexus of Air Quality and Climate Change" field experiment (Ryerson et al., 2013).  
470 They have been used to evaluate the simulated O<sub>3</sub> vertical profiles by the HTAP2 participating  
471 models. The detailed evaluation results have been shown by Cooper et al. (2016), and will be  
472 covered by subsequent publications.

Deleted: ↵

Deleted: ↵

Deleted: 2b

Formatted: Indent: First line: 0.5"

477 Over HTAP2's EAS source region, the global models' O<sub>3</sub> performance was evaluated  
478 against the monthly-mean surface in-situ O<sub>3</sub> measurements at 11 sites within the Acid Deposition  
479 Monitoring Network in East Asia (EANET, <http://www.eanet.asia>) that had data throughout the  
480 year of 2010. These include eight Japanese and three Korean sites (Figure 3a), all of which are  
481 located at low elevation regions (2-150 m). The reported monthly mean observations at these sites  
482 were based on weekly or daily sampled data, varying among sites.

### 484 2.3.2. Satellite products

485 In two case studies of high O<sub>3</sub> episodes, L2 and L3 O<sub>3</sub> and CO retrievals from several  
486 satellite instruments were used to assess the impacts of trans-Pacific pollution transport and  
487 stratospheric O<sub>3</sub> intrusions on NAM O<sub>3</sub> levels in early May. These include: 1) the early afternoon  
488 O<sub>3</sub> and CO profiles version 5 from the Tropospheric Emission Spectrometer (TES) (Beer et al.,  
489 2001; Beer, 2006) on the Aura satellite; 2) the mid-morning O<sub>3</sub> profiles from the METOP-Infrared  
491 Atmospheric Sounding Interferometer (IASI), which were retrieved using the Jet Propulsion  
492 Laboratory (JPL) TES optimal estimation retrieval algorithm (Bowman et al., 2006) for selected  
493 areas including the western US (Oetjen et al., 2014, 2016); as well as 3) the early afternoon L3 O<sub>3</sub>  
494 and CO maps (version 6, 1°×1°) from the Aqua Atmospheric Infrared Sounder (AIRS) instrument.  
495 The TES tropospheric O<sub>3</sub> retrieval is often sensitive to the mid- to lower free troposphere, and O<sub>3</sub>  
496 at these altitudes in the Eastern Pacific is known to possibly impact the downwind US surface air  
497 quality at later times (Huang et al., 2010; Parrish et al., 2010). TES O<sub>3</sub> is generally positively  
498 biased by <15% relative to high accuracy/precision reference datasets (e.g., Verstraeten et al.,  
499 2013). Although IASI is in general less sensitive than TES due to its coarse spectral resolution, the  
500 681–316 hPa partial column-averaged O<sub>3</sub> mixing ratios in the JPL product agree well with TES  
501 O<sub>3</sub> for the 2008–2011 period with a -3.9 ppbv offset (Oetjen et al., 2016). Note that IASI O<sub>3</sub> data  
502 are processed operationally in Europe using a different algorithm. For this work we used O<sub>3</sub>  
503 profiles from TES and IASI processed using a consistent algorithm at JPL, although the latter set  
504 of data represents only a small subset of the full set of the IASI radiance measurements. The IASI  
505 and TES L2 O<sub>3</sub> profiles (screened by the retrieval quality and the C-Curve flags) were used to  
506 evaluate the STEM O<sub>3</sub> vertical distributions in the different base simulations, and the satellite  
507 observation operators were applied in these comparisons. Taking TES as an example, its  
508 observation operator  $h_z$  for O<sub>3</sub> is written in (4):

$$509 h_z = z_c + A_{\text{TES}} (\ln(F_{\text{TES}}(c)) - z_c) \quad (4)$$

510 where  $z_c$  is the natural log form of the TES constraint vector (a priori) in volume mixing ratio.  
511  $A_{\text{TES}}$  is the averaging kernel matrix reflecting the sensitivity of retrieval to changes in the true state  
512 (Rodgers, 2000).  $F_{\text{TES}}$  projects the modeled O<sub>3</sub> concentration fields  $c$  to the TES grid using spatial  
513 and temporal interpolation. The exponential of  $h_z$  is then used to compute the mismatches between  
514 the model and TES O<sub>3</sub> retrievals as the model evaluation. A small mismatch between model with  
515 the satellite observation operators and the satellite retrievals may indicate either good model  
516 performance or may be the low sensitivity of the retrievals to the true O<sub>3</sub> profile. AIRS O<sub>3</sub> is  
517 sensitive to the altitudes near the tropopause, with positive biases over the ozonesondes in the  
518 upper troposphere (e.g., Bian et al., 2007); AIRS CO is most sensitive to 300–600 hPa (Warner et  
519 al., 2007) and is frequently used together with the AIRS O<sub>3</sub> to distinguish the stratospheric O<sub>3</sub>  
520 intrusions from long-range transported anthropogenic or biomass burning pollution. We use the  
521 L3 AIRS products in this study to get a broad overview of the areas that are strongly impacted by  
522 the stratospheric O<sub>3</sub> intrusions or/and LRT of pollution.

Formatted: Indent: First line: 0.5"

Deleted: a

Deleted: study

Field Code Changed

525 The bottom-up NO<sub>x</sub> emissions from the HTAP2 inventory were assessed on a monthly base  
 526 by comparing the GEOS-Chem nitrogen dioxide (NO<sub>2</sub>) columns with the de-striped KNMI (Royal  
 527 Netherlands Meteorological Institute) OMI column NO<sub>2</sub> product version 2.0 (Boersma et al.,  
 528 2011a, b). For this model evaluation against the OMI L2 products, the NO<sub>2</sub> fields calculated by the  
 529 GEOS-Chem adjoint model were saved daily at 13:30 local solar time, roughly coinciding with  
 530 the Aura and Aqua overpassing times. Other parameters used in the model column calculations  
 531 came from the GEOS-5/GEOS-Chem monthly mean conditions. The OMI data that passed the  
 532 tropospheric quality flag at 13-14 local time were selected based on the following screening criteria:  
 533 surface albedo<0.3; cloud fraction<0.2; solar zenith angle <75°; and viewing zenith angle <45°.  
 534 The averaging kernels (Eskes and Boersma, 2003) and Air Mass Factors (AMFs) in the KNMI  
 535 product were used to calculate the modeled tropospheric NO<sub>2</sub> vertical columns comparable to the  
 536 OMI's. Details of the method to compare the model-based NO<sub>2</sub> columns with the KNMI OMI's  
 537 can be found in Huang et al. (2014).  
 538

### 539 3. Results and Discussions

#### 540 3.1. Evaluation of the HTAP2 bottom-up NO<sub>x</sub> emissions and the model base simulations

##### 541 3.1.1. Evaluation of the bottom-up NO<sub>x</sub> emissions

542  
 543  
 544 The comparison of the GEOS-Chem adjoint NO<sub>2</sub> columns with the OMI product was used  
 545 to help assess the bottom-up HTAP2 NO<sub>x</sub> emissions. Figure 4 shows that NO<sub>2</sub> columns from  
 546 GEOS-Chem's base simulations over the US are overall overestimated. While grid-scale  
 547 differences in NO<sub>2</sub> columns may not be directly indicative of emissions biases (Qu et al., 2016),  
 548 these discrepancies are possibly due to a positive bias in the bottom-up emissions, mainly from the  
 549 anthropogenic sources, which have also been pointed out by Anderson et al. (2014) and Travis et  
 550 al. (2016). Larger OMI-model disagreement was found over the central/eastern US in June 2010  
 551 than in May, likely also due to the uncertainty in GEOS-Chem's soil or lightning NO<sub>x</sub> emissions,  
 552 which appear to be high over these regions (Figure S1). The NO<sub>2</sub> columns in the GEOS-Chem  
 553 base simulation were overestimated in many northern China rural areas and underpredicted in a  
 554 few urban areas in the East Asia as well as a broad area in the southwestern China. The mismatches  
 555 between model and OMI NO<sub>2</sub> fell within the ranges of the comparison between the GOME2 NO<sub>2</sub>  
 556 column product and six models' simulations over China in summer 2008 (Quennehen et al., 2016).  
 557 Also, the use of monthly-mean anthropogenic emissions as well as the overall rough treatment of  
 558 emission height and temporal profiles can be sources of uncertainty. These global model  
 559 evaluation results suggest that the EAS-NAM SR relationships analyzed using this inventory may  
 560 overall overestimate the NAM local contribution and underestimate the EAS contribution—Under  
 561 different chemical regimes, this statement would also rely on the quality of other O<sub>3</sub> precursors'  
 562 emissions in the HTAP2 inventory, and they may be associated with variable uncertainties  
 563 depending on the species or emission sector as introduced in Section 2.1. Therefore, careful  
 564 assessment of other key O<sub>3</sub> precursors' emissions in the inventory is needed in the future work. It  
 565 is important to note that uncertainty in satellite retrievals can prevent us from producing accurate  
 566 assessment on emissions (e.g., van Noije et al., 2006), and this comparison does not account for  
 567 the biases in the used OMI data, and would be further validated by using other OMI NO<sub>2</sub> products  
 568 as well as the bias-corrected (if applicable) in-situ NO<sub>2</sub> measurements. We also recommend more  
 569 global models to save their calculations more frequently, at least near the satellite overpassing

Deleted: p
Deleted: model base simulations and
Deleted: global model O <sub>3</sub> ensembles and the
Moved down [2]: The monthly-mean surface O <sub>3</sub> from multiple global models' free runs was evaluated with the CASTNET observations, at the stations with 95% of the hourly O <sub>3</sub> observation completeness for the 1 May-30 June 2010 period
Formatted: No underline
Formatted: Indent: First line: 0.5"
Deleted: , and the mean biases and RMSEs for these two months were summarized in Table 2 by US subregions. The three boundary condition-model as well as the eight-model ensembles overall underpredicted O <sub>3</sub> in the western US (by ~3-6 ppbv), similar to the HTAP1 model performance over these regions for May-June 2001.
Moved down [3]: This can be due to the underestimated trans-boundary pollution (as indicated by the evaluation of modeled O <sub>3</sub> profiles with ozonesondes and satellite O <sub>3</sub> products). In addition, the coarser model resolutions are less capable of resolving the local features that influence the pollutants' import processes, chemical transformation, as well as regional processes such as the cross-state pollution transport over complex terrains. The global RAQMS base simulation with satellite assimilation improved the free tropospheric O <sub>3</sub> structure as its comparisons with the ozonesondes shows, which also enhanced the simulated monthly-mean surface O <sub>3</sub> by up to
Deleted: over 10 ppbv in the western US and some coastal areas in the southeastern US (Figure S1, left). ... [2]
Moved down [4]: subregions (by 8-12 ppbv), close to HTAP1 model performance for May-June 2001 over the similar areas (Fiore et al., 2009) and in the Lapina et al.
Deleted: (2014) study for 2010, in large part due to the ... [3]
Moved down [5]: Satellite assimilation led to 2-6 ppb ... [4]
Moved down [7]: 2016; Travis et al.,
Formatted: Indent: First line: 0"
Deleted: Except in the northeastern US, the eight-mod ... [5]
Moved down [6]: in the literature (e.g., Geddes et al., 2016;
Deleted: 2016), but how serious these issues were in th ... [6]
Formatted: Underline
Deleted: 3
Deleted: , and larger disagreement was found over the ... [7]
Deleted: overall there does appear to be
Deleted: consistent with the findings of
Deleted: It is likely that other O <sub>3</sub> precursors' co-emitte ... [8]
Deleted: This
Deleted: precursors
Deleted: emission
Deleted: so
Deleted: also needed. Note

643 times, for a more comprehensive assessment of the emission inventory and a better understanding  
644 of the model biases.

### 645 3.1.2. Evaluation of the global model O<sub>3</sub> performance in NAM and EAS

646  
647 The monthly-mean surface O<sub>3</sub> from multiple global models' free runs was evaluated with  
648 the CASTNET observations, at the stations with 95% of the hourly O<sub>3</sub> observation completeness  
649 for the 1 May-30 June 2010 period. The mean biases and RMSEs for these two months were  
650 summarized in Table 2a by US subregions. The three boundary condition-model as well as the  
651 eight-model ensembles overall underpredicted O<sub>3</sub> in the western US (by ~3-6 ppbv), similar to the  
652 HTAP1 model performance over these regions for May-June 2001 presented in Fiore et al. (2009).  
653 This can be due to the underestimated trans-boundary pollution (as indicated by the evaluation of  
654 modeled O<sub>3</sub> profiles with ozonesondes and satellite O<sub>3</sub> products). In addition, the coarser model  
655 resolutions are less capable of resolving the local features that influence the pollutants' import  
656 processes, chemical transformation, as well as regional processes such as the cross-state pollution  
657 transport over complex terrains. The global RAQMS base simulation with satellite assimilation  
658 improved the free tropospheric O<sub>3</sub> structure as its comparisons with the ozonesondes shows, which  
659 also enhanced the simulated monthly-mean surface O<sub>3</sub> by up to >10 ppbv in the western US and  
660 some coastal areas in the southeastern US (Figure S2, left). The global models overall significantly  
661 overestimated O<sub>3</sub> in the other three subregions (by 8-12 ppbv), close to HTAP1 model performance  
662 for May-June 2001 over the similar areas (Fiore et al., 2009) and in the Lapina et al. (2014) study  
663 for 2010, in large part due to the uncertainties in the bottom-up emissions as discussed in Section  
664 3.1.1. Satellite assimilation led to 2-6 ppbv higher RAQMS surface O<sub>3</sub> in the  
665 central/southern/eastern US than in its free simulation, which are associated with higher positive  
666 biases.

667  
668 The surface O<sub>3</sub> performance by individual global models varies significantly, e.g., with the  
669 RMSEs at all CASTNET sites ranging from ~9 ppbv to >15 ppbv (Table 2b). As reported in the  
670 literature (e.g., Geddes et al., 2016; Travis et al., 2016), the representation of land use/land cover,  
671 boundary layer mixing and chemistry can be sources of uncertainty for certain global model (i.e.,  
672 GEOS-Chem), but how serious these issues were in the other models need to be investigated  
673 further. Some other possible reasons include the variation of these models' non-anthropogenic  
674 emission inputs and chemical mechanisms (Table 1c). Future work should emphasize on  
675 evaluating and comparing all models on process level to better understand their performance.  
676 Except in the northeastern US, the eight-model ensembles show better agreement with the  
677 CASTNET O<sub>3</sub> observations than the three boundary condition-model ensemble. Overall the three-  
678 model ensemble only outperforms one model but the eight-model ensemble outperforms seven  
679 individuals. This reflects that averaging the results from a larger number of models in this case  
680 more effectively cancelled out the positive or negative biases from the individual models.

681  
682 The monthly-mean surface O<sub>3</sub> from multiple global models' free runs was also evaluated  
683 with the EANET observations. Among the three boundary condition models, GEOS-Chem  
684 produced higher O<sub>3</sub> than the other two throughout the year, and C-IFS O<sub>3</sub> is the lowest from April  
685 to December. The three-model and eight-model ensembles are lower than the surface O<sub>3</sub>  
686 observations by <10 ppbv during high O<sub>3</sub> seasons (winter/spring), but show substantial (>10 ppbv)  
687 positive biases during low O<sub>3</sub> seasons especially in July and August (Figure 3b), similar to the  
688 HTAP1 model performance over Japan in 2001 (Fiore et al., 2009). During May-June 2010,

Deleted: .

Moved (insertion) [2]

Formatted: No underline

Formatted: Indent: First line: 0.5"

Moved (insertion) [3]

Moved (insertion) [4]

Moved (insertion) [5]

Moved (insertion) [6]

Moved (insertion) [7]

690 generally the models performed better at the Japanese sites than at the Korean sites (Table 2c),  
691 with significant positive biases occurring at low O<sub>3</sub> regions (e.g., in central Japan) and negative  
692 biases found at high O<sub>3</sub> regions, mainly owing to the uncertainty in the local and upwind emissions.  
693 The different approaches to generate the monthly-mean modeled and the observed O<sub>3</sub> data may  
694 have also contributed to these model-observation discrepancies. Overall O<sub>3</sub> performance by  
695 individual models varies less significantly than at the CASTNET sites, with RMSEs ranging from  
696 8.6 ppbv to ~13 ppbv (Table 2b). The three-model ensemble outperforms two individual models,  
697 and the eight-model ensemble outperforms six individual models. Unlike at the CASTNET sites,  
698 the three-model ensemble agrees better with the observations than the eight-model ensemble  
699 (Table 2c).

### 701 3.1.3. Evaluation of the STEM regional base simulations w/ three sets of boundary conditions

702  
703 The three STEM base simulations using different boundary conditions were evaluated with  
704 the hourly O<sub>3</sub> observations at the CASTNET sites in the four US subregions. The evaluation  
705 included the 8 May-30 June 2010 period to exclude the results during the one-week spin-up period.  
706 The time series plots of observed and modeled O<sub>3</sub> at the western US CASTNET sites show that  
707 STEM was capable of capturing several high O<sub>3</sub> periods, and it produced larger biases during the  
708 nighttime (Figure 2c), as a result of the poorer WRF performance. Figure 2c and the evaluation  
709 statistics in Table 3a-b indicate that STEM/C-IFS O<sub>3</sub> concentrations are associated with the highest  
710 positive bias and RMSE, while the STEM/GEOS-Chem and STEM/RAQMS predictions were  
711 positively and negatively biased by less than 2 ppbv, respectively, with similar RMSEs and  
712 correlations with the observations. The quality of the three STEM simulation mean is closest to  
713 the STEM/GEOS-Chem run, with the mean bias/RMSE of ~1.6/4.9 ppbv, much better than the  
714 three-boundary model ensemble (-5.7/10.4 ppbv). However, this good performance can be a net  
715 effect of incorrect partitioning between the trans-boundary and local source contributions, with the  
716 former being underestimated and offsetting the overestimation of the latter. Switching the STEM  
717 chemical boundary conditions to the assimilated RAQMS base simulation led to increases in the  
718 simulated surface O<sub>3</sub> concentrations by >9 ppbv in the western US (Figure S2, right), associated  
719 with higher positive biases (due to several factors discussed in the next paragraph). Regional-scale  
720 assimilation could further reduce uncertainties introduced from regional meteorological and  
721 emission inputs to obtain better modeled total O<sub>3</sub> and the partitioning of trans-boundary versus US  
722 contributions (e.g., Huang et al., 2015).

723  
724 The three STEM base simulations all significantly overpredicted O<sub>3</sub> over the rest of the US  
725 in part due to the overall overestimated NO<sub>x</sub> emissions, with the STEM/RAQMS associated with  
726 the lowest RMSEs and mean biases, but STEM/C-IFS correlated best with the observations (Table  
727 3b). These positive biases are higher than the global model ensembles', which can partially result  
728 from the possible unrealistic VOC speciation of the emission inventory and the SAPRC 99  
729 chemical mechanism: Although SAPRC mechanisms have been used in air quality modeling for  
730 regulatory applications in some US states such as California, they usually produced higher O<sub>3</sub> than  
731 other mechanisms such as the CB04 and the CB05 (which were used by some HTAP2 global  
732 models, see Table 1c) over the US, and the comparisons between SAPRC 99 and SAPRC 2007  
733 are still in progress (e.g., Luecken et al., 2008; Zhang et al., 2012; Cai et al., 2011). It is important  
734 to timely update the chemical mechanisms in the chemistry models, and we also suggest to timely  
735 upgrade the VOC speciation in the bottom-up emission inventories in the US to benefit the air

Deleted: averaged and

Deleted: The evaluation statistics is summarized in Table 3. The time series of observed and modeled O<sub>3</sub> at the western US CASTNET sites are shown in Figure 2a where the model overall simulated the surface O<sub>3</sub> fairly well, with a much smaller mean bias (~1.6 ppbv) than the global model ensembles.

Deleted: S1

Deleted: model

Deleted: mainly

Deleted: .

Deleted: CB05

748 quality modeling. Additionally, the uncertainty from non-anthropogenic emissions, such as the  
749 biogenic VOC emissions from WRF/MEGAN which is known to often have positive biases, can  
750 be another cause: As Hogrefe et al. (2011) presented, the MEGAN emissions resulted in a higher  
751 O<sub>3</sub> response to hypothetical anthropogenic NO<sub>x</sub> emission reductions compared with another set of  
752 biogenic emission input. [Huang et al. \(2017\)](#) showed that MEGAN's positive biases are in part  
753 due to the positively-biased temperature and radiation in WRF, and reducing ~2°C in WRF's  
754 temperature biases using a different land initialization approach led to ~20% decreases in  
755 MEGAN's isoprene emission estimates in September 2013 over some southeastern US regions.  
756 These temperature and radiation biases, can also be important sources of uncertainty in the  
757 modeled O<sub>3</sub> production. Quantifying the impacts of overestimated biogenic emissions and the  
758 biased weather fields that contributed to the biases in emissions on the modeled O<sub>3</sub> is still an  
759 ongoing work. Some existing studies also reported O<sub>3</sub> and NO<sub>2</sub> biases from other regional models  
760 in the eastern US, due to the chemical mechanism and biases in NO<sub>x</sub> and biogenic VOC emissions  
761 (e.g., [Canty et al., 2015](#)). We anticipate that the results from the Air Quality Model Evaluation  
762 International Initiative (AQMEII) experiment (e.g., [Schere et al., 2012](#); [Solazzo et al., 2012](#);  
763 [Galmarini et al., 2015, 2017](#)), which involves more regional model simulations over the US with  
764 the similar set of boundary conditions but different chemical mechanisms and non-anthropogenic  
765 emission inputs, can help better understand the causes of errors in the simulated total O<sub>3</sub>.

Deleted: Some factors that caused the overpredicted MEGAN emissions, such as positively-biased temperature in WRF, can also be important sources of uncertainty in the STEM modeled O<sub>3</sub>.

Deleted: 6

Deleted: other

Formatted: Indent: First line: 0.5"

### 767 3.2. The NAM surface O<sub>3</sub> sensitivity to extra-regional anthropogenic pollutants

#### 768 3.2.1. Global model ensembles

769  
770 The impact of all foreign (i.e. non-NAM) anthropogenic sources on NAM surface O<sub>3</sub> was  
771 first explored, including the spatial distributions of the RERER metric (eq. (2)) based on various  
772 global models' simulations (Figure 5), and the domain wide mean sensitivities R(O<sub>3</sub>, non-NAM,  
773 20%) (eq. (1d)) (Figure 6). Across the NAM, the strongest impacts were found in spring time  
774 (March-April-May, larger than 1.5 ppbv in average over the domain) and the weakest impacts are  
775 shown during the summertime (June-July-August, 1.0-1.3 ppbv), consistent with the existing  
776 knowledge on the seasonal variability of the non-local pollution impacts on NAM for other years  
777 (e.g., [Fiore et al., 2009](#); [Reidmiller et al., 2009](#)). All global models indicate strong non-NAM  
778 anthropogenic source impacts on the western US mainly due to the impact of its high elevation,  
779 and also near the US-Mexico border areas, especially southern Texas, due to their vicinity to the  
780 Mexican emission sources. Over the western states, stronger non-local impacts were reflected from  
781 the results based on higher-horizontal resolution global models (e.g., the >0.6 RERER values from  
782 the half degree EMEP model, corresponding to its higher R(O<sub>3</sub>, non-NAM, 20%) values than the  
783 other models'), similar to the findings in previous modeling studies ([Lin et al., 2010, 2012a](#)).  
784 [Although on a coarse horizontal resolution of 2.8°, OsloCTM3 suggests stronger extra-regional](#)  
785 [source influences on the northwestern US and the US-Canada border regions than the other models.](#)  
786 [Its largest number of vertical layers among all global models might be a cause.](#) Larger-than-1  
787 RERER values are often seen near the urban areas and large point sources due to the titration,  
788 especially evident from the higher resolution model results. The R(O<sub>3</sub>, EAS, 20%) values are larger  
789 than 1/3 of the R(O<sub>3</sub>, non-NAM, 20%) (0.2-0.5 ppbv from April to June), more than 3-4 times  
790 higher than R(O<sub>3</sub>, EUR, 20%) and R(O<sub>3</sub>, SAS, 20%). Note that all eight models contributed to the  
791 R(O<sub>3</sub>, EAS, 20%) calculations, but one or two models did not provide all necessary sensitivity runs  
792 to compute the RERER, R(O<sub>3</sub>, non-NAM, 20%), R(O<sub>3</sub>, EUR, 20%), or R(O<sub>3</sub>, SAS, 20%).  
793

Deleted: 4

Deleted: 5

Deleted: ; Brown-Steiner and Hess, 2011).

803 Comparing to the HTAP1 modeling results, the magnitudes of  $R(O_3, EUR, 20\%)$  from this  
 804 study are smaller by a factor of 2-3. In contrast, the  $R(O_3, non-NAM, 20\%)$  and  $R(O_3, EAS, 20\%)$   
 805 values are >50% higher than the HTAP1 modeling results. The different HTAP1 and HTAP2  
 806 results are possibly due to the following three reasons: 1) the substantial improvement in the  
 807 European air quality over the past decades that is shown in Crippa et al. (2016) and Pouliot et al.  
 808 (2015), which contrasts with the growing anthropogenic emissions from the East Asia and other  
 809 developing countries during 2001-2010; 2) the changes in the HTAP2 experiment setup from  
 810 HTAP1. This includes the differences in the participating models, and the different region  
 811 definitions, e.g., EUR by HTAP1's definition includes regions in Russia/Belarus/Ukraine,  
 812 Middle East and North Africa that are excluded from the HTAP2's EUR domain. For EAS and  
 813 SAS, however, the regions not overlapped by HTAP1 and HTAP2 are mostly in the less  
 814 populated/polluted regions; 3) the stronger-than-normal transport in 2010 than in 2000-2001, as  
 815 first introduced in Section 2.2.1. Interannual variability of  $R(O_3, EAS, 20\%)$  and  $R(O_3, non-NAM,$   
 816  $20\%)$  is also found between 2010 and 2008-2009, based on the SNU GEOS-Chem calculations  
 817 (Figure S3). Foreign anthropogenic pollution impact on NAM was stronger in 2010 than in 2008-  
 818 2009, especially in April-May. This can be in part due to the higher  $O_3$  precursors' emissions in  
 819 2010 from extra-regions including the East Asia (Table S1), as well as the spring 2010  
 820 meteorological conditions that favored the trans-Pacific pollution transport.

821  
 822 These monthly- and regional-mean  $R(O_3, EAS, 20\%)$  values suggest that despite dilution  
 823 along the great transport distance, the EAS anthropogenic sources still had distinguishable impact  
 824 on the NAM surface  $O_3$ . Similar to the findings from the HTAP1 studies, the large intermodel  
 825 variability (as indicated in Table 4) in the estimates of intercontinental SR relationships indicates  
 826 the uncertainties of these models in representing the key atmospheric processes which needs more  
 827 investigations in the future. Figure 6b compares the  $R(O_3, EAS, 20\%)$  estimated by individual  
 828 boundary condition models, their ensemble mean sensitivities, and the eight-global model mean.  
 829 The averaged  $R(O_3, EAS, 20\%)$  from the boundary condition model results are smaller than the  
 830 eight-global model mean, and except for July-October 2010, GEOS-Chem gives higher  $R(O_3, EAS,$   
 831  $20\%)$  than RAQMS and C-IFS, consistent with its highest  $O_3$  prediction in the EAS source region  
 832 (Figure 3b). Overall,  $R(O_3, EAS, 20\%)$  and its intermodel differences are much smaller than the  
 833 biases of the modeled total  $O_3$  in NAM. Other factors can contribute more significantly to the  
 834 biases in the modeled total  $O_3$ , such as the stratospheric  $O_3$  intrusion and the local  $O_3$  formation,  
 835 and assessing the impacts from these factors would be also helpful for understanding the  
 836 uncertainties in the modeled  $O_3$ .

837  
 838 The  $O_3$  sensitivities in response to the perturbations of individual species or sector  
 839 emissions in East Asia, estimated by the GEOS-Chem adjoint model, were also analyzed (Figure  
 840 S3). These sensitivities show similar seasonal variability to  $R(O_3, EAS, 20\%)$ , with the values  
 841 ~twice as high in the spring than in summer, also consistent with the results on previous years  
 842 based on the 20% emission perturbation approach (e.g., Fiore et al., 2009; Brown-Steiner and Hess,  
 843 2011; Emmons et al., 2012). However, this seasonal variability is weaker than the results based on  
 844 the tagged tracer approach for earlier years: Using the CAM-Chem model, Brown-Steiner and  
 845 Hess (2011) reported that during the springtime, Asian  $O_3$  created from the anthropogenic/biofuel  
 846  $NO_x$  emissions affected NAM  $O_3$  ~three times as strongly as in summer. This is because the  
 847 nonlinear  $O_3$  chemistry, which is stronger outside of summer, caused larger  $O_3$  responses to a 100%  
 848 reduction of  $NO_x$  emissions than 5 times of the  $O_3$  responses to a 20% reduction of  $NO_x$  emissions.

- Deleted: are smaller by a factor of 2-3, as a result of the substantial improvement in the European air quality over the past decades (Crippa et al., 2016; Pouliot et al., 2015), (... [9])
- Deleted: The  $R(O_3, EAS, 20\%)$  based on the emissio (... [10])
- Deleted: . The SNU GEOS-Chem-based  $R(O_3, EAS,$  (... [11])
- Deleted: ). Such interannual variability can also be due to
- Deleted: S
- Deleted: , as introduced in Section 2.2.1
- Formatted: Font color: Text 1
- Deleted: 5b
- Formatted: Font color: Text 1
- Deleted:
- Formatted: Font color: Text 1
- Formatted: Font color: Text 1
- Deleted:
- Formatted: Font color: Text 1
- Deleted: except for July-October 2010. The
- Formatted: Font color: Text 1
- Deleted:
- Formatted: Font color: Text 1
- Deleted: the
- Formatted: Font color: Text 1
- Deleted: overall
- Formatted: Font color: Text 1
- Formatted: Font color: Text 1
- Deleted: (<<5%) and their biases
- Formatted: Font color: Text 1
- Deleted: , as the impact of the EAS anthropogenic so (... [12])
- Formatted: Font color: Text 1
- Formatted: Font color: Text 1
- Deleted: s
- Formatted: Font color: Text 1
- Deleted: controlling
- Formatted: Font color: Text 1
- Deleted: local and regional emissions
- Formatted: Font color: Text 1
- Deleted: still
- Formatted: Font color: Text 1
- Deleted: more effective
- Formatted: Font color: Text 1
- Deleted: complying with
- Formatted: Font color: Text 1
- Deleted: tighter air quality standard
- Formatted: Font color: Text 1
- Deleted: S2).

897 The EAS anthropogenic NO<sub>x</sub> emissions more strongly impacted the NAM surface O<sub>3</sub> than the  
898 other major O<sub>3</sub> precursors, similar to the findings in Fiore et al. (2009) and Reidmiller et al. (2009)  
899 using the perturbation approach, as well as the conclusions in Lapina et al. (2014) based on the  
900 adjoint sensitivity analyses. Emissions from the power&industrial sectors are higher in East Asia  
901 than the other sectors (Table S1), resulting in its stronger influences on the NAM surface O<sub>3</sub>. As  
902 the observed NO<sub>2</sub> columns started to drop since 2010 due to the effective denitration devices  
903 implemented at the Chinese power and industrial plants (e.g., Liu et al., 2016), depending on the  
904 changes in the VOC emissions, it is anticipated to see different R(O<sub>3</sub>, EAS, 20%) values for the  
905 years after 2010. Therefore, continued studies to assess the East Asian anthropogenic pollution  
906 impacts on NAM during more recent years is needed. As emissions from various source sectors  
907 can differ by their emitted altitudes and temporal (from diurnal to seasonal) profiles, efforts should  
908 also be placed to have the models timely update the heights and temporal profiles of the emissions  
909 from those various sectors.

Deleted:

Deleted: .

Deleted: E

### 911 3.2.2. Regional model sensitivities and their connections with the boundary condition models'

912  
913 The monthly-mean STEM surface R(O<sub>3</sub>, EAS, 20%) sensitivities based on different  
914 boundary condition models were inter-compared, and also compared with the R(O<sub>3</sub>, EAS, 20%)  
915 estimated by their boundary condition models as well as the global model ensemble mean (Figure  
916 7). For both May and June 2010, the domain-wide mean R(O<sub>3</sub>, EAS, 20%) values from  
917 STEM/RAQMS were higher than the estimates from RAQMS by 0.03 ppbv; the STEM/GEOS-  
918 Chem R(O<sub>3</sub>, EAS, 20%) values are lower than those of GEOS-Chem by 0.01-0.06 ppbv, and the  
919 STEM/C-IFS R(O<sub>3</sub>, EAS, 20%) is 0.02 ppbv higher than C-IFS's in June but slightly (<<0.01 ppbv)  
920 lower in May. These differences are overall smaller than the inter-global model differences, and  
921 can be due to various factors including the uncertainties in boundary condition chemical species  
922 mapping, and the different meteorological/terrain fields/chemistry in the global and regional model  
923 pairs. The STEM R(O<sub>3</sub>, EAS, 20%) ensemble mean values, however, are less than 0.02 ppbv  
924 different from its boundary condition model's ensemble mean for both months. The STEM R(O<sub>3</sub>,  
925 EAS, 20%) ensemble mean value in June is also close to the eight-global model ensemble mean,  
926 but is ~0.05 ppbv lower than the eight-model mean in May. Choosing other/more global model  
927 outputs as STEM's boundary conditions may lead to different STEM ensemble mean R(O<sub>3</sub>, EAS,  
928 20%) estimates. We also found that the period mean R(O<sub>3</sub>, EAS, 20%) of ~0.2 ppbv sampled only  
929 at the CASTNET sites (Table 3a) are smaller than those averaged in all model grids. This indicates  
930 that currently the sparsely distributed surface network (especially over the western US that is more  
931 strongly affected by the extra-regional sources than the other US regions) may miss many LRT  
932 episodes that impact the NAM. The planned geostationary satellites with ~2-5 km footprint sizes  
933 and hourly sampling frequency (Hilsenrath and Chance, 2013) will help better capture the high O<sub>3</sub>  
934 and LRT episodes in these regions.

Deleted: 6

Deleted: CIFS

Deleted: models

Deleted: 3

936 The spatial patterns of the monthly-mean STEM surface R(O<sub>3</sub>, EAS, 20%) sensitivities  
937 based on the three boundary condition models are notably different, but overall resemble what's  
938 estimated by the corresponding boundary condition model, and the STEM sensitivities show more  
939 local details in certain high elevation regions in the US west (Figure 8 shows the June 2010  
940 conditions as an example). These different sensitivities were investigated further, by examining  
941 the R(O<sub>3</sub>, EAS, 20%) values near the source regions (i.e., East Asia) as well as near the receptor  
942 regions (Figure 9). More East Asian anthropogenic O<sub>3</sub> seems to be transported at the upper

Deleted: 7

Deleted: 8



952 troposphere in RAQMS than in the other two models. GEOS-Chem and RAQMS R(O<sub>3</sub>, EAS, 20%)  
953 sensitivities are similar over the EAS as well as the 500-900 hPa near the receptor in the eastern  
954 Pacific (at ~135°W), the altitudes US surface O<sub>3</sub> are most strongly sensitive to during the  
955 summertime as concluded from previous studies (e.g., Huang et al., 2010, 2013a; Parrish et al.,  
956 2010). Despite the close NAM domain-wide mean values from the STEM/GEOS-Chem and  
957 STEM/RAQMS, the spatial patterns of R(O<sub>3</sub>, EAS, 20%) over NAM differ in these two cases,  
958 with the latter case showing sharper gradients especially in the western US, partially due to the  
959 impact of its higher horizontal resolution. The R(O<sub>3</sub>, EAS, 20%) values from STEM/C-IFS are  
960 lower than from the other two cases both near the sources and at (near) NAM. The STEM surface  
961 (also near surface, not shown in figures) R(O<sub>3</sub>, EAS, 20%) does not spatially correlate well with  
962 the column R(O<sub>3</sub>, EAS, 20%), the latter of which contributed more to the base case O<sub>3</sub> columns,  
963 indicating that a good portion of the transported East Asian pollution did not descend to the lower  
964 altitudes to impact the boundary layer/ground level air quality. An additional regional simulation  
965 was performed in which the STEM boundary conditions were downscaled from a RAQMS  
966 simulation without the East Asian anthropogenic emissions. The non-linear emission perturbation-  
967 O<sub>3</sub> response relationships, as the larger-than-1 S<sub>O<sub>3</sub></sub> metric (eq. (3)) indicate, are seen across the  
968 domain, for both the surface and column O<sub>3</sub> (Figure 8). S<sub>O<sub>3</sub></sub> for column O<sub>3</sub>, ranging from 1.15-1.25  
969 in most regions, are overall ~0.05 higher than S<sub>O<sub>3</sub></sub> for the surface O<sub>3</sub>. Therefore, the full source  
970 contribution obtained by linearly scaling the receptor regional mean O<sub>3</sub> sensitivity to the 20%  
971 reduction in the source region emissions may be underestimated by at least ~10%.

Deleted: CIFS

Deleted: 7).

Deleted: .

Formatted: Indent: First line: 0"

Formatted: Underline

Deleted: 3

Deleted: Figure 2a

Deleted: S3

### 973 3.2.3. Regional model MDA8 sensitivities on all days and during the O<sub>3</sub> exceedances

974 The temporal variability of the STEM R(O<sub>3</sub>, EAS, 20%) ensemble sensitivities were also  
975 studied. For most US subregions, 3-6 LRT episodes (defined as when the sensitivities are above  
976 the period mean) were identified during May-June. Throughout this period, the hourly R(O<sub>3</sub>, EAS,  
977 20%) and the observed O<sub>3</sub> at the surface CASTNET sites are weakly correlated (Table 3a), but  
978 they display similar diurnal cycles (e.g., Figures 2c and 2d for the western US sites), possibly  
979 because the deeper boundary layer depth during the daytime enhanced entrainment down-mixing  
980 of the extra-regional pollutants to the surface. The identified diurnal variability of the R(O<sub>3</sub>, EAS,  
981 20%) can cause differences in the calculated MDA8 and all-hour mean R(O<sub>3</sub>, EAS, 20%) values.  
982 Figure S4 shows that the mean R(MDA8, EAS, 20%) values, usually at daytimes, are higher than  
983 the all-hour averaged R(O<sub>3</sub>, EAS, 20%) in most STEM model grids during both months. Therefore,  
984 it is important for more HTAP2 participating models to save their outputs hourly in order to  
985 conveniently compute the policy-relevant metrics for the O<sub>3</sub> sensitivities. Also, the hourly  
986 sampling frequency of the planned geostationary satellites is anticipated to be more helpful for  
987 evaluating the impacts of the LRT episodes.

Deleted: for May-June 2010 in

Deleted: 9

Deleted: Qualitatively consistent with the findings in Reidmiller et al. (2009), R(MDA8, EAS, 20%) is smaller during the high O<sub>3</sub> total days in all subregions. Note that the STEM base simulations overall substantially overpredicted the total O<sub>3</sub> in non-western US regions, so the R(MDA8, EAS, 20%) calculated during the days of O<sub>3</sub> exceedances can actually represent the sensitivities during the non-exceedances.

Formatted: Normal

988 The STEM R(MDA8, EAS, 20%) in all model grids within the four US subregions were  
989 averaged on all days during May-June 2010 and only on the days when the simulated total MDA8  
990 O<sub>3</sub> is over 70 ppbv (Figure 10). These sensitivities also show appreciable spatial variability: from  
991 0.35-0.58 ppbv in the western US (also with the largest standard deviations, not shown), which is  
992 slightly higher than the HTAP1 results reported by Reidmiller et al. (2009) for Spring 2001, to  
993 ~0.1-0.25 ppbv in the rest three subregions, which is close to the Reidmiller et al. (2009) results.

994 Comparing the solid bar plots in Figures 10-11, we found that on all days in the three non-  
995 western subregions, R(MDA8, EAS, 20%) values sampled at CASTNET sites are slightly smaller  
996  
997

1014 than those computed for all model grids, while in the non-western states the opposite differences  
1015 are seen. This again suggests that expanding observation network would help better capture the  
1016 high O<sub>3</sub> and LRT episodes.

1017  
1018 Figure 10 suggests smaller R(MDA8, EAS, 20%) values during the high O<sub>3</sub> days in all  
1019 subregions. However, STEM's total O<sub>3</sub> concentrations at CASTNET sites during the O<sub>3</sub>  
1020 exceedances were substantially overpredicted in non-western US regions while significantly  
1021 underpredicted in the western US (see mean biases above the bar plots in Figure 11). Therefore,  
1022 the R(MDA8, EAS, 20%) values shown in Figure 10 during O<sub>3</sub> exceedances can actually represent  
1023 the sensitivities during the non-exceedances in non-western US regions, and may not represent the  
1024 sensitivities during all O<sub>3</sub> exceedances in the western US. Figures 11-12 show that if calculated  
1025 only at the CASTNET sites during the exceedances, in non-western US regions, R(MDA8, EAS,  
1026 20%) is 0.02-0.07 ppbv smaller during the high O<sub>3</sub> total days. This is qualitatively consistent with  
1027 the findings in Reidmiller et al. (2009), and is possibly because that the LRT impacts were stronger  
1028 on some days with good dispersion conditions when the NAAQS was not exceeded, but weaker  
1029 on some high O<sub>3</sub> days under stagnant conditions. In contrast, western US R(MDA8, EAS, 20%) at  
1030 CASTNET sites was ~0.05 ppbv higher on high O<sub>3</sub> days than for all days, and this differences are  
1031 larger in rural/remote areas where local influences are less dominant. As a result, the  
1032 medium/strong positive correlations are found between modeled LRT of pollution and the total O<sub>3</sub>  
1033 in these regions (Table 3a; Lin et al., 2012a).

### 1034 3.3. Case studies of spring (9 May) and summer (10 June) LRT events mixed with stratospheric 1035 O<sub>3</sub> intrusions

1036  
1037 Lin et al. (2012a, b) and Neuman et al. (2012) showed that the trans-Pacific pollution  
1038 transport intensely impacted the western US during 8-10 May, 2010, intermingled with a  
1039 stratospheric intrusion that contributed to at least 1/3 of the total O<sub>3</sub> in some high elevation regions.  
1040 This episode is indeed indicated by the O<sub>3</sub> and CO products from AIRS and TES at ~500 hPa over  
1041 the Eastern Pacific (Figure 13), and the observed TES and IASI O<sub>3</sub> profiles over the western US  
1042 indicated elevated O<sub>3</sub> levels (>80 ppbv) at 700-900 hPa. Huang et al. (2013b) found that the  
1043 meteorological conditions during this period (i.e., a strong jet at ~700 hPa with wind speed >20  
1044 m/s shifted southwesterly when passing the southern California and continued to travel towards  
1045 the mountain states), along with the orographic lifting, efficiently exported the southern California  
1046 anthropogenic pollution, which was chemically coupled with the extra-regional pollution and  
1047 significantly enhanced the O<sub>3</sub> levels in the US intermountain west.  
1048

1049  
1050 We selected this episode to compare the STEM surface total O<sub>3</sub> concentrations as well as  
1051 the R(O<sub>3</sub>, EAS, 20%) sensitivities based on the different HTAP2 boundary condition models.  
1052 Figure 14 evaluates the simulated O<sub>3</sub> profiles in the western US from several STEM base  
1053 simulations against the TES and IASI O<sub>3</sub> retrievals, and Figures 15a-d indicate the performance of  
1054 the daily surface total MDA8 O<sub>3</sub> from these simulations. We found that the underestimated free  
1055 tropospheric O<sub>3</sub> from the STEM simulations that used any single free-running chemical boundary  
1056 conditions contributed to the underestimated STEM surface O<sub>3</sub> in the high elevation mountain  
1057 states; e.g., by 9-14 ppbv at three CASTNET sites (Grand Canyon National Park (NP), AZ;  
1058 Canyonlands NP, UT; and Rocky Mountain NP, CO) where O<sub>3</sub> exceedances were observed. The  
1059 unsatisfactory performance by free-running global models during high O<sub>3</sub> events would pose

- Deleted: y
- Deleted: the
- Deleted: 2010
- Formatted: Font:Not Italic, Underline
- Formatted: Normal, Indent: Left: 0"
- Deleted: .
- Deleted: E
- Deleted: 10

- Deleted: 11
- Deleted: 2

1068 difficulties for regional models (regardless of their resolutions and other configurations,  
1069 parameterization) to accurately estimate the SR relationships using boundary conditions  
1070 downscaled from these model runs. The STEM base simulation using the RAQMS assimilated  
1071 fields as the boundary conditions, agrees most with the observed O<sub>3</sub> at the CASTNET sites, as well  
1072 as the TES and IASI O<sub>3</sub> profiles in the western states. Similar to the conclusions drawn in Huang  
1073 et al. (2010, 2015) for summer 2008, we again demonstrated the robustness of satellite chemical  
1074 data assimilation for improving the boundary condition models' O<sub>3</sub> performance. As the  
1075 enhancement of O<sub>3</sub> due to the assimilation is much larger than the O<sub>3</sub> sensitivities to the EAS  
1076 anthropogenic emissions, the assimilation mainly improved the contributions from other sources,  
1077 such as the stratospheric O<sub>3</sub>.

1078  
1079 The quality of the model boundary conditions only indicates how well the total “transported  
1080 background” component is represented, and can not be directly connected with the accuracy of the  
1081 model estimated R(O<sub>3</sub>, EAS, 20%) sensitivities, which also show notable intermodel differences:  
1082 The estimated R(MDA8, EAS, 20%) in the different STEM cases range from <1.0 ppbv to ~1.3  
1083 ppbv, at least 40% higher than the May-June period mean in Figures 10-11. The mean R(MDA8,  
1084 EAS, 20%) at three high O<sub>3</sub> CASTNET sites range from 0.73 (STEM/GEOS-Chem) to 0.98 ppbv  
1085 (STEM/C-IFS), with the mean S<sub>O<sub>3</sub></sub> of ~1.14 at these sites based on the STEM/RAQMS runs due  
1086 to the nonlinear emission perturbation-O<sub>3</sub> response relationships (Figure 15e-h). The R(MDA8,  
1087 EAS, 100%) from the STEM/RAQMS case is as high as >7 ppbv over the high terrain regions.  
1088 These are of smaller magnitudes than the estimates in Lin et al. (2012a), possibly due to the  
1089 differences in the used models and the bottom-up emission inputs.

1090  
1091 A stratospheric O<sub>3</sub> intrusion also affected the NE US on the same day, as revealed by the  
1092 satellite free tropospheric O<sub>3</sub> and CO observations (Figure 13). This intrusion was mixed with LRT  
1093 East Asian pollution (Figure 15 and Figure S5). However, this intrusion did not enhance the NE  
1094 boundary layer/surface O<sub>3</sub> concentrations, which were actually anomalously low (MDA8<40 ppbv)  
1095 as indicated by the model base simulations and the CASTNET observations (Figure 15a-d).  
1096 Similar characteristics during summertime stratospheric O<sub>3</sub> intrusion events around this region  
1097 have been discussed by Ott et al. (2016). The East Asian pollution less intensely (<50%) affected  
1098 the surface O<sub>3</sub> levels in these regions than in the US west, due to the greater transport distances,  
1099 stronger local emission influence on chemical production/loss, as well as the impact of the overall  
1100 flat terrain in the US east.

1101  
1102 A summertime LRT event on 9-10 June is analyzed to contrast with the 9 May case study.  
1103 Lin et al. (2012b) showed that >80 ppbv of ozonesonde data in northern California at 2-6 km  
1104 measured the stratospheric O<sub>3</sub> remnants during this episode, and the transported stratospheric O<sub>3</sub>  
1105 contributed to as much as ~50% of the total O<sub>3</sub> in southern California based on their model  
1106 calculations. We show that on 10 June over 100 ppbv of O<sub>3</sub>, as well as <90 ppbv CO, was observed  
1107 by satellites at ~500 hPa above Nevada and northern California (Figure 16), which again was  
1108 substantially underestimated by all free-running models (Figure 17), resulting in the  
1109 underpredicted total O<sub>3</sub> at two CASTNET sites in southern California (Converse Station and  
1110 Joshua Tree NP) that experienced O<sub>3</sub> exceedances on this day (Figure 18a-c). The negative biases  
1111 in the “transported background” O<sub>3</sub> and surface MDA8 O<sub>3</sub> were successfully reduced by  
1112 incorporating satellite data (Figures 17 and 18d).

Deleted: .

Deleted: Figure 9. Strong

Deleted: are also shown during this period

Deleted: 12, lower

Deleted: 10

Deleted: 12

Deleted: S4

Deleted: 2

1122 Figures 18e-h show that LRT of EAS anthropogenic pollution also strongly affected  
 1123 southern California and Nevada. Notable intermodel differences are again found in the estimated  
 1124 R(MDA8, EAS, 20%), but they are overall lower than on 9 May (<1.0 ppbv). The mean R(MDA8,  
 1125 EAS, 20%) at the two high O<sub>3</sub> CASTNET sites range from 0.54 (STEM/C-IFS) to 0.86 ppbv  
 1126 (STEM/RAQMS), with the mean S<sub>O<sub>3</sub></sub> of ~1.13 at these sites based on the STEM/RAQMS runs  
 1127 (Figure 18e-h). The R(MDA8, EAS, 100%) from the STEM/RAQMS case is as high as >6 ppbv  
 1128 over southern California and Nevada. Compared to the spring event, R(MDA8, EAS, 20%) in the  
 1129 eastern US are discernable only over a limited region, due to weaker transport and stronger local  
 1130 chemical production/loss.

1131 **4. Conclusions and suggestions on future directions**

1132 In support of the HTAP Phase 2 experiment that involved high-resolution global models  
 1133 and regional models' participation to advance the understanding of the pollutants' SR relationships  
 1134 in the Northern Hemisphere, we conducted a number of regional scale STEM base and forward  
 1135 sensitivity simulations over NAM<sub>4</sub> during May-June 2010. STEM's<sub>4</sub> top and lateral chemical  
 1136 boundary conditions were downscaled from three global models' (i.e., GEOS-Chem, RAQMS,  
 1137 and ECMWF C-IFS) base and sensitivity simulations (in which the East Asian anthropogenic  
 1138 emissions were reduced by 20%). Despite dilution along the great transport distance, the East  
 1139 Asian anthropogenic sources still had distinguishable impact on the NAM<sub>4</sub> surface O<sub>3</sub>, with the  
 1140 period-mean NAM O<sub>3</sub> sensitivities to a 20% reduction of the East Asian anthropogenic emissions  
 1141 (i.e., R(O<sub>3</sub>, EAS, 20%)) ranging from ~0.24 ppbv (STEM/C-IFS) to ~0.34 ppbv (STEM/RAQMS).  
 1142 The spatial patterns of the STEM surface O<sub>3</sub> sensitivities over NAM<sub>4</sub> overall resembled those from  
 1143 its corresponding boundary condition model, with regional/period mean R(O<sub>3</sub>, EAS, 20%) differed  
 1144 slightly (<10%) from its corresponding boundary condition model's, which are smaller than those  
 1145 among its boundary condition models. The boundary condition models' two-month mean R(O<sub>3</sub>,  
 1146 EAS, 20%) was ~8% lower than the mean sensitivity estimated by multiple global models.  
 1147 Therefore, choosing other global model outputs as STEM's boundary conditions may lead to  
 1148 different STEM O<sub>3</sub> sensitivities. The biases and RMSEs in the simulated total O<sub>3</sub>, which differed  
 1149 significantly among models, can partially be due to the uncertainty in the bottom-up NO<sub>x</sub> emission  
 1150 inputs according to the model comparison with the OMI NO<sub>2</sub> columns, and future work on  
 1151 attributing the intermodel differences on process level is particularly important for better  
 1152 understanding the sources of uncertainties in the modeled total O<sub>3</sub> and its source contribution.

1153 The HTAP2 multi-model ensemble mean R(O<sub>3</sub>, EAS, 20%) values in 2010 were higher  
 1154 than the HTAP1 reported 2001 conditions, due to the impacts of the growing East Asian  
 1155 anthropogenic emissions, the interannual variability in atmospheric circulation (i.e., stronger trans-  
 1156 Pacific transport in spring 2010 following an El Niño event), and the different experiment designs  
 1157 of HTAP1 and HTAP2. The GEOS-Chem O<sub>3</sub> sensitivities in 2010 were also higher than the 2008-  
 1158 2009 conditions due to the increasing Asian emissions and the spring 2010 meteorological  
 1159 conditions that favored the trans-Pacific pollution transport. The GEOS-Chem sensitivity  
 1160 calculations indicate that the East Asian anthropogenic NO<sub>x</sub> emissions mattered more than the  
 1161 other East Asian O<sub>3</sub> precursors to the NAM<sub>4</sub> O<sub>3</sub>, qualitatively consistent with previous adjoint  
 1162 sensitivity calculations. Continued research is needed on temporal changes of emissions for  
 1163 different species and sectors in NAM<sub>4</sub> and foreign countries as well as their impacts on the SR  
 1164 relationships. As emissions from various source sectors can differ by emitted altitudes and

<b>Formatted:</b> Indent: First line: 0"
<b>Deleted:</b> North America
<b>Deleted:</b> The STEM
<b>Deleted:</b> CIFS
<b>Deleted:</b> The STEM
<b>Formatted:</b> Font color: Text 1
<b>Deleted:</b> (including the 24h mean and the policy-relevant MDA8 metric averaged throughout the study period and during a selected transport event) over North America
<b>Deleted:</b> the
<b>Deleted:</b> but can be quantitatively different from the mean sensitivities
<b>Deleted:</b> all
<b>Deleted:</b> model ensembles
<b>Deleted:</b> more
<b>Deleted:</b> ensemble mean
<b>Formatted:</b> Not Superscript/ Subscript
<b>Deleted:</b> Overall, the monthly-based US O <sub>3</sub> sensitivities to the 20% reduction of the East Asian anthropogenic emissions contributed to <<5% of the total O <sub>3</sub> and are of smaller magnitudes than the
<b>Deleted:</b> in the modeled total O <sub>3</sub> . Better quantifying the contributions from other factors, such as the stratospheric O <sub>3</sub> intrusion and the local O <sub>3</sub> formation, would still be the most effective way to help reduce the North American pollution levels and the model uncertainties. The US O <sub>3</sub> sensitivities to the East Asian anthropogenic emissions were episodically strong, contributing to the O <sub>3</sub> exceedances in some high terrain areas. Assessing the sources of
<b>Deleted:</b> are
<b>Deleted:</b> evaluating the East Asian pollution impacts during these episodes. The STEM O <sub>3</sub> sensitivities followed similar diurnal cycles as the total O <sub>3</sub> , emphasizing the importance of saving model results hourly for continentally calculate policy-relevant metrics, as well as the usefulness of hourly sampling frequency of the planned geostationary satellites for better evaluating the impacts of the LRT events.
<b>Deleted:</b> sensitivities
<b>Deleted:</b> as well as 1/5 of the original estimates for 2001-2005 using the tagged tracers. This indicates the increasing
<b>Deleted:</b> pollution on North America.
<b>Deleted:</b> S
<b>Deleted:</b> North American
<b>Deleted:</b> North America

1209 temporal profiles, efforts should also be placed to have the models timely update the height and  
1210 temporal profiles of the emissions from various sectors.

Deleted: .  
Deleted: E

1211  
1212 An additional STEM simulation was performed in which the boundary conditions were  
1213 downscaled from a RAQMS simulation without East Asian anthropogenic emissions (i.e., a 100%  
1214 emission reduction), to assess the scalability of the mean O<sub>3</sub> sensitivities to the size of the emission  
1215 perturbation. The scalability was found to be spatially varying, ranging from 1.15-1.25 for column  
1216 O<sub>3</sub> in most US regions, which were overall ~0.05 higher than the surface O<sub>3</sub>'s. Therefore, the full  
1217 source contribution obtained by linearly scaling the NAM regional mean O<sub>3</sub> sensitivity to the 20%  
1218 reduction in the East Asian emissions may be underestimated by at least 10%. The underestimation  
1219 in other seasons of the HTAP2 study period may be higher and will need to be quantified in future  
1220 work. Also, motivated by Lapina et al. (2014), additional calculations will be conducted in future  
1221 to explore the scalability of different O<sub>3</sub> metrics in these cases. For future source attribution  
1222 analysis, in general it is recommended to directly choose the suitable size of the emission  
1223 perturbation based on the specific questions to address, and to avoid linearly scaling O<sub>3</sub>  
1224 sensitivities that are based on other amounts of the perturbations.

Deleted: and

Deleted: . Motivated

1225  
1226 The STEM O<sub>3</sub> sensitivities to the East Asian anthropogenic emissions (based on three  
1227 boundary condition models separately and averagely) were strong during 3-6 episodes in May-  
1228 June 2010, following similar diurnal cycles as the total O<sub>3</sub>. Stronger-than-normal East Asian  
1229 anthropogenic pollution impacts were estimated during O<sub>3</sub> exceedances in the western US,  
1230 especially over the high terrain rural/remote areas; in contrast, non-local pollution impacts were  
1231 less strong during O<sub>3</sub> exceedances in other US regions. We emphasized the importance of saving  
1232 model results hourly for continentally calculate policy-relevant metrics, as well as the usefulness of  
1233 hourly sampling frequency of the planned geostationary satellites for better evaluating the impacts  
1234 of the LRT events.

1235  
1236 Based on model calculations, satellite O<sub>3</sub> (TES, JPL-IASI, and AIRS), CO (TES and AIRS)  
1237 and surface O<sub>3</sub> observations on 9 May 2010, we showed the different influences from stratospheric  
1238 O<sub>3</sub> intrusions along with the transported East Asian pollution on O<sub>3</sub> in the western and the eastern  
1239 US. This event was further compared with a summer event of 10 June 2010. During both events,  
1240 the unsatisfactory performance of free-running global models would pose difficulties for regional  
1241 models (regardless of their resolutions and other configurations, parameterization) to accurately  
1242 simulate the surface O<sub>3</sub> and its source contribution using boundary conditions downscaled from  
1243 these model runs. Incorporating satellite (OMI and MLS) O<sub>3</sub> data effectively improved the  
1244 modeled O<sub>3</sub>. As chemical data assimilation techniques keep developing (Bocquet et al., 2015),  
1245 several HTAP2 participating global models have already been able to assimilate single- or multi-  
1246 constitute satellite atmospheric composition data (e.g., Miyazaki et al., 2012; Parrington et al.,  
1247 2008, 2009; Huang et al., 2015; Inness et al., 2015; Flemming et al., 2017). Comparing the  
1248 performance of the assimilated fields from different models, and making the global model  
1249 assimilated chemical fields in the suitable format for being used as boundary conditions would be  
1250 very beneficial for future regional modeling, as well as for better interpreting the pollutants'  
1251 distributions especially during the exceptional events. Meanwhile, efforts should also be devoted  
1252 to advancing and applying higher-resolution regional scale modeling and chemical data  
1253 assimilation. Furthermore, although satellite observations have been applied for improving the  
1254 estimated US background O<sub>3</sub> (e.g., Huang et al., 2015), using satellite (and/or other types of)

Deleted: Satellite NO<sub>2</sub> (KNMI OMI) and O<sub>3</sub> (TES, JPL-IASI, OMI, MLS, and AIRS) products helped detect pollution episodes, quantify or/and reduce the uncertainties in the bottom-up NO<sub>x</sub> emissions and the model transported background O<sub>3</sub>. Based on model calculations and satellite/surface observations on a selected day of

Deleted: Continued studies on exceptional events during other seasons are in progress.

Deleted: 6

1268 observations to improve SR relationship studies also needs to be explored. Some of the possible  
1269 methods include: 1) The combination of data assimilation and the tagging approach; 2) Introducing  
1270 observation-constrained emission estimates in the emission perturbation analyses.

## 1271 **Acknowledgements**

1272 The global and regional modeling results used in this study have been submitted to the  
1273 AeroCom database following the HTAP2 data submission guidelines (<http://iek8wikis.iek.fz->  
1274 [juelich.de/HTAPWiki/HTAP-2-data-submission](http://iek8wikis.iek.fz-juelich.de/HTAPWiki/HTAP-2-data-submission)), or can be made available upon request.  
1275 Technical support from Anna Carlin Benedictow, Brigitte Koffi, Jan Griesfeller, and Michael  
1276 Schulz regarding formatting and submitting the data to the AeroCom is acknowledged. MH thanks  
1277 the research resources at the University of Iowa and JPL/Caltech that supported this study, as well  
1278 as the travel funding from the US EPA for attending the related HTAP2 workshops. DKH and YD  
1279 recognize support from NASA AQAST. [FD Acknowledges support from the Administrative](#)  
1280 [Arrangement](#). Part of this research was carried out at the Jet Propulsion Laboratory, California  
1281 Institute of Technology, under contract to the National Aeronautics and Space Administration.  
1282 Reference herein to any specific commercial product, process or service by trade name, trademark,  
1283 manufacturer or otherwise does not constitute or imply its endorsement by the United States  
1284 Government or the Jet Propulsion Laboratory, California Institute of Technology. The views,  
1285 opinions, and findings contained in this report are those of the author(s) and should not be  
1286 construed as an official National Oceanic and Atmospheric Administration or U.S. Government  
1287 position, policy, or decision. [We also acknowledge the feedbacks from Dr. Gail Tonnesen, two](#)  
1288 [anonymous reviewers, and Dr. Meiyun Lin on earlier versions of this paper, that helped improve](#)  
1289 [its quality](#).

## 1292 **References**

- 1293 Anderson, D. C., Loughner, C. P., Diskin, G., Weinheimer, A., Canty, T., P., Salawitch, R. J.,  
1294 Worden, H. M., Fried, A., 25 Mikoviny, T., Wisthaler, A., and Dickerson, R., R. (2014),  
1295 Measured and modeled CO and NO<sub>v</sub> in DISCOVER-AQ: An evaluation of emissions and  
1296 chemistry over the eastern US, *Atmos. Environ.*, 96, 78-87, doi:  
1297 10.1016/j.atmosenv.2014.07.004.
- 1300 Allen, D. J., Pickering, K. E., Pinder, R. W., Henderson, B. H., Appel, K. W., and Prados, A.  
1301 (2012), Impact of lightning-NO on eastern United States photochemistry during the summer  
1302 of 2006 as determined using the CMAQ model, *Atmos. Chem. Phys.*, 12, 1737-1758, doi:  
1303 10.5194/acp-12-1737-2012.
- 1304 Ambrose, J.L., Reidmiller, D.R., and Jaffe, D.A. (2011), Causes of high O<sub>3</sub> in the lower free  
1305 troposphere over the Pacific Northwest as observed at the Mt. Bachelor Observatory. *Atmos.*  
1306 *Environ.*, 45, 5302–5315, doi: 10.1016/j.atmosenv.2011.06.056.
- 1307 Anenberg, S. C., L. W. Horowitz, D. Q. Tong, and J. J. West (2010), An estimate of the global  
1308 burden of anthropogenic ozone and fine particulate matter on premature human mortality using  
1309 atmospheric modeling, *Environ. Health Perspect.*, 118(9), 1189–1195.
- 1310 Avnery, S, D.L. Mauzerall, J. Liu, L.W. Horowitz (2011a), Global Crop Yield Reductions due to  
1311 Surface Ozone Exposure: 1. Year 2000 Crop Production Losses and Economic  
1312 Damage, *Atmos. Environ.*, 45, 2284-2296.

Formatted: None, Indent: First line: 0.5", Don't suppress line numbers

Deleted: .

... [13]

1315 Avnery, S, D.L. Mauzerall, J. Liu, L.W. Horowitz (2011b), Global Crop Yield Reductions due to  
1316 Surface Ozone Exposure: 2. Year 2030 Potential Crop Production Losses and Economic  
1317 Damage under Two Scenarios of O<sub>3</sub> Pollution, *Atmos. Environ.*, 45, 2297-2309.

1318 Beer, R., T. A. Glavich, and D. M. Rider (2001), Tropospheric emission spectrometer for the Earth  
1319 Observing System's Aura satellite, *Applied Optics*, 40, 2356 – 2367.

1320 Beer, R (2006), TES on the Aura Mission: Scientific Objectives, Measurements, and Analysis  
1321 Overview, *IEEE Transaction on Geoscience and Remote Sensing*, 44, 1102-1105.

1322 Bian, J., A. Gettelman, H. Chen, and L. L. Pan (2007), Validation of satellite ozone profile  
1323 retrievals using Beijing ozonesonde data, *J. Geophys. Res.*, 112, D06305,  
1324 doi:10.1029/2006JD007502.

1325 Bocquet, M., Elbern, H., Eskes, H., Hirtl, M., Žabkar, R., Carmichael, G. R., Flemming, J., Inness,  
1326 A., Pagowski, M., Pérez Camaño, J. L., Saide, P. E., San Jose, R., Sofiev, M., Vira, J.,  
1327 Baklanov, A., Carnevale, C., Grell, G., and Seigneur, C. (2015), Data assimilation in  
1328 atmospheric chemistry models: current status and future prospects for coupled chemistry  
1329 meteorology models, *Atmos. Chem. Phys.*, 15, 5325-5358, doi:10.5194/acp-15-5325-2015.

1330 Boersma, K. F., Braak, R., van der A, R. J. (2011a), Dutch OMI NO<sub>2</sub> (DOMINO) data product  
1331 v2.0 HE5 data file user manual. [http://www.temis.nl/docs/OMI\\_NO2\\_HE5\\_2.0\\_2011.pdf](http://www.temis.nl/docs/OMI_NO2_HE5_2.0_2011.pdf).

1332 Boersma, K. F., Eskes, H. J., Dirksen, R. J., van der A, R. J., Veeffkind, J. P., Stammes, P., Huijnen,  
1333 V., Kleipool, Q. L., Sneep, M., Claas, J., Leitão, J., Richter, A., Zhou, Y., Brunner, D. (2011b),  
1334 An improved tropospheric NO<sub>2</sub> column retrieval algorithm for the Ozone Monitoring  
1335 Instrument, *Atmos. Meas. Tech.*, 4, 1905-1928.

1336 Bowman, K. W., Rodgers, C. D., Kulawik, S. S., Worden, J., Sarkissian, E., Osterman, G., Steck,  
1337 T., Lou, M., Eldering, A., Shephard, M., Worden, H., Lampel, M., Clough, S., Brown, P.,  
1338 Rinsland, C., Gunson, M., and Beer, R. (2006), Tropospheric Emission Spectrometer:  
1339 Retrieval method and error analysis, *IEEE Transaction on Geoscience and Remote Sensing*,  
1340 44 (5), 1297–1307, doi: 10.1109/TGRS.2006.871234.

1341 Bowman, K., and D. K. Henze (2012), Attribution of direct ozone radiative forcing to spatially  
1342 resolved emissions, *Geophys. Res. Lett.*, 39, L22704, doi:10.1029/2012GL053274.

1343 [Brioude, J., Angevine, W. M., Ahmadov, R., Kim, S.-W., Evan, S., McKeen, S. A., Hsie, E.-Y.,](#)  
1344 [Frost, G. J., Neuman, J. A., Pollack, I. B., Peischl, J., Ryerson, T. B., Holloway, J., Brown, S.](#)  
1345 [S., Nowak, J. B., Roberts, J. M., Wofsy, S. C., Santoni, G. W., Oda, T., and Trainer, M. \(2013\),](#)  
1346 [Top-down estimate of surface flux in the Los Angeles Basin using a mesoscale inverse](#)  
1347 [modeling technique: assessing anthropogenic emissions of CO, NO<sub>x</sub> and CO<sub>2</sub> and their](#)  
1348 [impacts, \*Atmos. Chem. Phys.\*, 13, 3661-3677, doi:10.5194/acp-13-3661-2013.](#)

1349 Brown-Steiner, B., and P. Hess (2011), Asian influence on surface ozone in the United States: A  
1350 comparison of chemistry, seasonality, and transport mechanisms, *J. Geophys. Res.*, 116,  
1351 D17309, doi:10.1029/2011JD015846.

1352 Cai, C., J. T. Kelly, J. C. Avise, A. P. Kaduwela, and W. R. Stockwell (2011), Photochemical  
1353 Modeling in California with Two Chemical Mechanisms: Model Intercomparison and  
1354 Response to Emission Reductions, *J. Air & Waste Manage. Assoc.*, 61:5, 559-572, doi:  
1355 10.3155/1047-3289.61.5.559.

1356 [Canty, T. P., Hembeck, L., Vinciguerra, T. P., Anderson, D. C., Goldberg, D. L., Carpenter, S. F.,](#)  
1357 [Allen, D. J., Loughner, C. P., Salawitch, R. J., and Dickerson, R. R. \(2015\), Ozone and NO<sub>x</sub>](#)  
1358 [chemistry in the eastern US: evaluation of CMAQ/CB05 with satellite \(OMI\) data, \*Atmos.\*](#)  
1359 [Chem. Phys., 15, 10965-10982, doi:10.5194/acp-15-10965-2015.](#)

Moved (insertion) [8]

Moved (insertion) [9]

1360 Carmichael, G.R., Tang, Y., Kurata, G., Uno, I., Streets, D.G., Thongboonchoo, N., Woo, J.H.,  
1361 Guttikunda, S., White, A., Wang, T., Blake, D.R., Atlas, E., Fried, A., Potter, B., Avery, M.A.,  
1362 Sachse, G.W., Sandholm, S.T., Kondo, Y., Talbot, R.W., Bandy, A., Thornton, D., and Clarke,  
1363 A.D. (2003a), Evaluating regional emission estimates using the TRACE-P observations, *J.*  
1364 *Geophys. Res.*, 108 (D21), 8810, doi: 10.1029/2002JD003116.

1365 Carmichael, G.R., Tang, Y., Kurata, G., Uno, I., Streets, D., Woo, J.H., Huang, H., Yienger, J.,  
1366 Lefter, B., Shetter, R., Blake, D., Atlas, E., Fried, A., Apel, E., Eisele, F., Cantrell, C., Avery,  
1367 M., Barrick, J., Sachse, G., Brune, W., Sandholm, S., Kondo, Y., Singh, H., Talbot, R., Bandy,  
1368 A., Thornton, D., Clarke, A., and Heikes, B. (2003b), Regional-scale chemical transport  
1369 modeling in support of the analysis of observations obtained during the TRACE-P experiment,  
1370 *J. Geophys. Res.*, 108 (D21), 8823, doi: 10.1029/2002JD003117.

1371 Carter, W. P. L. (2000), Documentation of the SAPRC-99 chemical mechanism for VOC  
1372 Reactivity Assessment, final report to California Air Resources Board, Contract No. 92-329  
1373 and 95-308.

1374 Cooper, O. R., et al. (2010), Increasing springtime ozone mixing ratios in the free troposphere over  
1375 western North America, *Nature*, 463, doi: 10.1038/nature08708.

1376 Cooper, O. R., Oltmans, S. J., Johnson, B. J., Brioude, J., Angevine, W., Trainer, M., Parrish, D.  
1377 D., Ryerson, T. R., Pollack, I., Cullis, P. D., Ives, M. A., Tarasick, D. W., Al-Saadi, J., and  
1378 Stajner, I. (2011), Measurement of western U.S. baseline ozone from the surface to the  
1379 tropopause and assessment of downwind impact regions, *J. Geophys. Res.*, 116, D00V03, doi:  
1380 10.1029/2011JD016095.

1381 Cooper, O., et al. (2016), Western NA Performance Evaluation for HTAP2, HTAP2 workshop,  
1382 Potsdam, Germany, 2016.

1383 Crippa, M., Janssens-Maenhout, G., Dentener, F., Guizzardi, D., Sindelarova, K., Muntean, M.,  
1384 Van Dingenen, R., and Granier, C. (2016), Forty years of improvements in European air  
1385 quality: regional policy-industry interactions with global impacts, *Atmos. Chem. Phys.*, 16,  
1386 3825-3841, doi:10.5194/acp-16-3825-2016.

1387 Emmons, L. K., Hess, P. G., Lamarque, J.-F., and Pfister, G. G. (2012), Tagged ozone mechanism  
1388 for MOZART-4, CAM-chem and other chemical transport models, *Geosci. Model Dev.*, 5,  
1389 1531-1542, doi:10.5194/gmd-5-1531-2012.

1390 Eskes, H. J. and Boersma, K. F. (2003), Averaging kernels for DOAS total-column satellite  
1391 retrievals, *Atmos. Chem. Phys.*, 3, 1285-1291.

1392 Fiore, A. M., et al. (2009), Multimodel estimates of intercontinental source receptor relationships  
1393 for ozone pollution, *J. Geophys. Res.*, 114, D04301, doi:10.1029/2008JD010816.

1394 Fiore, A. M., J. T. Oberman, M. Y. Lin, L. Zhang, O. E. Clifton, D. J. Jacob, V. Naik, L. W.  
1395 Horowitz, J. P. Pinto, and G. P. Milly (2014), Estimating North American background ozone  
1396 in U.S. surface air with two independent global models: Variability, uncertainties, and  
1397 recommendations, *Atmos. Environ.*, 96, 284-300, doi: 10.1016/j.atmosenv.2014.07.045.

1398 Flemming, J., Huijnen, V., Arteta, J., Bechtold, P., Beljaars, A., Blechschmidt, A.-M., Diamantakis,  
1399 M., Engelen, R. J., Gaudel, A., Inness, A., Jones, L., Josse, B., Katragkou, E., Marecal, V.,  
1400 Peuch, V.-H., Richter, A., Schultz, M. G., Stein, O., and Tsikerdekis, A. (2015), Tropospheric  
1401 chemistry in the Integrated Forecasting System of ECMWF, *Geosci. Model Dev.*, 8, 975-1003,  
1402 doi:10.5194/gmd-8-975-2015.

1403 Flemming, J., Benedetti, A., Inness, A., Engelen, R., Jones, L., Huijnen, V., Remy, S., Parrington,  
1404 M., Suttie, M., Bozzo, A., Peuch, V.-H., Akritidis, D., and Katragkou, E. (2017), The CAMS

<b>Moved (insertion) [10]</b>
<b>Formatted:</b> Default Paragraph Font, Font color: Black
<b>Moved (insertion) [11]</b>
<b>Formatted:</b> Default Paragraph Font, Font color: Black
<b>Deleted:</b> 6



1406 interim Reanalysis of Carbon Monoxide, Ozone and Aerosol for 2003–2015, *Atmos. Chem.*  
 1407 *Phys.*, **17**, 1945-1983, doi:10.5194/acp-17-1945-2017.

1408 Galmarini, S., C. Hogrefe, D. Brunner, P. Makar, A. Baklanov (2015), Preface to the AQMEII p2  
 1409 Special issue, *Atmos. Environ.*, **115**, 340-344.

1410 Galmarini, S., Koffi, B., Solazzo, E., Keating, T., Hogrefe, C., Schulz, M., Benedictow, A.,  
 1411 Griesfeller, J. J., Janssens-Maenhout, G., Carmichael, G., Fu, J., and Dentener, F. (2017),  
 1412 Technical note: Coordination and harmonization of the multi-scale, multi-model activities  
 1413 HTAP2, AQMEII3, and MICS-Asia3: simulations, emission inventories, boundary conditions,  
 1414 and model output formats, *Atmos. Chem. Phys.*, **17**, 1543-1555, doi:10.5194/acp-17-1543-  
 1415 2017.

1416 Geddes, J. A., Heald, C. L., Silva, S. J., and Martin, R. V. (2016), Land cover change impacts on  
 1417 atmospheric chemistry: simulating projected large-scale tree mortality in the United States,  
 1418 *Atmos. Chem. Phys.*, **16**, 2323-2340, doi:10.5194/acp-16-2323-2016.

1419 Gery, M. W., G. Z. Whitten, J. P. Killus, and M. C. Dodge (1989), A photochemical kinetics  
 1420 mechanism for urban and regional scale computer modeling, *J. Geophys. Res.*, **94**, 12,925 –  
 1421 12,956, doi:10.1029/JD094iD10p12925.

1422 Granier, C., Lamarque, J. F., Mieville, A., Muller, J. F., Olivier, J., Orlando, J., Peters, J., Petron,  
 1423 G., Tyndall, G., and Wallens, S. (2005), POET, a database of surface emissions of ozone  
 1424 precursors, <http://www.aero.jussieu.fr/projet/ACCENT/POET.php>.

1425 Gratz, L.E., Jaffe, D.A., and Hee, J.R. (2014), Causes of increasing ozone and decreasing carbon  
 1426 monoxide in springtime at the Mt. Bachelor Observatory from 2004 to 2013, *Atmos. Environ.*,  
 1427 **109**, 323–330, doi: 10.1016/j.atmosenv.2014.05.076.

1428 Guenther, A. B., X. Jiang, C. L. Heald, T. Sakulyanontvittaya, T. Duhl, L. K. Emmons, and X.  
 1429 Wang (2012), The Model of Emissions of Gases and Aerosols from Nature version 2.1  
 1430 (MEGAN2.1): an extended and updated framework for modeling biogenic emissions, *Geosci.*  
 1431 *Model Dev.*, **5** (6), 1471-1492.

1432 Henze, D. K., Hakami, A., and Seinfeld, J. H. (2007), Development of the adjoint of GEOS-Chem,  
 1433 *Atmos. Chem. Phys.*, **7**, 2413–2433, doi:10.5194/acp-7-2413-2007.

1434 Hilsenrath, E., and K. Chance (2013), NASA ups the TEMPO on monitoring air pollution, *Earth*  
 1435 *Obs.*, **25**, 10–15.

1436 Hogrefe, C., Isukapalli, S., Tang, X., Georgopoulos, P., He, S., Zalewsky, E., Hao, W., Ku, J.,  
 1437 Key, T., and Sistla, G. (2011), Impact of biogenic emission uncertainties on the simulated  
 1438 response of ozone and fine Particulate Matter to anthropogenic emission reductions, *J. Air*  
 1439 *Waste Manage.*, **61**, 92–108.

1440 Huang, M., Carmichael, G. R., Adhikary, B., Spak, S. N., Kulkarni, S., Cheng, Y. F., Wei, C.,  
 1441 Tang, Y., Parrish, D. D., Oltmans, S. J., D'Allura, A., Kaduwela, A., Cai, C.,  
 1442 Weinheimer, A. J., Wong, M., Pierce, R. B., Al-Saadi, J. A., Streets, D. G., and Zhang, Q.  
 1443 (2010), Impacts of transported background ozone on California air quality during the  
 1444 ARCTAS-CARB period – a multi-scale modeling study, *Atmos. Chem. Phys.*, **10**, 6947-6968,  
 1445 doi: 10.5194/acp-10-6947-2010.

1446 Huang, M., Carmichael, G. R., Chai, T., Pierce, R. B., Oltmans, S. J., Jaffe, D. A.,  
 1447 Bowman, K. W., Kaduwela, A., Cai, C., Spak, S. N., Weinheimer, A. J., Huey, L. G., and  
 1448 Diskin, G. S. (2013a), Impacts of transported background pollutants on summertime western  
 1449 US air quality: model evaluation, sensitivity analysis and data assimilation, *Atmos. Chem.*  
 1450 *Phys.*, **13**, 359-391, doi: 10.5194/acp-13-359-2013.

Deleted: . Discuss.,  
 Deleted: 2016-666, in review

Deleted: 6  
 Deleted: Harmonization  
 Deleted: HTAP, AQMEII

Deleted: . Discuss.,  
 Deleted: 2016-828, in review.

Deleted: Grewe, V., Dahmann, K., Matthes, S., and  
 Steinbrecht, W. (2012), Attributing ozone to NOx  
 emissions: Implications for climate mitigation measures,  
 Atmos.

Moved down [12]: Environ.,

Formatted: Default Paragraph Font, Font:(Asian)+Theme  
 Body Asian (DengXian), (Asian) Chinese (PRC)

Deleted: 59, 102-107, doi:  
 10.1016/j.atmosenv.2012.05.002.

1465 Huang, M., Bowman, K. W., Carmichael, G. R., Pierce, R. B., Worden, H. M., Luo, M., Cooper,  
1466 O. R., Pollack, I. B., Ryerson, T. B., Brown, S. S. (2013b), Impact of southern California  
1467 anthropogenic emissions on ozone pollution in the mountain states, *J. Geophys. Res.*, 118,  
1468 12784-12803, doi: 10.1002/2013JD020205.

1469 Huang, M., et al. (2014), Changes in nitrogen oxides emissions in California during 2005–2010  
1470 indicated from top-down and bottom-up emission estimates, *J. Geophys. Res.*, 119, 12,928–  
1471 12,952, doi: 10.1002/2014JD022268, 2014.

1472 Huang, M., et al. (2015), Improved Western US Background Ozone Estimates via Constraining  
1473 Nonlocal and Local Source Contributions using Aura TES and OMI Observations, *J. Geophys.*  
1474 *Res.*, 120, 3572–3592, doi: 10.1002/2014JD022993.

1475 Huang, M., Carmichael, G. R., Crawford, J. H., Wisthaler, A., Zhan, X., Hain, C. R., Lee, P., and  
1476 Guenther, A. B. (2017), Linkages between land initialization of the NASA-Unified WRF v7  
1477 and biogenic isoprene emission estimates during the SEAC4RS and DISCOVER-AQ airborne  
1478 campaigns, *Geosci. Model Dev. Discuss.*, doi:10.5194/gmd-2017-13, in review.

1479 Inness, A., Blechschmidt, A.-M., Bouarar, I., Chabrillat, S., Crepulja, M., Engelen, R. J., Eskes,  
1480 H., Flemming, J., Gaudel, A., Hendrick, F., Huijnen, V., Jones, L., Kapsomenakis, J.,  
1481 Katragkou, E., Keppens, A., Langerock, B., de Mazière, M., Melas, D., Parrington, M., Peuch,  
1482 V. H., Razinger, M., Richter, A., Schultz, M. G., Suttie, M., Thouret, V., Vrekoussis, M.,  
1483 Wagner, A., and Zerefos, C. (2015), Data assimilation of satellite-retrieved ozone, carbon  
1484 monoxide and nitrogen dioxide with ECMWF's Composition-IFS, *Atmos. Chem. Phys.*, 15,  
1485 5275-5303, doi:10.5194/acp-15-5275-2015.

1486 Jaffe, D.A. (2011), Relationship between surface and free tropospheric ozone in the Western U.S.,  
1487 *Environ. Sci. Technol.*, 45, 432–438, doi: 10.1021/es1028102.

1488 Janssens-Maenhout, G., Crippa, M., Guizzardi, D., Dentener, F., Muntean, M., Pouliot, G.,  
1489 Keating, T., Zhang, Q., Kurokawa, J., Wankmüller, R., Denier van der Gon, H., Kuenen, J. J.  
1490 P., Klimont, Z., Frost, G., Darras, S., Koffi, B., and Li, M. (2015), HTAP\_v2.2: a mosaic of  
1491 regional and global emission grid maps for 2008 and 2010 to study hemispheric transport of  
1492 air pollution, *Atmos. Chem. Phys.*, 15, 11411-11432, doi:10.5194/acp-15-11411-2015.

1493 Jacob, D. J., Logan, J. A., and Murti, P. P. (1999), Effect of rising Asian emissions on surface  
1494 ozone in the United States, *Geophys. Res. Lett.*, 26, 2175-2178, doi: 10.1029/1999GL900450.

1495 Jerret, M., R. T. Burnett, C. A. Popo, III, K. Ito, G. Thurston, D. Krewski, Y. Shi, E. Calle, and M.  
1496 Thun (2009), Long-Term Ozone Exposure and Mortality, the New England Journal of  
1497 *Medicine*, 360, 1085-1096, doi: 10.1056/NEJMoa0803894.

1498 Kaiser, J. W., Heil, A., Andreae, M. O., Benedetti, A., Chubarova, N., Jones, L., Morcrette, J.-J.,  
1499 Razinger, M., Schultz, M. G., Suttie, M., and van der Werf, G. R. (2012), Biomass burning  
1500 emissions estimated with a global fire assimilation system based on observed fire radiative  
1501 power, *Biogeosciences*, 9, 527–554, doi:10.5194/bg-9-527-2012.

1502 Kalnay, E., and Co-authors (1996), The NCEP/NCAR 40-Year Reanalysis Project, *Bulletin of the*  
1503 *American Meteorological Society*, 77, 437–471.

1504 Kim, S.-W., B. C. McDonald, S. Baidar, S. S. Brown, B. Dube, R. A. Ferrare, G. J. Frost, R. A.  
1505 Harley, J. S. Holloway, H.-J. Lee, et al. (2016), Modeling the weekly cycle of NO<sub>x</sub> and CO  
1506 emissions and their impacts on O<sub>3</sub> in the Los Angeles-South Coast Air Basin during the CalNex  
1507 2010 field campaign, *J. Geophys. Res. Atmos.*, 121, 1340–1360, doi:10.1002/2015JD024292.

1508 Koffi, B., Dentener, F., Janssens-Maenhout, G., Guizzardi, D., Crippa, M., Diehl, T., Galmarini,  
1509 S., and Solazzo, E.; Hemispheric Transport Air Pollution (HTAP): Specification of the HTAP2

Deleted: F.
Deleted: G.
Deleted: D.
Deleted: M.
Deleted: T.
Deleted: S.
Deleted: E.
Deleted: (2016).

1518 experiments – Ensuring harmonized modelling, EUR 28255 EN – Scientific and Technical  
 1519 Research Reports, doi:10.2788/725244, 2016.

1520 Langford, A. O., Brioude, J., Cooper, O.R., Senff, C.J., Alvarez II, R.J., Hardesty, R.M., Johnson,  
 1521 B.J., and Oltmans, S.J. (2011), Stratospheric influence on surface ozone in the Los Angeles  
 1522 area during late spring and early summer of 2010, *J. Geophys. Res. Atmos.*, 117, D00V06, doi:  
 1523 10.1029/2011JD016766.

1524 Lapina, K., D. K. Henze, J. B. Milford, M. Huang, M. Lin, A. M. Fiore, G. Carmichael, G. G.  
 1525 Pfister, and K. Bowman (2014), Assessment of source contributions to seasonal vegetative  
 1526 exposure to ozone in the U.S., *J. Geophys. Res. Atmos.*, 119, 324–340,  
 1527 doi:10.1002/2013JD020905.

1528 Levelt, P.F., E. Hilsenrath, G.W. Leppelmeier, G.H.J. van den Oord, P.K. Bhartia, J. Tamminen,  
 1529 J.F. de Haan and J.P. Veefkind (2006), Science Objectives of the Ozone Monitoring Instrument,  
 1530 *IEEE Transaction on Geoscience and Remote Sensing*, 44, 1199-1208.

1531 Li, M., Zhang, Q., Kurokawa, J.-I., Woo, J.-H., He, K., Lu, Z., Ohara, T., Song, Y., Streets, D. G.,  
 1532 Carmichael, G. R., Cheng, Y., Hong, C., Huo, H., Jiang, X., Kang, S., Liu, F., Su, H., and  
 1533 Zheng, B. (2017), MIX: a mosaic Asian anthropogenic emission inventory under the  
 1534 international collaboration framework of the MICS-Asia and HTAP, *Atmos. Chem. Phys.* 17,  
 1535 935-963, doi:10.5194/acp-17-935-2017.

1536 Lin, M., Holloway, T., Carmichael, G. R., and Fiore, A. M. (2010), Quantifying pollution inflow  
 1537 and outflow over East Asia in spring with regional and global models, *Atmos. Chem. Phys.*,  
 1538 10, 4221-4239, doi:10.5194/acp-10-4221-2010.

1539 Lin, M., A. M. Fiore, L. W. Horowitz, O. R. Cooper, V. Naik, J. Holloway, B. J. Johnson, A.  
 1540 Middlebrook, S. J. Oltmans, I. B. Pollack, T. B. Ryerson, J. X. Warner, C. Wiedinmyer, J.  
 1541 Wilson, B. Wyman (2012a), Transport of Asian ozone pollution into surface air over the  
 1542 western United States in spring, *J. Geophys. Res.*, 117, D00V07, doi: 10.1029/2011JD016961.

1543 Lin, M., A. Fiore, O. R. R. Cooper, L. W. Horowitz, A. O. O. Langford, H. Levy II, B. J. Johnson,  
 1544 V. Naik, S. J. Oltmans, and C. J. Senff (2012b), Springtime high surface ozone events over the  
 1545 western United States: Quantifying the role of stratospheric intrusions, *J. Geophys. Res.*, 117,  
 1546 D00V22, doi: 10.1029/2012JD018151.

1547 Lin, M., L.W. Horowitz, S. J. Oltmans, A. M. Fiore, S. Fan (2014), Tropospheric ozone trends at  
 1548 Manna Loa Observatory tied to decadal climate variability, *Nature Geoscience*, 7, 136-143,  
 1549 doi:10.1038/NNGEO2066.

1550 Lin, M., L. W. Horowitz, O. R. Cooper, D. Tarasick, S. Conley, L. T. Iraci, B. Johnson, T. Leblanc,  
 1551 I. Petropavlovskikh, and E. L. Yates (2015), Revisiting the evidence of increasing springtime  
 1552 ozone mixing ratios in the free troposphere over western North America, *Geophys. Res. Lett.*,  
 1553 42, 8719–8728, doi:10.1002/2015GL065311.

1554 Lin, M., Horowitz, L. W., Payton, R., Fiore, A. M., and Tonnesen, G. (2016), US surface ozone  
 1555 trends and extremes from 1980–2014: Quantifying the roles of rising Asian emissions,  
 1556 domestic controls, wildfires, and climate, *Atmos. Chem. Phys. Discuss.*, doi:10.5194/acp-  
 1557 2016-1093, in review.

1558 Liu, F., Q. Zhang, R. J. van der A, B. Zheng, D. Tong, L. Yan, Y. Zheng, and K. He (2016), Recent  
 1559 reduction in NO<sub>x</sub> emissions over China: Synthesis of satellite observations and emission  
 1560 inventories, *Environ. Res. Lett.*, 11 (11), 114002, doi: 10.1088/1748-9326/11/11/114002.

1561 Livesey, N.J., M.J. Filipiak, L. Froidevaux, W.G. Read, A. Lambert, M.L. Santee, J.H. Jiang, H.C.  
 1562 Pumphrey, J.W. Waters, R.E. Cofield, D.T. Cuddy, W.H. Daffer, B.J. Drouin, R.A. Fuller, R.F.  
 1563 Jarnot, Y.B. Jiang, B.W. Knosp, Q.B. Li, V.S. Perun, M.J. Schwartz, W.V. Snyder, P.C. Stek,

Deleted: -

Deleted: in preparation.

Deleted: . B

Deleted: . F

Deleted: . P

Deleted: . J

Deleted: . C

Deleted: 5

Deleted: for

Deleted: the

Deleted: projects

Deleted: . Discuss., 15, 34813-34869

Deleted: acpd-15-34813-2015

Moved (insertion) [13]

1577 R.P. Thurstans, P.A. Wagner, M. Avery, E.V. Browell, J-P. Cammas, L.E. Christensen, G.S.  
1578 Diskin, R-S. Gao, H-J. Jost, M. Loewenstein, J.D. Lopez, P. Nedelec, G.B. Osterman, G.W.  
1579 Sachse, and C.R. Webster (2008), Validation of Aura Microwave Limb Sounder O<sub>3</sub> and CO  
1580 observations in the upper troposphere and lower stratosphere, *J. Geophys. Res.* 113, D15S02,  
1581 doi:10.1029/2007JD008805.

1582  
1583 Luecken, D.J., S. Phillips, G. Sarwar, C. Jang, Effects of using the CB05 vs. SAPRC99 vs. CB4  
1584 chemical mechanism on model predictions (2008), *Ozone and gas-phase photochemical*  
1585 *precursor concentrations*, *Atmos. Environ.*, 42 (23), 5805-5820, doi:  
1586 10.1016/j.atmosenv.2007.08.056.

1587 Maas, R. and P. Grennfelt (eds) (2016), *Towards Cleaner Air Scientific Assessment Report 2016*.  
1588 EMEP Steering Body and Working Group on Effects of the Convention on Long-Range  
1589 Transboundary Air Pollution, Oslo,  
1590 [http://www.unece.org/fileadmin/DAM/env/lrtap/ExecutiveBody/35th\\_session/CLRTAP\\_Scientific\\_Assessment\\_Report\\_-\\_Final\\_20-5-2016.pdf](http://www.unece.org/fileadmin/DAM/env/lrtap/ExecutiveBody/35th_session/CLRTAP_Scientific_Assessment_Report_-_Final_20-5-2016.pdf).

1591 Madronich, S., Flocke, S., Zeng, J., Petropavlovskikh, I., and Lee-Taylor, J. (2002), *The*  
1592 *Tropospheric Ultra-violet Visible (TUV) model Manual*,  
1593 [https://www2.acom.ucar.edu/modeling/tropospheric-ultraviolet-and-visible-tuv-radiation-](https://www2.acom.ucar.edu/modeling/tropospheric-ultraviolet-and-visible-tuv-radiation-model)  
1594 [model](https://www2.acom.ucar.edu/modeling/tropospheric-ultraviolet-and-visible-tuv-radiation-model).

1595  
1596 Mauzerall, D. L. and Wang, X. (2001), *Protecting Agricultural Crops from the Effects of*  
1597 *Tropospheric Ozone Exposure: Reconciling Science and Standard Setting in the United States,*  
1598 *Europe and Asia, Annual Review of Energy and the Environment*, 26, 237-268.

1599 McDonald-Buller, E. C., et al. (2011), *Establishing policy relevant background (PRB) ozone*  
1600 *concentrations in the United States*, *Environ. Sci. Technol.*, 45, 9484-9497.

1601 [Meijer, E. W., van Velthoven, P. F. J., Brunner, D. W., Huntrieser, H., and Kelder, H. \(2001\),](#)  
1602 [Improvement and evaluation of the parameterization of nitrogen oxide production by lightning,](#)  
1603 [Phys. Chem. Earth Pt. C, 26, 577-583.](#)

1604 Mesinger, F., DiMego, G., Kalnay, E., Mitchell, K., Shafran, P. C., Ebisuzaki, W., Jovic, D.,  
1605 Woollen, J., Rogers, E., Berbery, E. H., Ek, M. B., Fan, Y., Grumbine, R., Higgins, W., Li, H.,  
1606 Lin, Y., Manikin, G., Parrish, D. and Shi, W. (2006), *North American Regional Reanalysis*,  
1607 *Bulletin of the American Meteorological Society*, 87(3), 343-360, doi: 10.1175/BAMS-87-3-  
1608 343.

1609 Miyazaki, K., Eskes, H. J., Sudo, K., Takigawa, M., van Weele, M., Boersma, K. F. (2012),  
1610 *Simultaneous assimilation of satellite NO<sub>2</sub>, O<sub>3</sub>, CO, and HNO<sub>3</sub> data for the analysis of*  
1611 *tropospheric chemical composition and emissions*, *Atmos. Chem. Phys.*, 12, 9545-9579.

1612 Monks, P. S., Archibald, A. T., Colette, A., Cooper, O., Coyle, M., Derwent, R., Fowler, D.,  
1613 Granier, C., Law, K. S., Mills, G. E., Stevenson, D. S., Tarasova, O., Thouret, V., von  
1614 Schneidemesser, E., Sommariva, R., Wild, O., and Williams, M. L. (2015), *Tropospheric*  
1615 *ozone and its precursors from the urban to the global scale from air quality to short-lived*  
1616 *climate forcer*, *Atmos. Chem. Phys.*, 15, 8889-8973, doi:10.5194/acp-15-8889-2015.

1617 [Murray, L. T., D. J. Jacob, J. A. Logan, R. C. Hudman, and W. J. Koshak \(2012\), Optimized](#)  
1618 [regional and interannual variability of lightning in a global chemical transport model](#)  
1619 [constrained by LIS/OTD satellite data, J. Geophys. Res., 117, D20307,](#)  
1620 [doi:10.1029/2012JD017934.](#)

**Moved up [13]:** Liu, F., Q. Zhang, R. J. van der A, B. Zheng, D. Tong, L. Yan, Y. Zheng, and K. He (2016), Recent reduction in NO<sub>x</sub> emissions over China: Synthesis of satellite observations and emission inventories, *Environ. Res. Lett.*, 11 (11), 114002, doi: 10.1088/1748-9326/11/11/114002.

1627 National Research Council (NRC) (2009), global sources of local pollution-An Assessment of  
 1628 Long-Range Transport of Key Air Pollutants to and from the United States, 35-66,  
 1629 [http://books.nap.edu/openbook.php?record\\_id=12743&page=35](http://books.nap.edu/openbook.php?record_id=12743&page=35).

1630 Neuman, J. A., et al. (2012), Observations of ozone transport from the free troposphere to the Los  
 1631 Angeles basin, *J. Geophys. Res. Atmos.*, 117, D00V09, doi: 10.1029/2011JD016919.

1632 Oetjen, H., Payne, V. H., Kulawik, S. S., Eldering, A., Worden, J., Edwards, D. P., Francis, G. L.,  
 1633 Worden, H. M., Clerbaux, C., Hadji-Lazarou, J., and Hurtmans, D. (2014), Extending the  
 1634 satellite data record of tropospheric ozone profiles from Aura-TES to MetOp-IASI:  
 1635 characterisation of optimal estimation retrievals, *Atmos. Meas. Tech.*, 7, 4223–4236,  
 1636 doi:10.5194/amt-7-4223-2014.

1637 Oetjen, H., Payne, V. H., Neu, J. L., Kulawik, S. S., Edwards, D. P., Eldering, A., Worden, H. M.,  
 1638 and Worden, J. R. (2016), A joint data record of tropospheric ozone from Aura-TES and  
 1639 MetOp-IASI, *Atmos. Chem. Phys.*, 16, 10229-10239, doi:10.5194/acp-16-10229-2016.

1640 Ott, L. E., B. N. Duncan, A. M. Thompson, G. Diskin, Z. Fasnacht, A. O. Langford, M. Lin, A. M.  
 1641 Molod, J. E. Nielsen, S. E. Pusede, et al. (2016), Frequency and impact of summertime  
 1642 stratospheric intrusions over Maryland during DISCOVER-AQ (2011): New evidence from  
 1643 NASA's GEOS-5 simulations, *J. Geophys. Res. Atmos.*, 121, 3687–3706,  
 1644 doi:10.1002/2015JD024052.

1645 Park, R. J., D. J. Jacob, B. D. Field, R. M. Yantosca, and M. Chin (2004), Natural and  
 1646 transboundary pollution influences on sulfate-nitrate-ammonium aerosols in the United States:  
 1647 Implications for policy, *J. Geophys. Res.*, 109, D15204, doi:10.1029/2003JD004473.

1648 Parrington, M., D. B. A. Jones, K. W. Bowman, L. W. Horowitz, A. M. Thompson, D. W. Tarasick,  
 1649 and J. C. Witte (2008), Estimating the summertime tropospheric ozone distribution over North  
 1650 America through assimilation of observations from the Tropospheric Emission Spectrometer,  
 1651 *J. Geophys. Res.*, 113, D18307, doi:10.1029/2007JD009341.

1652 Parrington, M., D. B. A. Jones, K. W. Bowman, A. M. Thompson, D. W. Tarasick, J. Merrill, S.  
 1653 J. Oltmans, T. Leblanc, J. C. Witte, and D. B. Millet (2009), Impact of the assimilation of  
 1654 ozone from the Tropospheric Emission Spectrometer on surface ozone across North America,  
 1655 *Geophys. Res. Lett.*, 36, L04802, doi:10.1029/2008GL036935.

1656 Parrish, D. D., D. B. Millet, and A. H. Goldstein (2009), Increasing ozone in marine boundary  
 1657 layer inflow at the west coasts of North America and Europe, *Atmos. Chem. Phys.*, 9, 1303–  
 1658 1323, doi:10.5194/acp-9-1303-2009.

1659 Parrish, D. D., Aikin, K. C., Oltmans, S. J., Johnson, B. J., Ives, M., and Sweeny, C. (2010), Impact  
 1660 of transported background ozone inflow on summertime air quality in a California ozone  
 1661 exceedance area, *Atmos. Chem. Phys.*, 10, 10093-10109, doi:10.5194/acp-10-10093-2010.

1662 Parrish, D. D., et al. (2012), Long-term changes in lower tropospheric baseline ozone  
 1663 concentrations at northern mid-latitudes, *Atmos. Chem. Phys.*, 12, 11,485–11,504,  
 1664 doi:10.5194/acp-12-11485-2012.

1665 Pierce, R. B., et al. (2007), Chemical data assimilation estimates of continental U.S. ozone and  
 1666 nitrogen budgets during the Intercontinental Chemical Transport Experiment–North America,  
 1667 *J. Geophys. Res.*, 112, D12S21, doi:10.1029/2006JD007722.

1668 Pierce, R. B., et al. (2009), Impacts of background ozone production on Houston and Dallas, Texas,  
 1669 air quality during the Second Texas Air Quality Study field mission, *J. Geophys. Res.*, 114,  
 1670 D00F09, doi:10.1029/2008JD011337.

1671 Pouliot, G., H. A.C. Denier van der Gon, J. Kuenen, J. Zhang, M. D. Moran, P.A. Makar (2015),  
1672 Analysis of the emission inventories and model-ready emission datasets of Europe and North  
1673 America for phase 2 of the AQMEII project, *Atmos. Environ.*, 115, 345-360.  
1674 Qu, Z., D. K. Henze, S. L. Capps, Y. Wang, X. Xu, J. Wang (2016), Monthly top-down NO<sub>x</sub>  
1675 emissions for China (2005-2012): a hybrid inversion method and trend analysis, submitted.  
1676 Quennehen, B., Raut, J.-C., Law, K. S., Daskalakis, N., Ancellet, G., Clerbaux, C., Kim, S.-W.,  
1677 Lund, M. T., Myhre, G., Oliv  , D. J. L., Safieddine, S., Skeie, R. B., Thomas, J. L., Tsyro, S.,  
1678 Bazureau, A., Bellouin, N., Hu, M., Kanakidou, M., Klimont, Z., Kupiainen, K.,  
1679 Myriokefalitakis, S., Quaas, J., Rumbold, S. T., Schulz, M., Cherian, R., Shimizu, A., Wang,  
1680 J., Yoon, S.-C., and Zhu, T. (2016), Multi-model evaluation of short-lived pollutant  
1681 distributions over east Asia during summer 2008, *Atmos. Chem. Phys.*, 16, 10765-10792,  
1682 doi:10.5194/acp-16-10765-2016.  
1683 Reidmiller, D. R., Fiore, A. M., Jaffe, D. A., Bergmann, D., Cuvelier, C., Dentener, F. J., Duncan,  
1684 B. N., Folberth, G., Gauss, M., Gong, S., Hess, P., Jonson, J. E., Keating, T., Lupu, A., Marmar,  
1685 E., Park, R., Schultz, M. G., Shindell, D. T., Szopa, S., Vivanco, M. G., Wild, O., and Zuber,  
1686 A. (2009), The influence of foreign vs. North American emissions on surface ozone in the US,  
1687 *Atmos. Chem. Phys.*, 9, 5027-5042, doi:10.5194/acp-9-5027-2009.  
1688 Rodgers, C. D. (2000), *Inverse Methods for Atmospheric Sounding: Theory and Practice*, World  
1689 Sci., Singapore.  
1690 Ryerson, T. B., Andrews, A. E., Angevine, W. M., Bates, T. S., Brock, C. A., Cairns, B., Cohen,  
1691 R. C., Cooper, O. R., de Gouw, J. A., Fehsenfeld, F. C., Ferrare, R. A., Fischer, M. L., Flagan,  
1692 R. C., Goldstein, A. H., Hair, J. W., Hardesty, R. M., Hostetler, C. A., Jimenez, J. L., Langford,  
1693 A. O., McCauley, E., McKeen, S. A., Molina, L. T., Nenes, A., Oltmans, S. J., Parrish, D. D.,  
1694 Pederson, J. R., Pierce, R. B., Prather, K., Quinn, P. K., Seinfeld, J. H., Senff, C. J., Sorooshian,  
1695 A., Stutz, J., Surratt, J. D., Trainer, M., Volkamer, R., Williams, E. J., Wofsy, S. C. (2013),  
1696 The 2010 California Research at the Nexus of Air Quality and Climate Change (CalNex) field  
1697 study, *J. Geophys. Res.*, 118, 5830–5866.  
1698 Schere, K. J. Flemming, R. Vautard, C. Chemel, A. Colette, C. Hogrefe, B. Bessagnet, F. Meleux,  
1699 R. Mathur, S. Roselle, R.-M. Hu, R. S. Sokhi, S. T. Rao, S. Galmarini (2012), Trace gas/aerosol  
1700 boundary concentrations and their impacts on continental-scale AQMEII modeling domains,  
1701 *Atmos. Environ.*, 53, 38-50, doi: 10.1016/j.atmosenv.2011.09.043.  
1702 Shindell, D. T., G. Faluvegi, D. M. Koch, G. A. Schmidt, N. Unger, and S. E. Bauer (2009),  
1703 Improved attribution of climate forcing to emissions, *Science*, 326, 716–718, doi:  
1704 10.1126/science.1174760.  
1705 Shindell, D. T., et al. (2013), Radiative forcing in the ACCMIP historical and future climate  
1706 simulations, *Atmos. Chem. Phys.*, 13, 2939–2974, doi:10.5194/acp-13-2939-2013.  
1707 Simpson, D., Benedictow, A., Berge, H., Bergstr  m, R., Emberson, L. D., Fagerli, H., Flechard,  
1708 C. R., Hayman, G. D., Gauss, M., Jonson, J. E., Jenkin, M. E., Nyiri, A., Richter, C.,  
1709 Semeena, V. S., Tsyro, S., Tuovinen, J.-P., Valdebenito, A., and Wind, P. (2012), The EMEP  
1710 MSC-W chemical transport model – technical description, *Atmos. Chem. Phys.*, 12, 7825–  
1711 7865, doi:10.5194/acp-12- 7825-2012.  
1712 Sindelarova, K., Granier, C., Bouarar, I., Guenther, A., Tilmes, S., Stavrakou, T., M  ller, J.-F.,  
1713 Kuhn, U., Stefani, P., and Knorr, W. (2014), Global data set of biogenic VOC emissions  
1714 calculated by the MEGAN model over the last 30 years, *Atmos. Chem. Phys.*, 14, 9317–9341,  
1715 doi:10.5194/acp-14-9317-2014.

Moved (insertion) [14]

Formatted: apple-style-span, Font:Arial, Font color: Black,  
Pattern: Clear (White)

1716 Skamarock, W. C., J. B. Klemp, J. Dudhia, D. Gill, D. M. Barker, W. Wang, and J. G. Powers  
 1717 (2008), A description of the Advanced Research WRF version 3 (Available at  
 1718 www.mmm.ucar.edu/wrf/users/docs/arwv3.pdf).

1719 Smith, K. R., Jerrett, M., and Anderson, H. R. et al. (2009), Public health benefits of strategies to  
 1720 reduce greenhouse-gas emissions: health implications of short-lived greenhouse pollutants,  
 1721 Lancet, doi: 10.1016/S0140-6736 (09) 61716-5.

1722 Solazzo, E. R. Bianconi, R. Vautard, K. W. Appel, M. D. Moran, C. Hogrefe, B. Bessagnet, J.  
 1723 Brandt, J. H. Christensen, C. Chemel, I. Coll, H. D. van der Gon, J. Ferreira, R. Forkel, X. V.  
 1724 Francis, G. Grell, P. Grossi, A. B. Hansen, A. Jeričević, L. Kraljević, A. I. Miranda, U.  
 1725 Nopmongcol, G. Pirovano, M. Prank, A. Riccio, K. N. Sartelet, M. Schaap, J. D. Silver, R. S.  
 1726 Sokhi, J. Vira, J. Werhahn, R. Wolke, G. Yarwood, J. Zhang, S.T. Rao, S. Galmarini (2012),  
 1727 Model evaluation and ensemble modelling of surface-level ozone in Europe and North  
 1728 America in the context of AQMEII, Atmos. Environ., 53, 60-74, , doi:  
 1729 10.1016/j.atmosenv.2012.01.003.

1730 Søvde, O. A., Prather, M. J., Isaksen, I. S. A., Berntsen, T. K., Stordal, F., Zhu, X., Holmes, C. D.,  
 1731 and Hsu, J. (2012), The chemical transport model Oslo CTM3, Geosci. Model Dev., 5, 1441–  
 1732 1469, doi:10.5194/gmd-5-1441-2012.

1733 Sudo, K., M. Takahashi, J. Kurokawa, and H. Akimoto (2002), Chaser: A global chemical model  
 1734 of the troposphere. I. Model description, J. Geophys. Res., 107(D17), 4339,  
 1735 doi:10.1029/2001JD001113.

1736 Stevenson, D. S., et al. (2006), Multimodel ensemble simulations of present-day and near-future  
 1737 tropospheric ozone, J. Geophys. Res., 111, D08301, doi:10.1029/2005JD006338.

1738 Stevenson, D. S., et al. (2013), Tropospheric ozone changes, radiative forcing and attribution to  
 1739 emissions in the Atmospheric Chemistry and Climate Model Intercomparison Project  
 1740 (ACCMIP), Atmos. Chem. Phys., 13, 3063–3085, doi:10.5194/acp-13-3063-2013.

1741 Susaya, J., Kim, K.-H., Shon, Z.-H., Brown R. J. (2013), Demonstration of long-term increases in  
 1742 tropospheric O<sub>3</sub> levels: Causes and potential impacts, Chemosphere, 92, 1520–1528.

1743 Task Force on Hemispheric Transport of Air Pollution (HTAP) (2010), 2010 Final Assessment  
 1744 report, Part A: Ozone and particulate matter,  
 1745 http://www.htap.org/activities/2010\_Final\_Report/HTAP%202010%20Part%20A%2011040  
 1746 7.pdf.

1747 Tilmes, S., Lamarque, J.-F., Emmons, L. K., Kinnison, D. E., Marsh, D., Garcia, R. R., Smith, A.  
 1748 K., Neely, R. R., Conley, A., Vitt, F., Val Martin, M., Tanimoto, H., Simpson, I., Blake, D. R.,  
 1749 and Blake, N. (2016), Representation of the Community Earth System Model (CESM1)  
 1750 CAM4-chem within the Chemistry- Climate Model Initiative (CCMI), Geosci. Model Dev., 9,  
 1751 1853– 1890, doi:10.5194/gmd-9-1853-2016.

1752 Travis, K. R., Jacob, D. J., Fisher, J. A., Kim, P. S., Marais, E. A., Zhu, L., Yu, K., Miller, C. C.,  
 1753 Yantosca, R. M., Sulprizio, M. P., Thompson, A. M., Wennberg, P. O., Crouse, J. D., St.  
 1754 Clair, J. M., Cohen, R. C., Laughner, J. L., Dibb, J. E., Hall, S. R., Ullmann, K., Wolfe, G. M.,  
 1755 Pollack, I. B., Peischl, J., Neuman, J. A., and Zhou, X. (2016), Why do models overestimate  
 1756 surface ozone in the Southeast United States?, Atmos. Chem. Phys., 16, 13561-13577,  
 1757 doi:10.5194/acp-16-13561-2016.

1758 United Nations Environment Programme and World Meteorological Organization (2011),  
 1759 Integrated Assessment of Black Carbon and Tropospheric Ozone: Summary for Decision  
 1760 Makers, http://www.unep.org/dewa/Portals/67/pdf/Black\_Carbon.pdf.

Moved (insertion) [15]

Moved up [10]: H.,

Deleted: Stjern, C.

Moved up [8]: W.,

Deleted: Samset, B.

Moved up [11]: Flemming, J.,

Deleted: Phys., 16, 13579-13599, doi:10.5194/acp-16-13579-2016.

Formatted: Default Paragraph Font, Font color: Black

Deleted: Haslerud, A. S., Henze, D

Moved up [14]: ., Jonson, J.

Formatted: Default Paragraph Font, Font color: Black

Moved up [15]: Sudo, K.,

Moved up [9]: Chem.

Deleted: Myhre, G., Bian, H., Chin, M., Davila, Y., Dentener, F., Emmons, L.,

Formatted: apple-style-span, Font color: Black, Pattern: Clear (White)

Deleted: E., Kucsera, T., Lund, M. T., Schulz, M.,

Deleted: Takemura, T., and Tilmes, S. (2016), Atmos.

1776 US EPA (2016a), Implementation of the 2015 Primary Ozone NAAQS: Issues Associated with  
 1777 Background Ozone White Paper for Discussion,  
 1778 <https://www.epa.gov/sites/production/files/2016-03/documents/whitepaper-bgo3-final.pdf>.  
 1779 US EPA (2016b), High level summary of background ozone workshop,  
 1780 [https://www.epa.gov/sites/production/files/2016-03/documents/bgo3-high-level-](https://www.epa.gov/sites/production/files/2016-03/documents/bgo3-high-level-summary.pdf)  
 1781 [summary.pdf](https://www.epa.gov/sites/production/files/2016-03/documents/bgo3-high-level-summary.pdf).  
 1782 [van der Werf, G. R., Randerson, J. T., Giglio, L., Collatz, G. J., Mu, M., Kasibhatla, P. S., Morton,](#)  
 1783 [D. C., DeFries, R. S., Jin, Y., and van Leeuwen, T. T. \(2010\), Global fire emissions and the](#)  
 1784 [contribution of deforestation, savanna, forest, agricultural, and peat fires \(1997–2009\), \*Atmos.\*](#)  
 1785 [\*Chem. Phys.\*, 10, 11707-11735, doi:10.5194/acp-10-11707-2010.](#)  
 1786 [van Noije, T. P. C., Eskes, H. J., Dentener, F. J., Stevenson, D. S., Ellingsen, K., Schultz, M. G.,](#)  
 1787 [Wild, O., Amann, M., Atherton, C. S., Bergmann, D. J., Bey, I., Boersma, K. F., Butler, T.,](#)  
 1788 [Cofala, J., Drevet, J., Fiore, A. M., Gauss, M., Hauglustaine, D. A., Horowitz, L. W., Isaksen,](#)  
 1789 [I. S. A., Krol, M. C., Lamarque, J.-F., Lawrence, M. G., Martin, R. V., Montanaro, V., Müller,](#)  
 1790 [J.-F., Pitari, G., Prather, M. J., Pyle, J. A., Richter, A., Rodriguez, J. M., Savage, N. H., Strahan,](#)  
 1791 [S. E., Sudo, K., Szopa, S., and van Roozendaal, M. \(2006\), Multi-model ensemble simulations](#)  
 1792 [of tropospheric NO<sub>2</sub> compared with GOME retrievals for the year 2000, \*Atmos. Chem. Phys.\*,](#)  
 1793 [6, 2943-2979, doi:10.5194/acp-6-2943-2006.](#)  
 1794 Verstraeten, W. W., K. F. Boersma, J. Zörner, M. A. F. Allaart, K. W. Bowman, and J. R. Worden  
 1795 (2013), Validation of six years of TES tropospheric ozone retrievals with ozonesonde  
 1796 measurements: Implications for spatial patterns and temporal stability in the bias, *Atmos. Meas.*  
 1797 *Tech.*, 6, 1413–1423.  
 1798 Verstraeten, W.W., J. L. Neu, J. E. Williams, K. W. Bowman, J. R. Worden, and K. F. Boersma  
 1799 (2015), Rapid increases in tropospheric ozone production and export from China, *Nature*  
 1800 *Geoscience*, 8, 690–695, doi:10.1038/ngeo2493.  
 1801 [Wang, H., D. J. Jacob, P. L. Sager, D. G. Streets, R. J. Park, A. B. Gilliland, and A. van Donkelaar](#)  
 1802 [\(2009\), Surface ozone background in the United States: Canadian and Mexican pollution](#)  
 1803 [influences, \*Atmos. Environ.\*, 43\(6\), 1310–1319, doi:10.1016/j.atmosenv.2008.11.036.](#)  
 1804 [Wang, Y., Konopka, P., Liu, Y., Chen, H., Müller, R., Plöger, F., Riese, M., Cai, Z., and Lü, D.](#)  
 1805 [\(2012\), Tropospheric ozone trend over Beijing from 2002–2010: ozonesonde measurements](#)  
 1806 [and modeling analysis, \*Atmos. Chem. Phys.\*, 12, 8389-8399, doi:10.5194/acp-12-8389-2012.](#)  
 1807 Warneke, C., J. A. deGouw, J. S. Holloway, J. Peischl, T. B. Ryerson, E. Atlas, D. Blake, M.  
 1808 Trainer, and D. D. Parrish (2012), Multiyear trends in volatile organic compounds in Los  
 1809 Angeles, California: Five decades of decreasing emissions, *J. Geophys. Res.*, 117, D00V17,  
 1810 doi:10.1029/2012JD017899.  
 1811 Warner, J. X., McCourt Comer, M., Barnett, C. D., McMillan, W. W., Wolf, W., Maddy, E., and  
 1812 Sachse, G. (2007), A comparison of satellite tropospheric carbon monoxide measurements  
 1813 from AIRS and MOPITT during INTEX-A, *J. Geophys. Res.*, 112, D12S17,  
 1814 doi:10.1029/2006JD007925, 2007.  
 1815 Wiedinmyer, C., Akagi, S. K., Yokelson, R. J., Emmons, L. K., Al-Saadi, J. A., Orlando, J. J., and  
 1816 Soja, A. J. (2011), The Fire INventory from NCAR (FINN): a high resolution global model to  
 1817 estimate the emissions from open burning, *Geosci. Model Dev.*, 4, 625-641, doi:10.5194/gmd-  
 1818 4-625-2011.  
 1819 Wigder, N.L., Jaffe, D.A., Herron-Thorpe, F.L., and Vaughan, J.K. (2013), Influence of daily  
 1820 variations in baseline ozone on urban air quality in the United States Pacific Northwest, *J.*  
 1821 *Geophys. Res.*, 118, 3343–3354, doi: 10.1029/2012JD018738.

Formatted: Default Paragraph Font, Font:Arial, Font color: Auto, Pattern: Clear

Moved (insertion) [12]

Formatted: Default Paragraph Font, Font:Arial



1822 Wild, O., Fiore, A. M., Shindell, D. T., Doherty, R. M., Collins, W. J., Dentener, F. J., Schultz, M.  
1823 G., Gong, S., MacKenzie, I. A., Zeng, G., Hess, P., Duncan, B. N., Bergmann, D. J., Szopa,  
1824 S., Jonson, J. E., Keating, T. J., and Zuber, A. (2012), Modelling future changes in surface  
1825 ozone: a parameterized approach, *Atmos. Chem. Phys.*, 12, 2037-2054, doi:10.5194/acp-12-  
1826 2037-2012.

1827 Wu, S., B. N. Duncan, D. J. Jacob, A. M. Fiore, and O. Wild (2009), Chemical nonlinearities in  
1828 relating intercontinental ozone pollution to anthropogenic emissions, *Geophys. Res. Lett.*, 36,  
1829 L05806, doi:10.1029/2008GL036607.

1830 Yarwood, G., Rao, S., Yocke, M., and Whitten, G. (2005), Updates to the carbon bond chemical  
1831 mechanism: CB05. Final report to the US EPA, EPA Report Number: RT-0400675.

1832 Zhang, L., Jacob, D. J., Boersma, K. F., Jaffe, D. A., Olson, J. R., Bowman, K. W., Worden, J. R.,  
1833 Thompson, A. M., Avery, M. A., Cohen, R. C., Dibb, J. E., Flock, F. M., Fuelberg, H. E.,  
1834 Huey, L. G., McMillan, W. W., Singh, H. B., and Weinheimer, A. J. (2008), Transpacific  
1835 transport of ozone pollution and the effect of recent Asian emission increases on air quality in  
1836 North America: an integrated analysis using satellite, aircraft, ozonesonde, and surface  
1837 observations, *Atmos. Chem. Phys.*, 8, 6117-6136, doi:10.5194/acp-8-6117-2008.

1838 Zhang, L., Jacob, D. J., Kopacz, M., Henze, D. K., Singh, K., and Jaffe, D. A. (2009),  
1839 Intercontinental source attribution of ozone pollution at western U.S. sites using an adjoint  
1840 method, *Geophys. Res. Lett.*, 36, L11810, doi: 10.1029/2009GL037950.

1841 Zhang, L., D. J. Jacob, N. V. Downey, D. A. Wood, D. Blewitt, C. C. Carouge, A. van Donkelaar,  
1842 D. B. A. Jones, L. T. Murray, and Y. Wang (2011), Improved estimate of the policy-relevant  
1843 background ozone in the United States using the GEOS-Chem global model with 1/2°×2/3°  
1844 horizontal resolution over North America, *Atmos. Environ.*, 45, 6769–6776, doi:  
1845 10.1016/j.atmosenv.2011.07.054.

1846 Zhang, Q., Yuan, B., Shao, M., Wang, X., Lu, S., Lu, K., Wang, M., Chen, L., Chang, C.-C., and  
1847 Liu, S. C. (2014), Variations of ground-level O<sub>3</sub> and its precursors in Beijing in summertime  
1848 between 2005 and 2011, *Atmos. Chem. Phys.*, 14, 6089-6101, doi:10.5194/acp-14-6089-2014.

1849 Zhang, Y., Y. Chen, G. Sarwar, and K. Schere (2012), Impact of gas-phase mechanisms on  
1850 Weather Research Forecasting Model with Chemistry (WRF/Chem) predictions: Mechanism  
1851 implementation and comparative evaluation, *J. Geophys. Res.*, 117, D01301,  
1852 doi:10.1029/2011JD015775.

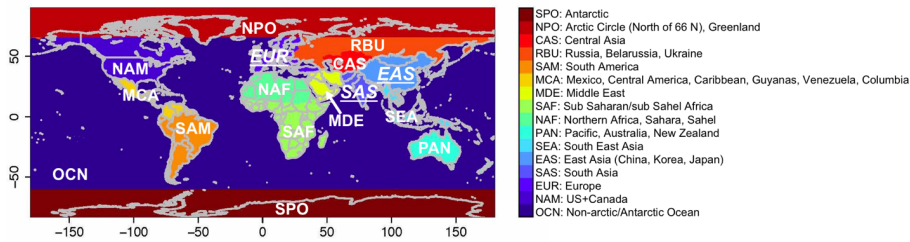


**Figure 1.** Definitions of the 16 source regions used in HTAP2 SR relationship study (More details in Koffi et al., 2016). The map is plotted based on data on a  $0.1^\circ \times 0.1^\circ$  resolution grid. We focus in this study on the impact of anthropogenic pollution from selected non-North American source regions (i.e., EAS, SAS, and EUR), whose names are underlined and in italic.

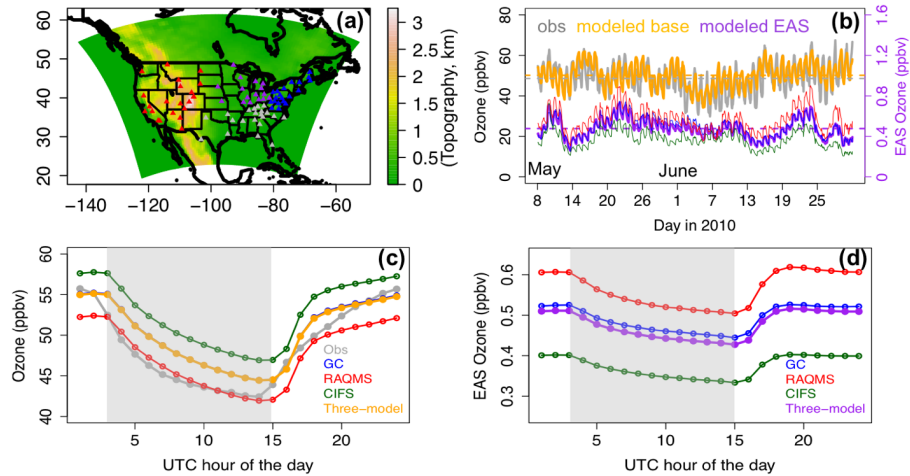
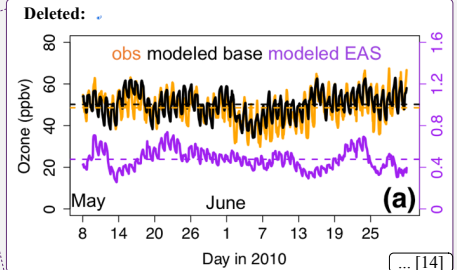


**Figure 2.** (a) The 60 km STEM NAM domain, colored by the model topography. The CASTNET sites used in the STEM base  $O_3$  evaluation are marked as triangles in different colors that identify the subregions they belong to (red: western US; grey: southern US; purple: Midwest; blue: northeastern US). (b) Evaluation of the STEM modeled (averaged from the three base simulations using the GEOS-Chem, ECMWF C-IFS, and RAQMS base runs as the chemical boundary conditions) hourly  $O_3$  at the western US (i.e., EPA regions 8, 9, and 10) CASTNET sites. Observations, modeled base  $O_3$  and the modeled  $R(O_3, EAS, 20\%)$  are in grey, orange, and purple lines, respectively. The horizontal dashed lines indicate the period mean values. The  $R(O_3, EAS, 20\%)$  values from STEM calculations using three different chemical boundary conditions are shown separately in thin lines (blue: GEOS-Chem; red: RAQMS; green: C-IFS). The period-mean diurnal variability of the STEM modeled (c) base and (d)  $R(O_3, EAS, 20\%)$  at the western US CASTNET sites. The STEM calculations using three different chemical boundary conditions are shown separately as well as averagely. Light grey-shaded areas indicate the local standard nighttime (from 6/7 pm to 7/8 am).

Formatted: Font:Bold



Deleted: .

Deleted: as highlighted

Deleted:

Moved down [16]: The horizontal dashed lines indicate the period mean values.

Formatted: Font:Bold

Deleted: (b

Moved (insertion) [16]

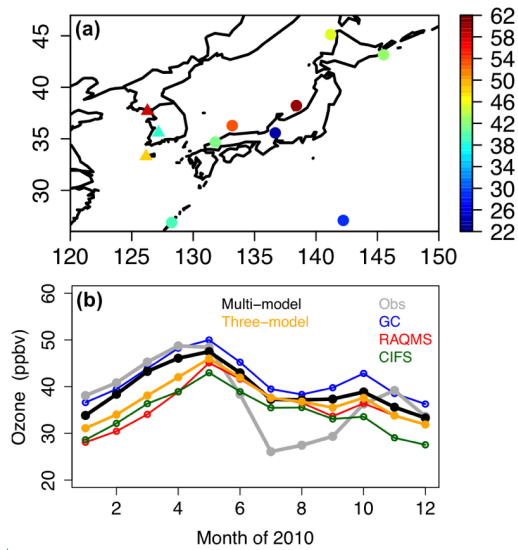


**Figure 3.** (a) May-June 2010 period mean surface O<sub>3</sub> observations in ppbv at eight Japanese (filled circles) and three Korean (filled triangles) EANET sites. (b) Observed and modeled monthly-mean surface O<sub>3</sub> in 2010 at all eleven EANET sites. The “Multi-model” and “Three-model” in the legend indicate the mean values of all eight global models and only of the three boundary condition models, respectively.

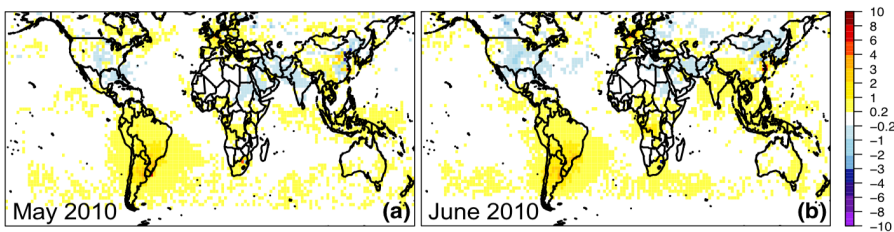


**Figure 4.** Evaluation of the GEOS-Chem adjoint base NO<sub>2</sub> product (recorded at near the satellite overpassing time) with the OMI NO<sub>2</sub> columns. The differences between OMI and GEOS-Chem (OMI-modeled) tropospheric NO<sub>2</sub> columns ( $\times 10^{15}$  molec./cm<sup>2</sup>) are shown for (a) May and (b) June 2010. Details of the comparison are included in Section 2.3.2.

Formatted: Font:Bold

Formatted: Font:Bold

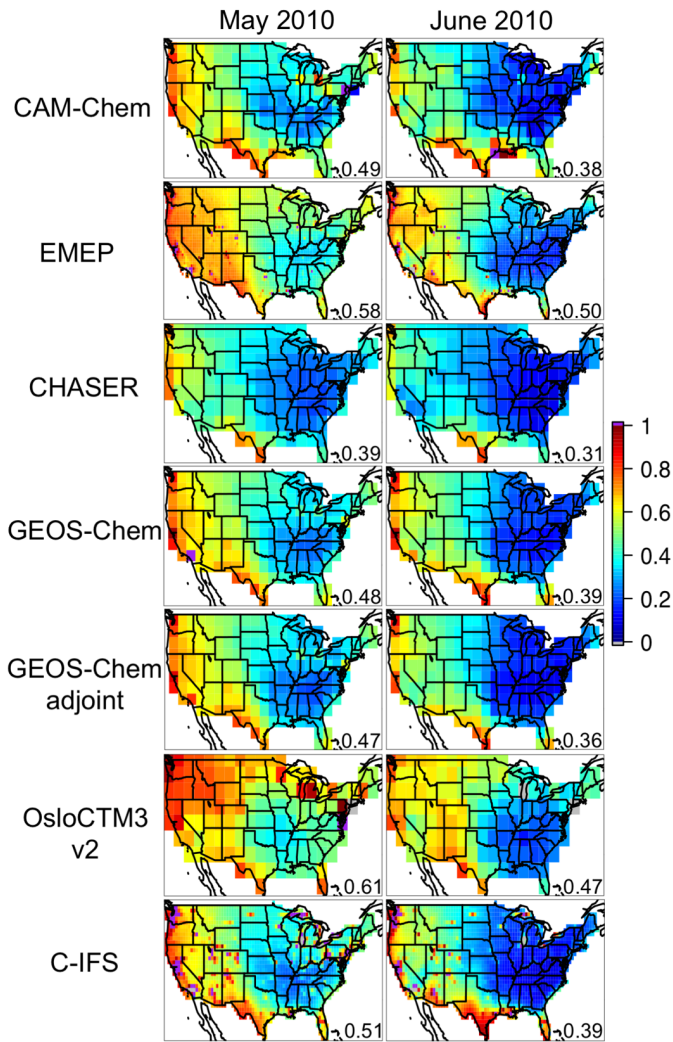
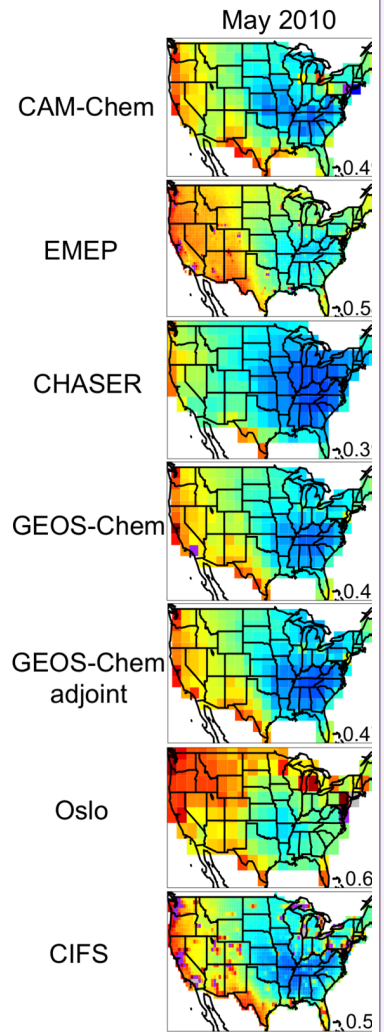


**Figure 5.** The RERER maps in May (left) and June (right) 2010 over the continental US, calculated based on the monthly mean O<sub>3</sub> from multiple global models' base and emission sensitivity simulations. The RERER metric (unitless) was defined in eq. (2) in the text. Values larger than 1 and smaller than 0 are shown in purple and grey, respectively. The US (including continental US as well as Hawaii which is not shown in the plots) mean values are indicated for each panel at the lower right corner. All models show declining RERER values from May to June, and the 7-model mean RERER values for May and June 2010 are ~0.5 and ~0.4, respectively.

Formatted: Font:Bold



Deleted:

Deleted: 4

Deleted: The

1895  
1896  
1897  
1898  
1899  
1900  
1901  
1902

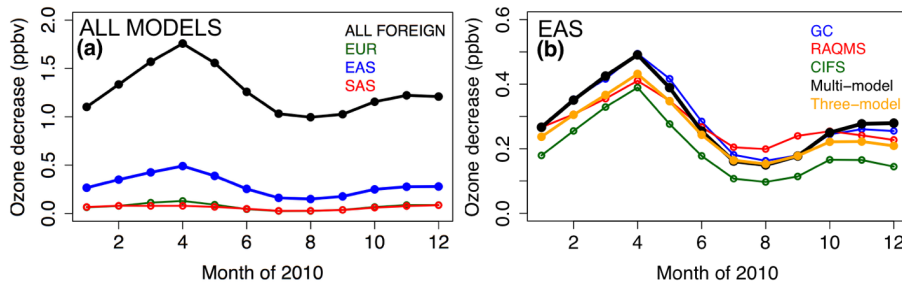


**Figure 6.** (a) North American (130-65°W; 20-50°N) mean O<sub>3</sub> sensitivity to 20% anthropogenic emission reductions in various non-North American regions, averaged from multiple (six-eight, see details in text) global models. (b) North American surface R(O<sub>3</sub>, EAS, 20%) values, as estimated by single (the three STEM boundary condition models) or multi- global model means. The “Multi-model” and “Three-model” in the legend indicate the mean sensitivities of all eight global models and only of the three boundary condition models, respectively.

Deleted: 5

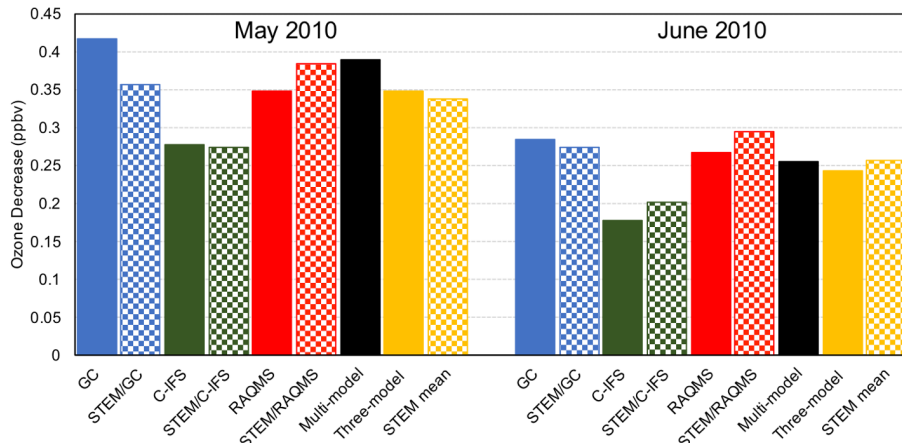


**Figure 7.** Monthly-mean North American (130-65°W; 20-50°N) surface R(O<sub>3</sub>, EAS, 20%) values from multiple global and regional model simulations for May (left) and June (right) 2010. STEM model mean values were calculated from its hourly output from 8 May and on. The “Multi-model” and “Three-model” in the legend indicate the mean sensitivities of all eight global models and only of the three boundary condition models, respectively.

Deleted: 6

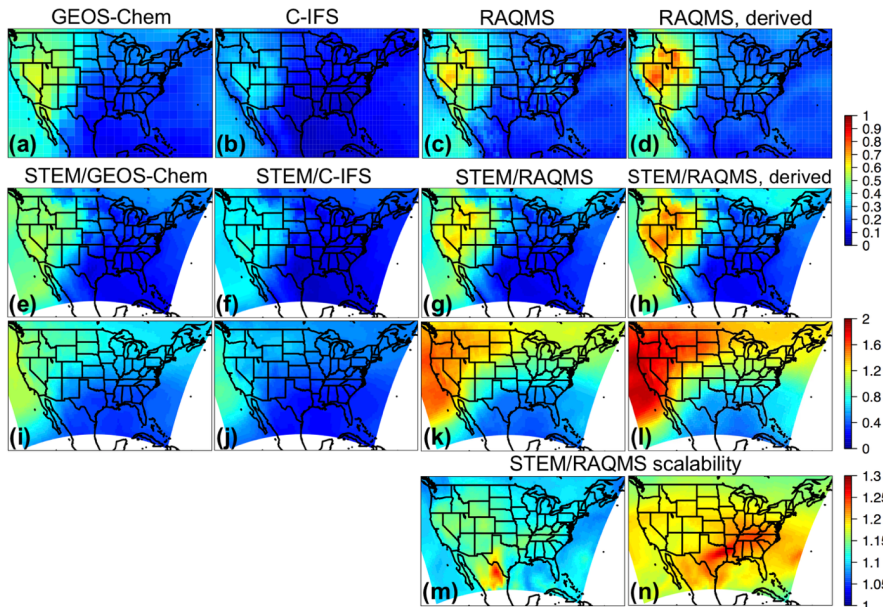


**Figure 8.** The monthly-mean  $R(O_3, \text{EAS}, 20\%)$  in June 2010 for: **(a-d)** surface  $O_3$  (ppbv) from the three boundary condition models, **(e-h)** STEM surface  $O_3$  (ppbv), and **(i-l)** STEM column  $O_3$  ( $\times 10^{16}$  molecules/ $\text{cm}^2$ ).  $R(O_3, \text{EAS}, 20\%)$  values from the simulations associated with GEOS-Chem, ECMWF C-IFS, and RAQMS are shown in **(a;e;i)**, **(b;f;j)** and **(c;g;k)**, respectively. **(d;h;l)** show 1/5 of the  $R(O_3, \text{EAS}, 100\%)$  from the simulations related to RAQMS. STEM/RAQMS-based “Scalability”  $S_{O_3}$  (eq. (3)) values over the NAM are shown for **(m)** surface and **(n)** column  $O_3$ .

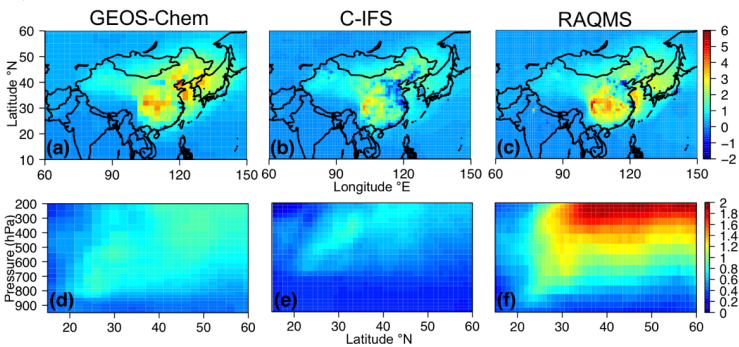
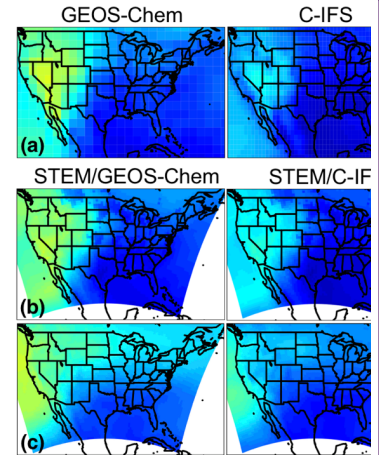


**Figure 9.** The monthly-mean  $R(O_3, \text{EAS}, 20\%)$  in ppbv in June 2010 from the three boundary condition models at the source and near the receptor regions: **(a-c)** surface  $O_3$  in the East Asia; and

Formatted: Font:Bold



Deleted:  
Figure 7.

Moved (insertion) [17]

Deleted: b

Deleted: c

Deleted: Columns 1-3 show

Deleted: ,

Deleted: Column 4 shows

Deleted: (d) The

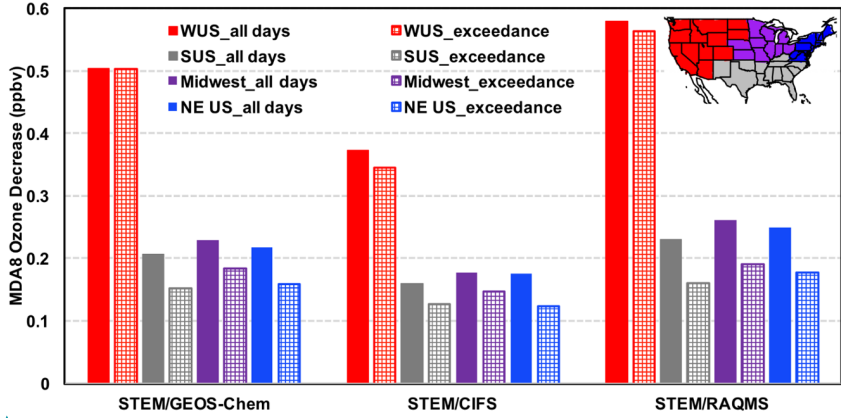
Deleted: of

Deleted: (left)

Deleted: (right) in June 2010

Moved up [17]: Figure 8.

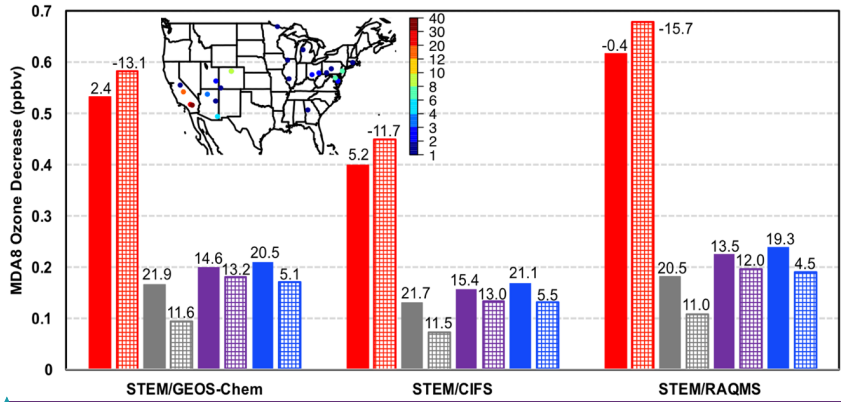
1945 (d) O<sub>x</sub> (GEOS-Chem) or (e-f) O<sub>3</sub> (ECMWF C-IFS and RAQMS) along the cross section of 135°W  
 1946 (near the west boundary of the STEM model domain as defined in Figure 2a).



Deleted: 2b  
 Formatted: Font:Bold

1947  
 1948 **Figure 10.** STEM R(MDA8, EAS, 20%) for May-June 2010 in four US subregions (defined in the  
 1949 inset panel, also consistent with the definitions in Figures 2/S4 and Tables 2-3), averaged on all  
 1950 days (bars with solid fill) and only on the days when the simulated total MDA8 O<sub>3</sub> concentrations  
 1951 were over 70 ppbv (bars with grid pattern fill). The results from the STEM runs using GEOS-  
 1952 Chem, ECMWF C-IFS and RAQMS boundary conditions are shown separately.

Deleted: 9  
 Deleted: of  
 Deleted: S3



Formatted: Font:Bold

1954 **Figure 11.** STEM R(MDA8, EAS, 20%) for May-June 2010 at the CASTNET sites in four US  
 1955 subregions (same definition as in Figure 10 inset), averaged on all days (bars with solid fill) and  
 1956 only on the days when the observed MDA8 O<sub>3</sub> concentrations were over 70 ppbv (bars with grid  
 1957 pattern fill). The results from the STEM runs using GEOS-Chem, ECMWF C-IFS and RAQMS  
 1958 boundary conditions are shown separately. Biases for the corresponding model base runs  
 1959 are shown above the bar plots. Inset shows at various CASTNET sites the number of days when the  
 1960 observed MDA8 O<sub>3</sub> concentrations were over 70 ppbv.

1966  
 1967  
 1968  
 1969  
 1970  
 1971

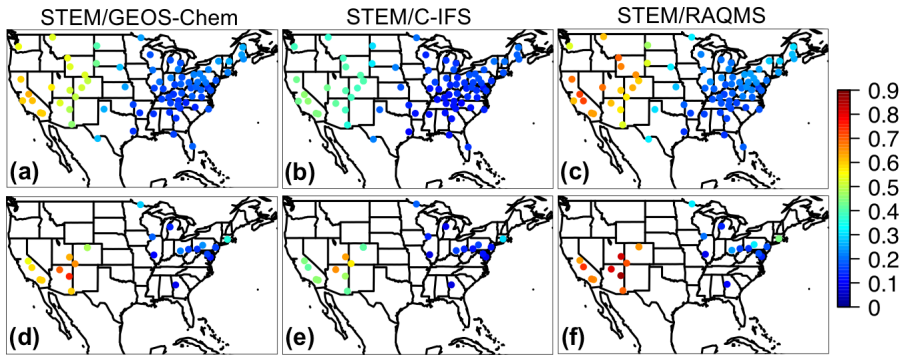


**Figure 12.** STEM R(MDA8, EAS, 20%) in ppbv for May-June 2010 at the CASTNET sites on (a-c) all days and (d-f) the days when the observed MDA8 O<sub>3</sub> concentrations were over 70 ppbv. The results from the STEM runs using (a;d) GEOS-Chem, (b;e) ECMWF C-IFS and (c;f) RAQMS boundary conditions are shown separately.

1972  
 1973  
 1974  
 1975  
 1976  
 1977

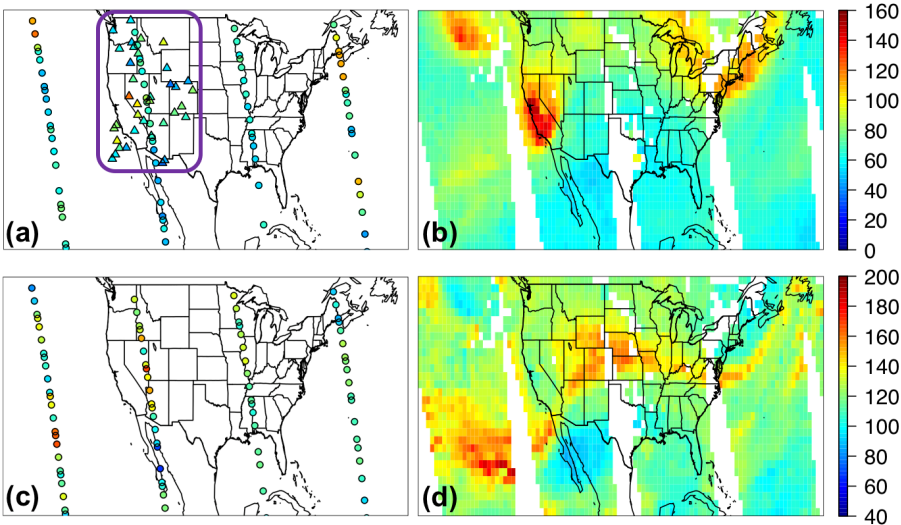
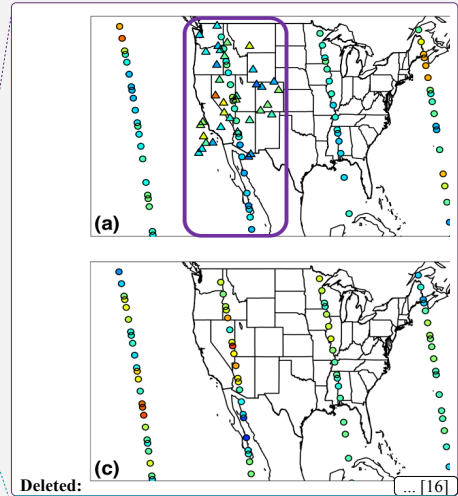


**Figure 13.** Case study of 9 May 2010: (a-b) Ozone (ppbv) and (c-d) CO (ppbv) at ~500 hPa from the L2 (a;c) TES retrievals (circles) and (b;d) L3 AIRS products at early afternoon local time. The L2 IASI O<sub>3</sub> (ppbv) at ~500 hPa retrieved using the TES algorithm (details in Section 2.3.2) at the mid-morning local times is shown on panel (b) as triangles. The O<sub>3</sub> profiles within the purple box in panel (a) were used in the model evaluation shown in Figure 14.

Formatted: Font:Bold



Deleted: ... [16]

Formatted: Font:Bold

Deleted: 11



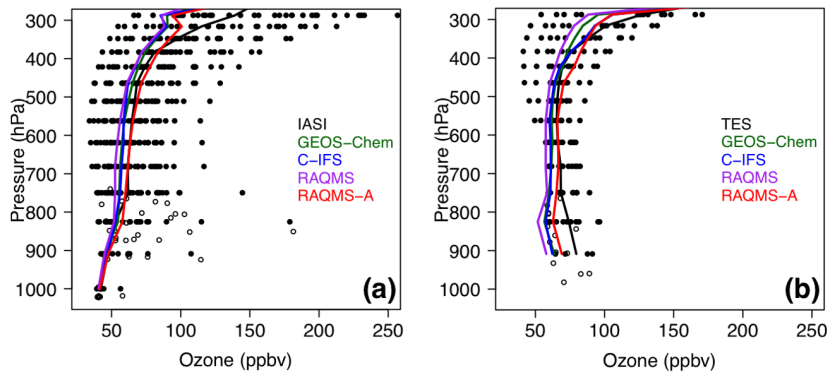


**Figure 14.** Case study of 9 May 2010: The comparisons between (a) IASI and (b) TES O<sub>3</sub> in the western US with the simulated O<sub>3</sub> in the STEM runs using the GEOS-Chem (green), C-IFS (blue), RAQMS (purple), and assimilated RAQMS (red) boundary conditions. The O<sub>3</sub> profiles within the purple box in Figure 10a were used in the evaluation. Observation operators were applied in the comparisons (details in Section 2.3.2). Solid and open dots are TES/IASI data at the TES retrieval reporting levels and at the variable surface pressure levels, respectively. Solid lines are median O<sub>3</sub> profiles from the satellite observations and the different STEM simulations, calculated only on the TES retrieval reporting levels.

Deleted: 11

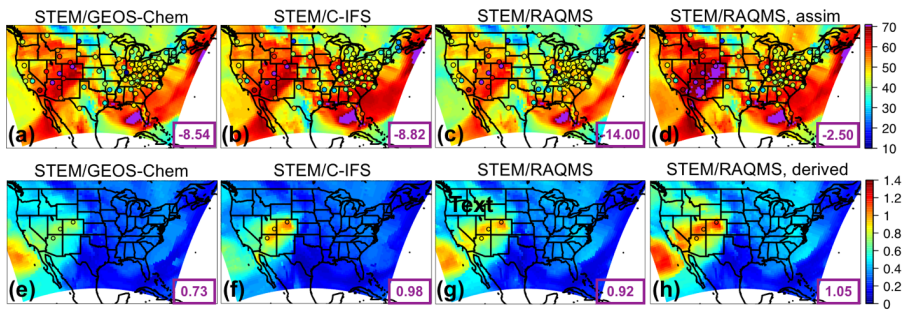
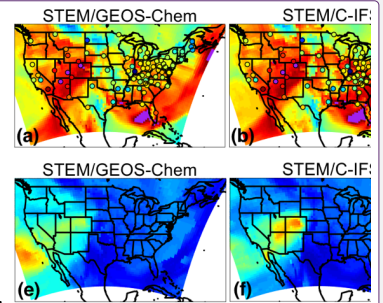


**Figure 15.** Case study of 9 May 2010: (a-d) Surface MDA8 total O<sub>3</sub> and (e-h) surface R(MDA8, EAS, 20%) from the STEM simulations using the (a;e) GEOS-Chem, (b;f) ECMWF C-IFS, and (c;g) RAQMS free run as the boundary conditions. (d) Surface MDA8 total O<sub>3</sub> in a STEM base simulation using the RAQMS assimilation run as the boundary conditions. CASTNET observations are overlaid in filled circles in panels (a-d). (h) 1/5 of the surface R(MDA8, EAS, 100%) from STEM/RAQMS simulations. The conditions at ~400-500 hPa are shown in Figure S5. Purple numbers at the lower right corners of (a-d) and (e-h) are mean model biases and mean R(MDA8, EAS, 20%) values in ppbv at the three mountain sites (Grand Canyon NP, AZ; Canyonlands NP, UT; and Rocky Mountain NP, CO) where O<sub>3</sub> exceedances were observed on this day. The locations of these sites are shown in panel (e-h) as open circles.

Formatted: Font:Bold



Deleted:

Deleted: 12

Deleted: S4

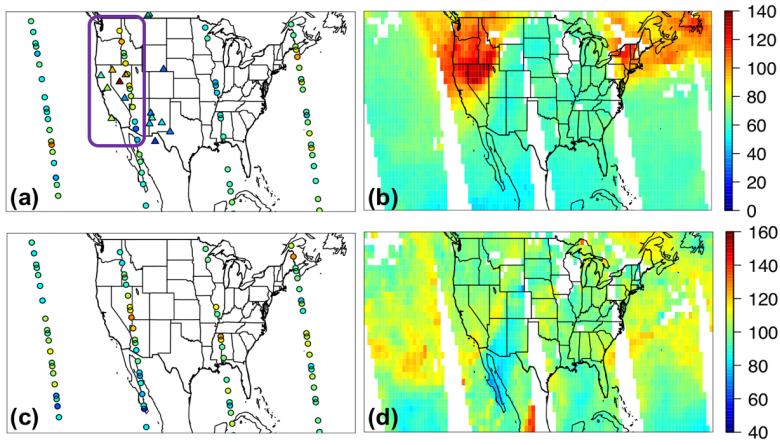


Figure 16. Same as Figure 13, but for a case study of 10 June 2010.

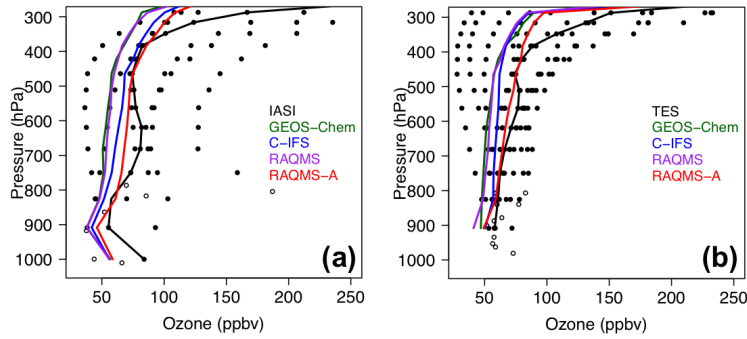
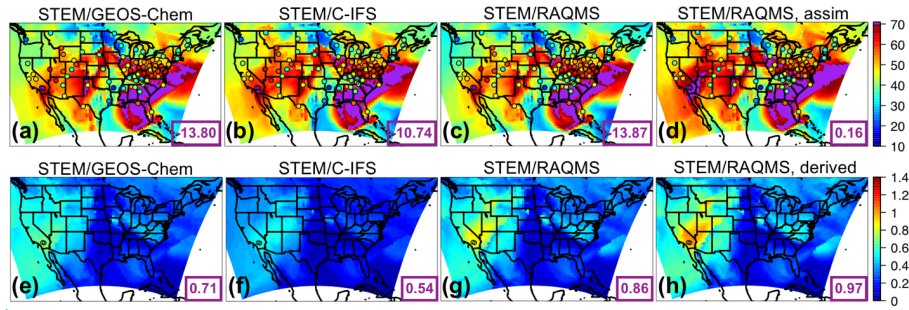


Figure 17. Same as Figure 14, but for a case study of 10 June 2010.



Formatted: Font:Bold

2014  
2015  
2016  
2017

**Figure 18.** Same as Figure 15, but for a case study of 10 June 2010. The CASTNET sites with O<sub>3</sub> exceedances on this day are Converse Station and Joshua Tree NP in southern California.  
**Table 1a.** HTAP2 base and sensitivity simulations by various global models. The STEM boundary condition models are highlighted in bold.

Global model, Resolution: lon×lat×vertical layer. (References)	BASE	EASALL (-20%)	EASALL (-100%)	GLOALL (-20%)	NAMALL (-20%)	EURALL (-20%)	SASALL (-20%)
CAM-Chem, 2.5°×1.9°×56 (Tilmes et al., 2016)	✓	✓		✓	✓	✓	✓
CHASER T42, ~2.8°×2.8°×32 (Sudo et al., 2002)	✓	✓		✓	✓	✓	✓
EMEP rv48, 0.5°×0.5°×20 (Simpson et al., 2012)	✓	✓		✓	✓	✓	✓
<b>SNU GEOS-Chem v9-01-03, 2°×2.5°×47</b> (Park et al., 2004; <a href="http://iek8wikis.iek.fz-juelich.de/HTAPWiki/WP_2.3?action=AttachFile&amp;do=view&amp;target=README_GEOS-Chem.pdf">http://iek8wikis.iek.fz-juelich.de/HTAPWiki/WP_2.3?action=AttachFile&amp;do=view&amp;target= README GEOS-Chem.pdf</a> )	✓	✓		✓	✓		
CU-Boulder GEOS-Chem adjoint v35f, 2°×2.5°×47 (Henze et al., 2007)	✓	✓		✓	✓	✓	✓
<b>RAQMS, 1°×1°×35, free running</b> (Pierce et al., 2007, 2009)	✓	✓	✓				
<b>RAQMS, 1°×1°×35, with satellite assimilation</b> (Pierce et al., 2007, 2009)	✓						
OsloCTM3 v2, ~2.8°×2.8°×60 (Søvde et al., 2012)	✓	✓		✓	✓	✓	✓
<b>ECMWF C-IFS, ~0.7°×0.7°×54, 1.125°×1.125°×54, as the STEM chemical boundary conditions</b> (Flemming et al., 2015)	✓	✓		✓	✓	✓	✓

2018  
2019  
2020  
2021  
2022  
2023  
2024  
2025

Acronyms:  
CAM-Chem: Community Atmosphere Model with Chemistry  
C-IFS: Composition-Integrated Forecasting System  
ECMWF: European Center for Medium range Weather Forecasting  
EMEP: European Monitoring and Evaluation Programme  
GEOS-Chem: Goddard Earth Observing System with Chemistry  
RAQMS: Realtime Air Quality Modeling System  
SNU: Seoul National University

Deleted: ...	[18]
Deleted: Relevant references for the RAQMS model	[19]
Formatted	[20]
Formatted Table	[21]
Formatted	[23]
Formatted	[25]
Formatted	[27]
Formatted	[29]
Formatted	[31]
Formatted	[33]
Formatted	[22]
Deleted: -	
Formatted	[24]
Deleted: %	
Deleted: -	
Formatted	[26]
Deleted: %	
Deleted: -	
Formatted	[28]
Deleted: %	
Deleted: -	
Formatted	[30]
Deleted: %	
Deleted: -	
Formatted	[32]
Deleted: %	
Deleted: -	
Formatted	[34]
Deleted: %	
Deleted: and horizontal resolution	
Formatted	[35]
Deleted: °	
Formatted	[36]
Deleted: °	
Formatted	[37]
Deleted: °	
Formatted	[38]
Deleted: °	
Formatted	[39]
Deleted: °	
Formatted	[40]
Deleted: °,	
Formatted	[41]
Formatted	[42]
Deleted: °, w/	
Formatted	[43]
Deleted: Oslo	
Formatted	[44]
Deleted: °	
Formatted	[45]
Deleted: CIFS	
Formatted	[46]
Deleted: °/	
Formatted	[47]
Deleted: ° (used	
Formatted	[48]
Formatted	[49]

2095

**Table 1b.** STEM regional simulations for HTAP2

Boundary condition model, Resolution: lon×lat×vertical layer,	BASE	EASALL (-20%)	EASALL (-100%)
SNU GEOS-Chem v9-01-03, 2°×2.5°×47,	✓	✓	
RAQMS, 1°×1°×35, free running	✓	✓	✓
RAQMS, 1°×1°×35, with satellite assimilation	✓		
ECMWF C-IFS, 1.125°×1.125°×54,	✓	✓	

Formatted: Justified, Level 1, Indent: Left: 0", Suppress line numbers

- Deleted:
- Deleted: -
- Deleted: %
- Deleted: -
- Deleted: %
- Deleted: °
- Deleted: °,
- Deleted: °, w/
- Deleted: CIFS
- Deleted: °

2096

**Table 1c.** STEM and its boundary condition models' key inputs and chemical mechanisms, with references. More details on the models can be found in Table 1a and the text.

Model	Meteorology	Biogenic VOCs: NO <sub>x</sub>	Lightning	Biomass Burning	Chemical Mechanism
<u>GEOS-Chem</u>	<u>GEOS-5</u>	<u>MEGAN v2.1</u> (Guenther et al., 2012); <u>Wang et al., 2009</u>	based on <u>GEOS-5 deep convective cloud top heights and climatological observations</u> (Murray et al., 2012)	<u>GFED v3.0</u> (van der Werf et al., 2010)	<u>GEOS-Chem standard NO<sub>x</sub>-O<sub>3</sub>-hydrocarbon-aerosol</u> ( <a href="http://acmg.seas.harvard.edu/geos/doc/archive/man.v9-01-03/appendix_1.html">http://acmg.seas.harvard.edu/geos/doc/archive/man.v9-01-03/appendix_1.html</a> )
<u>RAQMS</u>	Online (Pierce et al., 2007)				<u>CB-IV</u> (Gery et al., 1989) with adjustments
<u>ECMWF C-IFS</u>	<u>IFS</u>	<u>MEGAN-MACC</u> , (Sindelarova et al., 2014); <u>POET</u> database for 2000 (Granier et al., 2005)	based on <u>IFS convective precipitation</u> (Meijer et al., 2001)	<u>GFAS v1.0</u> (Kaiser et al., 2012)	<u>CB05</u> (Yarwood et al., 2005)
<u>STEM</u>	<u>WRF-ARW v3.3.1</u>	<u>WRF-MEGAN v2.1</u>	based on <u>scaled WRF convective precipitation</u>	<u>FINN v1.0</u> (Wiedinmyer et al., 2011)	<u>SAPRC99</u> (Carter, 2000)

2099

Acronyms:

2100

CB: Carbon Bond

2101

FINN: Fire INventory from NCAR

2102

GFAS: Global Fire Assimilation System

2103

GFED: Global Fire Emissions Database

2104

IFS: Integrated Forecasting System

2105

MACC: Monitoring Atmospheric Composition and Climate

2106

MEGAN: Model of Emissions of Gases and Aerosols from Nature

2107

POET: Precursors of Ozone and their Effects in the Troposphere

2118 WRF-ARW: Advanced Research Weather Research and Forecasting Model  
 2119 **Table 2a**, Evaluation of the period mean (1 May-30 June, 2010) multi- global model free  
 2120 simulations against the CASTNET observations, only at the sites where 95% of the hourly O<sub>3</sub>  
 2121 observations are available. Evaluation of the individual models is summarized in Table 2b.

Deleted: [50]

Subregion	US EPA regions contained	Number of sites	Mean bias (ppbv)		RMSE (ppbv)	
			3 BC <sup>a</sup> models	8 global models	3 BC models	8 global models
Western US	8, 9, 10	19	-5.68	-2.52	10.37	7.05
Southern US	4, 6	18	11.61	10.24	13.62	11.96
Midwest	5, 7	13	8.03	7.66	9.16	8.67
Northeast	1, 2, 3	17	9.55	10.63	10.28	11.24
All	1-10	67	5.49	6.22	11.11	9.96

Formatted Table

2122 <sup>a</sup>BC: Boundary Conditions

2123 **Table 2b**. Evaluation of the period mean (May-June 2010) global model free simulations against  
 2124 the EANET and CASTNET observations. The STEM boundary condition models are highlighted  
 2125 in bold.  
 2126

Formatted: Font:Bold  
 Formatted: Justified

Network	Number of sites	RMSE (ppbv)							
		CAM-Chem	EMEP	CHASER	SNU GEOS-Chem	GEOS-Chem adjoint	RAQMS	OsloCTM3 v2	C-IFS
CASTNET	67	13.30	11.61	15.43	<b>15.55</b>	13.48	<b>9.32</b>	11.05	<b>11.00</b>
EANET	11	10.38	9.96	11.39	<b>9.18</b>	11.04	<b>8.60</b>	12.97	<b>10.86</b>

2127 **Table 2c**. Evaluation of the period mean (May-June 2010) multi- global model free simulations  
 2128 against the EANET observations in Japan and Korea. Evaluation of the individual models is  
 2129 summarized in Table 2b.  
 2130

Country	Number of sites	Mean bias (ppbv)		RMSE (ppbv)	
		3 BC <sup>a</sup> models	8 global models	3 BC models	8 global models
Japan	8	0.36	1.01	8.77	9.25
Korea	3	1.14	3.98	8.37	10.51
All	11	0.57	1.82	8.66	9.61

2131 <sup>a</sup>BC: Boundary Conditions

2133 **Table 3a.** Evaluation of the hourly STEM simulated total O<sub>3</sub> (averaged from the three base  
 2134 simulations that used the different free-running boundary conditions) against the CASTNET  
 2135 surface observations for 8 May-30 June, 2010. The subregional mean R(O<sub>3</sub>, EAS, 100%) and its  
 2136 correlation coefficient with the observed O<sub>3</sub> are also shown.

Deleted: 3

Deleted: %, as well as

Subregion	US EPA regions contained	Number of sites	Mean elevation (km): actual/model	Mean bias (ppbv)	RMSE (ppbv)	Correlation (model base; obs)	Correlation (obs; modeled EAS)	Mean EAS sensitivity (ppbv)
Western US	8, 9, 10	22	1.75/1.71	1.60	4.86	0.76	0.34	0.48
Southern US	4, 6	22	0.38/0.31	20.33	22.13	0.58	0.27	0.15
Midwest	5, 7	16	0.29/0.28	15.64	17.97	0.70	0.15	0.17
Northeast	1, 2, 3	20	0.36/0.26	20.94	24.16	0.47	0.17	0.21
All	1-10	80	0.73/0.68	16.17	18.30	0.66	0.13	0.20

Formatted Table

2137 **Table 3b.** Evaluation of the hourly STEM simulated total O<sub>3</sub> (separately for three base simulations  
 2138 that used the different free-running boundary conditions) against the CASTNET surface  
 2139 observations for 8 May-30 June, 2010.  
 2140

Subregion	US EPA regions contained	Number of sites	Mean bias (ppbv)/RMSE (ppbv)/Correlation (model base; obs)		
			SNU GEOS-Chem	C-IFS	RAQMS
Western US	8, 9, 10	22	1.68/4.83/0.77	4.16/6.63/0.70	-1.03/4.81/0.76
Southern US	4, 6	22	21.18/22.94/0.57	20.34/22.07/0.60	19.48/21.45/0.56
Midwest	5, 7	16	15.77/18.17/0.70	16.41/18.46/0.72	14.73/17.35/0.69
Northeast	1, 2, 3	20	21.25/24.36/0.47	21.86/24.80/0.48	19.71/23.40/0.45
All	1-10	80	16.57/18.62/0.66	16.89/18.84/0.67	15.03/17.52/0.64

Formatted: Justified

2141

2144 **Table 4.** The ranges and standard deviations (ppbv, separated by “;”) of R(O<sub>3</sub>, *source region*, 20%)  
 2145 by 6-8 global models (defined in eq. (1a-d)), summarized by months in 2010. The monthly multi-  
 2146 model mean values are shown in Figures 5-6.

Month/ Source region	All Foreign/ Non-NAM (ppbv)	EUR (ppbv)	EAS (ppbv)	SAS (ppbv)
Jan	0.38-1.69; 0.41	0.002-0.12; 0.05	0.02-0.72; 0.24	0.001-0.11; 0.04
Feb	0.92-2.07; 0.37	0.02-0.15; 0.05	0.16-0.91; 0.28	0.02-0.12; 0.04
Mar	1.30-2.37; 0.38	0.07-0.21; 0.06	0.24-1.03; 0.30	0.03-0.12; 0.03
Apr	1.42-2.46; 0.33	0.09-0.23; 0.05	0.33-1.07; 0.28	0.04-0.12; 0.03
May	1.24-1.91; 0.21	0.06-0.17; 0.04	0.24-0.75; 0.19	0.05-0.11; 0.02
Jun	1.03-1.41; 0.13	0.03-0.07; 0.02	0.14-0.39; 0.09	0.04-0.07; 0.01
Jul	0.86-1.18; 0.13	0.02-0.04; 0.01	0.08-0.22; 0.06	0.01-0.04; 0.01
Aug	0.80-1.19; 0.13	0.01-0.04; 0.01	0.07-0.20; 0.05	0.02-0.04; 0.01
Sep	0.85-1.18; 0.13	0.03-0.05; 0.01	0.10-0.25; 0.06	0.02-0.06; 0.01
Oct	0.96-1.31; 0.14	0.04-0.10; 0.02	0.17-0.42; 0.09	0.03-0.08; 0.02
Nov	0.90-1.48; 0.19	0.05-0.15; 0.04	0.17-0.54; 0.14	0.04-0.10; 0.02
Dec	0.73-1.67; 0.29	0.03-0.18; 0.05	0.14-0.66; 0.19	0.04-0.12; 0.03

2147